ELECTRODE FABRICATION FOR *in vitro* MONITORING OF CATECHOLAMINE SECRETION: CONSEQUENCES AND EXPLANATIONS FOR DOCA-SALT SENSITIVE IMPAIRMENT OF ADRENAL CHROMAFFIN CELL SECRETION

By

Matthew J. Fhaner

A DISSERTATION

Submitted to
Michigan State University
in partial fulfillment of the requirements
for the degree of

DOCTOR OF PHILOSOPHY

Chemistry

2012

ABSTRACT

ELECTRODE FABRICATION FOR *in vitro* MONITORING OF CATECHOLAMINE SECRETION: CONSEQUENCES AND EXPLANATIONS FOR DOCA-SALT SENSITIVE IMPAIRMENT OF ADRENAL CHROMAFFIN CELL SECRETION

By

Matthew J. Fhaner

Sympathetic activity is increased in multiple forms of hypertension. This observation led our group to hypothesize that increased sympathetic activity play an integral role in the on-set and long term maintenance of blood pressure in salt-sensitive hypertension (SSH). This form of hypertension is unique, as it is characterized by increased salt retention in the kidneys, leading to an increase in blood volume and in turn blood pressure. Studies were performed investigating the release of norepinephrine from sympathetic neurons innervating smooth muscle cells of mesenteric blood vessels, which determined that sympathetic neurons isolated from DOCA-salt rats released a higher amount of norepinephrine. This increase in overflow is partly attributed to impairment in the auto-regulatory α_2-AR and the norepinephrine reuptake transporter. A gap remained in this work due to the spatial limitations of performing electrochemistry at individual neuronal junctions. To solve this, my work will use adrenal chromaffin cells to elucidate the affects of DOCA-salt hypertension on the frequency and kinetics of individual vesicle secretion. To accomplish this goal, electrode fabrication and optimization for single cell electrochemistry is required, alongside the isolation of single adrenal chromaffin cells.

The results of this work revealed significant findings in both electrode fabrication processes and biological alterations in chromaffin cell signaling. 1) Applying a novel nucleation process to our published boron-doped diamond electrode fabrication process decreased the growth time needed to deposit a continuous diamond film in half. These electrodes will be useful for *in vitro* electrochemistry work for larger tissue such as mesenteric blood vessels and gastrointestinal neurotransmission; however carbon-fibers are superior for single cell work due to the ease at which they can be manipulated into a disk-shape. 2) Chromaffin cells isolated from DOCA-salt rats had a higher frequency of release events, with individual events occurring more rapidly, than Sham chromaffin cells. 3) These alterations appear to at least in part be caused by impairment in the function of BK and ATP-sensitive potassium channels in DOCA-salt cells. Further mechanistic investigation led to the conclusion that calcium influx, reactive oxygen species levels and catecholamines metabolism are not responsible for any alterations observed in DOCA-salt chromaffin cell secretion patterns. 4) Finally, fast-scan voltammetry determined that the ratio of norepinephrine:epinephrine secreting cells remains unchanged in DOCA-salt hypertension.

These results suggest that increased release frequency along with more rapid secretion may also contribute to the alterations found in sympathetic neurons by previous group members. Also, potassium channels may provide a viable treatment option for managing salt-sensitive hypertension. Finally, for future work requiring BDD electrodes, application of a pre-growth carbon layer greatly enhances film deposition rates.

Acknowledgments

My time and subsequent success in graduate school was made possible by the combined effort of a number of people.

I would like to first thank my advisors, Dr. Greg Swain and Dr. James Galligan. They provided me with a unique research environment which allowed encouraged me not to fear failing, as it is part of the scientific process. Their support led to me being awarded a pre-doctoral fellowship, which would have been impossible to obtain without their guidance and comments. I am truly indebted to both of them for their understanding, patience and encouragement throughout my research.

I would also like to personally thank a number of the great faculty we have here at Michigan State University. First I thank my committee members Dr. Gary Blanchard and Dr. Dana Spence. Each of them acted in a variety of positions ranging from sounding board to professional guidance. I would also like to thank Dr. Gavin Reid and Dr. Daniel Jones who were generous enough to provide me with professional development advice over the years. The community nature of the department's faculty was a great help throughout my time here.

I would also like to thank past and current group members for their help and advice. Dr. Hua Dong, Dr. Shihua Wang and Dr. Matt Swope helped train me to become the scientist I am today, for better or worse. I would also like to sincerely thank Xingyi Yang, Yan Zhu, LiangLiang Li, and Catherine Munson along with all the other Swain Group members. A special appreciation is also given to the members of Dr. Galligan's group who welcomed me as I spent nearly half my time doing research in their labs.

Finally, a solid core of friends and family is needed to get through graduate school. I want to especially thank John McIlroy, Stephen Halpin and Adam Giebink for providing me with both academic and personal support. I would also like to thank Hannah Garver for all her hard work maintaining the animals I needed to accomplish my research goals. I would also like to thank my extended family for their patience and understanding when I had to decline family functions for work reasons. Last, but certainly not least, I want to thank my wife Cassie Fhaner. Her constant support, understanding and unwavering patience allowed me to keep my sanity when times became overwhelming.

Table of Contents

LIST OF TABLES

LIST OF FIGURES

Chapter 1

Introduction

1.1 Hypertension

Hypertension is a chronic elevation in blood pressure defined as a sustained systolic pressure above 140 mmHg and a diastolic pressure above 90 mmHg[1]. Consequences of prolonged hypertension include a decrease in renal function, vascular endothelial function and output[2]. The multifactoral effects of hypertension can lead to serious health complications in chronic patients including renal injury, heart attack and stroke[2]. Hypertension can be a challenging disease to treat because of the unidentifiable causes in many patients and often goes undetected due to the lack of obvious outward symptoms. For this reason, the disease is known as the “silent killer”.

Hypertension can be classified into two forms. The first is essential hypertension, or primary hypertension. Essential hypertension is the most common type and accounts for nearly 95% of hypertensive patients[3]. This form of the disease has no identifiable cause. The second is referred to as secondary hypertension. Secondary hypertension is the direct result of some identifiable cause. Examples include smoking, neurotransmitter secreting tumors or even diet[1, 4-5].

Our research group is focused understanding neurogenic effects in a specific type of essential hypertension known as salt-sensitive hypertension (SSH). Salt sensitivity occurs in 30 percent of people who have normal blood pressure and 50 percent who are hypertensive[6]. SSH occurs more frequently in African Americans, the elderly and those suffering kidney disorders[6]. SSH is characterized by a deficiency in sodium clearance, which leads to an increase in blood volume[7]. Salt-sensitive patients can develop chronic hypertension if the disease is not properly managed[8]. Further understanding of the pathophysiology of this disease may provide for more comprehensive and effective treatments.

1.2 Regulation of Blood Pressure

Mean arterial blood pressure (MAP) is the product of cardiac output (CO) and total peripheral resistance (TPR)[9]. TPR is the combination of the resistance to blood flow through peripheral vessels and is determined by the diameter of small arteries and arterioles. The MAP is regulated by feedback from chemo and cardiopulmonary receptors and also by the baroreflex[10]. The baroreflex stabilizes short term changes in blood pressure to the carotid MAP. These same receptors are also involved in long-term regulation of blood pressure[11]. Baroreflexes and central nerve signals from the brain dominate real-time control of blood pressure through both the sympathetic and parasympathetic nervous systems which are both part of the autonomic nervous system[12]. Activation of the sympathetic nervous system (SNS) can increase both TPR and CO, which increases in blood pressure. It is also important to note that the kidneys

are under the control of the SNS which regulates renal blood flow[13]. Other factors that can influence blood pressure are aldosterone levels, circulating epinephrine levels, vascular function and the endothelin system[14-17].

1.3 Sympathetic Nervous System

The sympathetic nervous system (Figure 1-1) is a division of the autonomic nervous system and is positioned between the first thoracic segment of the spinal cord and the second or third lumbar. Heart rate, digestive secretions, pupil dilation and blood vessel contraction are all regulated by the sympathetic nervous system[18]. Nerve activity in the sympathetic system is a critical factor controlling vasoconstriction in the splanchnic circulation[19-20]. Neurotransmitters, such as epinephrine (EPI), norepinephrine (NE) and ATP[21-22] are involved in regulating basal levels of vaso- and venoconstriction. When neurotransmitter levels are elevated, for example when sympathetic nerve activity is increased, there is a greater likely hood of hypertension development[23]. It is known that increased sympathetic activity is associated with both essential and secondary hypertension[24-25]. For this reason, work in our group has focused on the role of sympathetic nerve activity and the development of hypertension. Due the large volume of blood stored in the splanchnic circulation[26], our group has focused attention on sympathetic nerves innervating these blood vessels as a location

that would be highly affected by increased sympathetic nerve activity in deoxycorticosterone acetate (DOCA)-salt hypertension.

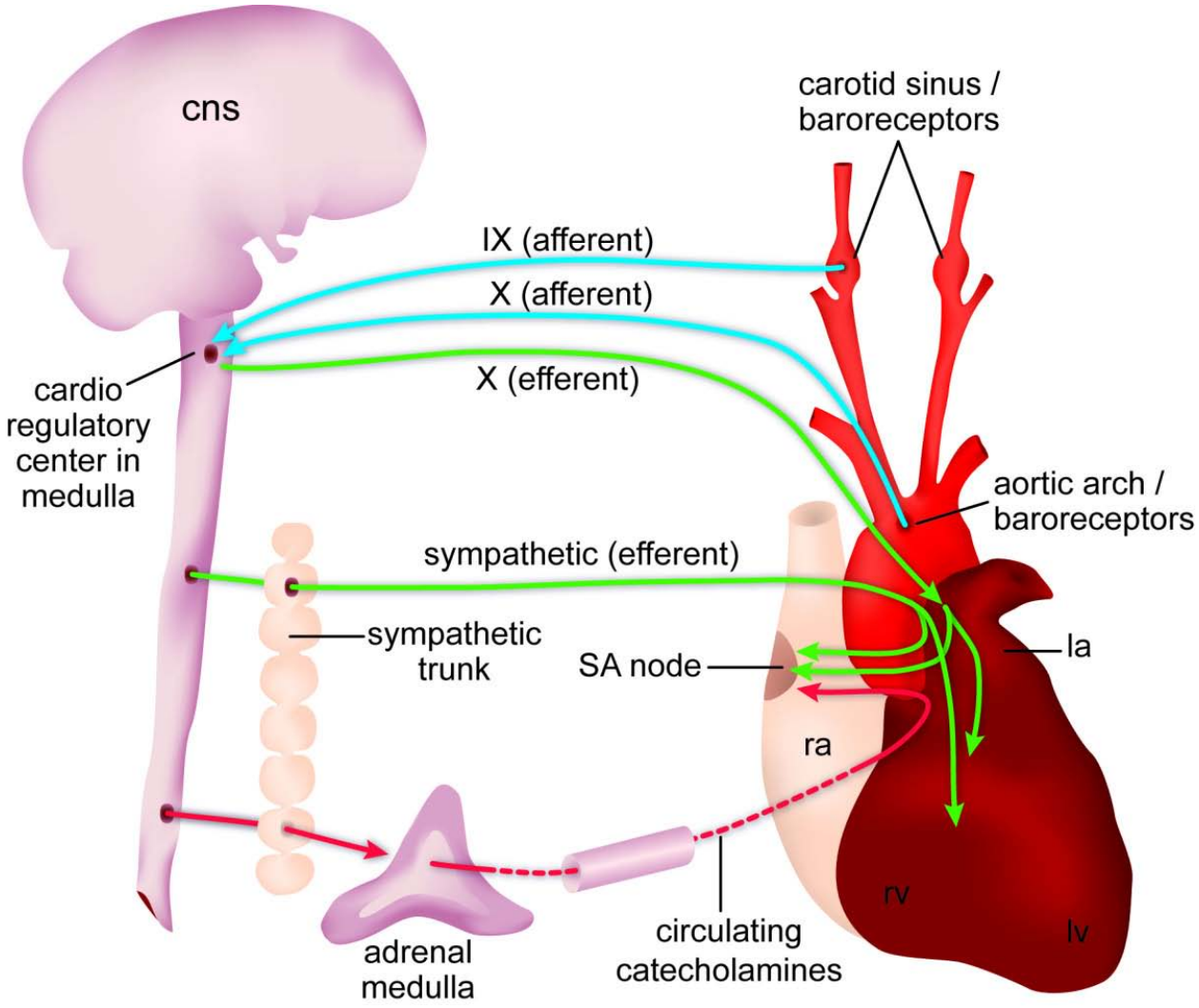

Figure 1-1. Overview of the sympathetic nervous system. Reprinted from McNeill *et al*. Neural Development 2010, 5:6. For interpretation of the references to color in this and all other figures, the reader is referred to the electronic version of this dissertation.

1.4 Mesenteric Blood Vessels

The splanchnic region of the body consists of the pancreas, spleen, liver, small and large intestines. This region is home to roughly 33% of the body's total blood volume[26]. The blood vessels within the mesentery are supplied by the sympathetic nervous system. Importantly, the basal firing frequency of these nerves is elevated in hypertension[27]. Hyperactivation of sympathetic nerves has been found to cause a 60% reduction in the stored blood within the mesenteric veins[28]. Blood that is forced out of mesenteric veins due to heightened constriction moves to more resistive arteries causing an increase in blood pressure. This increased cardiac output leads to an increase in mean arterial pressure. Therefore, people with heightened SNS activity are at risk for developing hypertension. Vascular tone is controlled by, among other factors, the neurotransmitters released from sympathetic nerves including NE and ATP. Neurotransmitters are stored in vesicles[29] and are released from sympathetic nerve terminals. It acts at the alpha$_1$-adrenoreceptor (α_1-AR) located on vascular smooth muscle cells to evoke constriction[30]. Upon activation of the α_1-AR, calcium influx into the smooth muscle cells will cause constriction[31]. Understanding neuroeffector signaling mediated by NE and ATP is a target of research in our group as they are potent vasoconstrictors[32]. Unlike ATP, NE is electrochemically active and can be measured locally as an oxidation current using a small carbon microelectrode. Dynamic changes in NE concentration at the adventitia surface can be measured using

electrochemical methods[33-34]. The simultaneous monitoring of NE availability along with the blood vessel diameter using video microscopy offers insight into sympathetic neurogenic control of blood vessel tone in hypertension. Figure 1-2 shows a diagram depiciting the sympathetic innervation of mesenteric blood vessels.

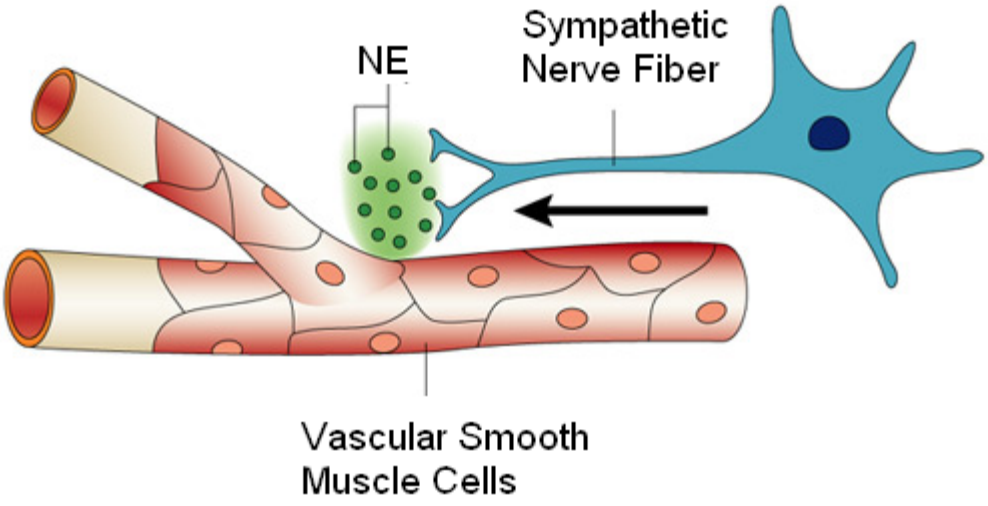

Figure 1-2. Sympathetic nerve innervation of a mesenteric blood vessel and the signaling by NE, which is one vasoconstricting neurotransmitter stored and released by sympathetic nerves. Reprinted by permission from Macmillan Publishers Ltd: [Nature Reviews Genetics] (Blood vessels and nerves: common signals, pathways and diseases), copyright (2003).

Prior work in our group focused on characterizing sympathetic neuroeffector signaling in the DOCA model of salt-sensitive hypertension in using vitro electrochemistry and video microscopy[35]. NE released from nerve terminals has several fates. First, NE can diffuse across the neuroeffector junction and bind to and activate α_1-ARs located on vascular smooth muscle cells. This binding evokes

constriction. NE can also diffuse to bind with the prejunctional alpha$_2$-adrenoreceptor (α_2-ARs), which through negative feedback terminates further NE release. Most of the NE molecules secreted are taken back up into the nerve terminal by the norepinephrine transporter (NET) protein. Uptake by NET is the predominate fate and occurs on the millisecond time scale so that the nerve can be "reset" for the next signaling event. After uptake into the releasing nerve terminal, NE may be repackaged into vesicles for "re-release" or metabolized. A key finding from this work is that in this animal model of hypertension, there is impaired function of prejunctional the α_2-adrenergic autoreceptors and clearance by and the NET[33, 36-37]. The functional impairment of both α_2-AR and NET leads to greater availability of NE in the neuroeffector junction and this increases vascular smooth muscle cell constriction. Another alteration found in DOCA-salt blood vessels are different innervation patterns for sympathetic neurons on mesenteric veins and arteries[35].

One mechanistic factor that could not be determined from our prior work is how NE storage and individual secretory kinetics are altered in this model of hypertension. Due to the small size of neuroeffector junctions, there is no way to place a microelectrode in the neuronal-junction gap to monitor secretion from a single nerve ending. This means that the transient oxidation current recorded amperometrically at a blood vessel surface results from NE release from multiple nearby varicosities. Additionally, information about release kinetics is convoluted with the kinetics of reuptake making it challenging to know if any aspect of the storage and exocytotic

release are altered in the disease state. An attractive alternative is to use model systems with larger vesicles and higher concentrations of the neurotransmitter to monitor exocytosis[38]. Such a model system is the adrenal medullary chromaffin cell line[39-41]. Over the years, electrochemical methods have been used to measure chemical secretion from a variety of single cells isolated in culture including mouse mast cells[42], human pancreatic β-cells[43], and rat pheochromocytoma (PC12) cells[44]. Measurements using single cell model systems provide direct information about quantal release from individual vesicles (number of molecules per release event), the number of release events per stimulus and the release kinetics of secretory events. In order to better understand how exocytotic release from sympathetic nerves might be altered in DOCA-salt hypertension, adrenal medullary chromaffin cells were used as a model.

1.5 Adrenal Gland and Chromaffin Cells

The adrenal gland is located above the kidneys and is an integral part in the body's response (hypothalamus-pituitary-adrenal axis) to stress[45]. The glands are supplied by a number of suprarenal arteries and veins and, along with the thyroid gland, have the greatest blood supply per gram of tissue of any organ[46]. The adrenal gland is composed of two zones. The cortex, or the outer zone, is where mineral- and glucocorticoids are produced. Of particular importance is the mineralcorticoid, aldosterone. Aldosterone promotes salt and water retention by the kidneys[47]. This causes an increase in blood pressure as blood volume increases making these organs

an integral piece in development of SSH. The second zone of the adrenal gland is the adrenal medulla. The adrenal medulla is home to the chromaffin cells, which synthesize, store and secrete the neurotransmitters NE and EPI[48]. Secretion is stimulated by pre-ganglionic sympathetic nerves originating between the T1 – T10 spinal segments[49]. These nerves release acetylcholine, the physiological stimulant of catecholamine secretion from adrenal chromaffin cells. Adrenal chromaffin cells secrete EPI and NE at approximately a 3:1 ratio. These cells are the primary source of EPI released into the blood stream[48]. Both molecules are electroactive and can be monitored as an oxidation current.

Chromaffin cells have been extensively studied as a model for exocytosis[38, 40-41, 50-54]. They are an ideal platform for investigating the kinetics of exocytosis due to their large size, as compared to neurons, lack of expressed transporter protein, and ease of isolation in culture[55]. Chromaffin cells store and release neurotransmitters in a manner similar to sympathetic neurons. They contain voltage-sensitive Na^{+}, K^{+} and Ca^{+2} channels, receptor-mediated K^{+} and Ca^{+2} channels and nicotinic acetylcholine receptors[48]. Upon chemical stimulation, these cells exhibit Ca^{+2}-dependent exocytosis. Prior to secretion, NE and EPI are synthesized inside the chromaffin cells[56]. The synthesis, which is outlined in Figure 1-3, begins with the conversion of tyrosine into 3,4-dihydroxyphenylalanine (DOPA) and finally converted into dopamine. The reactions

are catalyzed by specific enzymes at each step. Dopamine is packaged into chromaffin granules by the vesicular monoamine transporter (VMAT) using a pH gradient from the 5.5 value inside of chromaffin vesicle to the 7.2 value of the cytoplasm[57]. Once inside the chromaffin granule, dopamine is converted to NE via DOPA decarboxylase. NE can diffuse out of granules and if there is phenylethanolamine N-methyltransferase (PNMT) present in the cytoplasm, NE can be converted to EPI. The EPI is then repackaged into vesicles for secretion. The two predominate vesicles are those that contain only NE or only EPI. There is also a smaller subset of vesicles that contain both NE and EPI.

The major stimulant for granule secretion is a rise in intracellular calcium[58]. Calcium enters the cell in response to an external stimulus, such as acetylcholine, via the nicotinic acetylcholine receptor (nAChR). nAChRs are non-specific cationic channels that allow sodium and calcium to enter after activation with acetylcholine (ACh). Cation influx leads to a local depolarization of the cell membrane[59]. This local change in cell membrane potential activates voltage-gated calcium channels, facilitating greater calcium entry. Influx of extracellular calcium causes intracellular calcium to be released from the mitochondria and endoplasmic reticulum resulting in a complete depolarization of the cell membrane[60]. Calcium is also important for soluble *N*-ethylamide-sensitive factor attachment protein receptor (SNARE) proteins, which tether the granules to the cell membrane, leaving it primed for vesicle fusion and secretion[61]. Further information regarding the steps involved in vesicle packaging and secretion are provided in the following section.

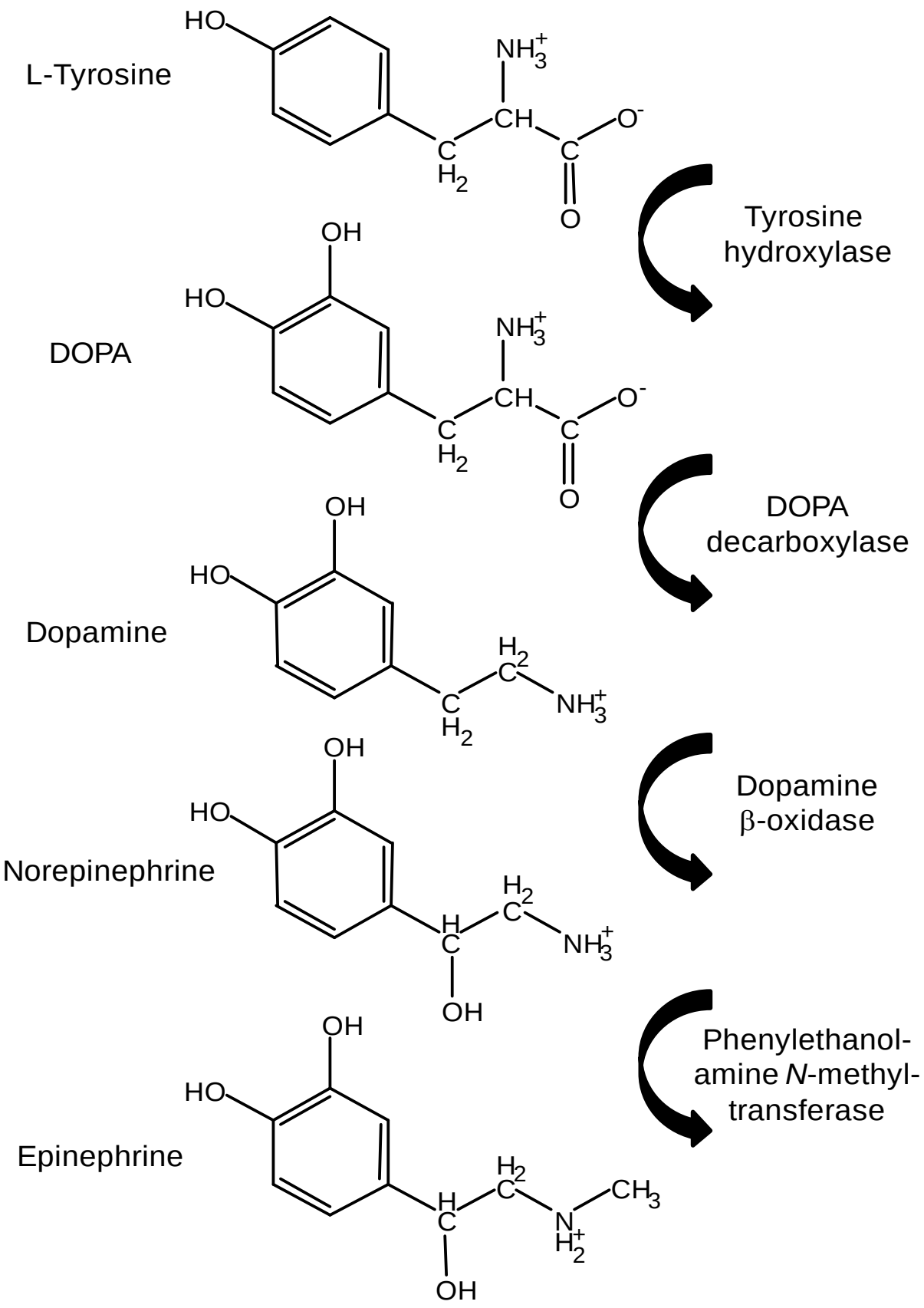
L-Tyrosine
Tyrosine hydroxylase
DOPA
DOPA decarboxylase
Dopamine
Dopamine β-oxidase
Norepinephrine
Phenylethanol-amine N-methyl-transferase
Epinephrine

Figure 1-3. Catecholamine synthesis inside adrenal chromaffin cells. L-Tyrosine is converted to DOPA (Tyrosine Hydroxylase), which is converted to dopamine (DOPA decarboxylase). Dopamine is converted to norepinephrine (dopamine beta-hydroxylase) and then finally into epinephrine (phenylethanolamine *N*-methyltransferase).

1.6 Chromaffin Granule Secretion

Chromaffin granules (also known as vesicles) start their life in the Golgi region of the intracellular complex[62] (Figure 1-4). Various peptides are synthesized in the endoplasmic reticulum and then transported to the Golgi apparatus for packing into granules. After incorporation of peptides into the vesicular matrix, granules break away from the Golgi and move into the cytoplasm. At this point, vesicles start to become packed with neurotransmitters. The synthesis of NE and EPI occurs as described in Figure 1-3. Neurotransmitter packaging is a dynamic process as catecholamines continuously leak out of vesicles and are repackaged via VMAT. At this point of the granule life-cycle, they take in ATP and catecholamines without bias[63]. Granules become mature and completely filled with neurotransmitters within 12-24 h after creation[64-65]. When fully mature, vesicles will contain a variety of small molecules including NE, EPI, ATP, nucleotides, ascorbic acid, neuropeptide Y and chromogranin with the majority of the contents (>90%) in vesicles being due to catecholamine packaging[66].

Transport of newly formed vesicles occurs along the dense microtubule network that supports the organelle architecture[67]. Also, F-actin plays a key role in granule

transport in both the interior and cortical region of the cytoplasm[68-69]. The majority of granules will be held within the actin network until stimulation[70], upon which the actin network will undergo changes to promote granule movement towards the cell membrane[71]. There is a pool of vesicles that reside near the cell membrane and are

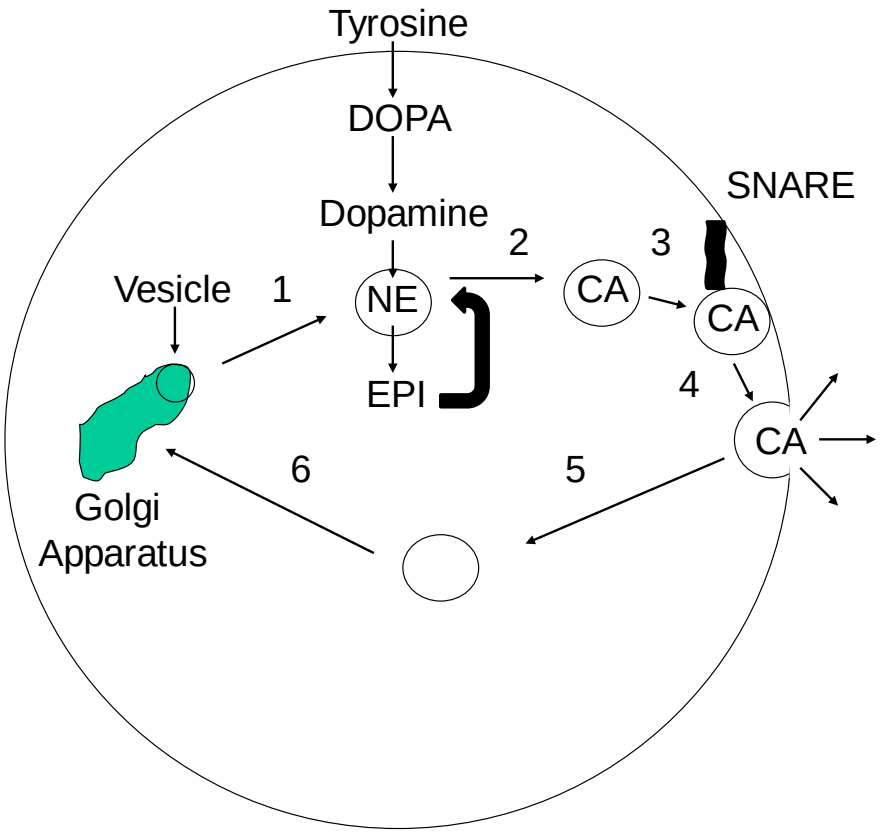

Figure 1-4. Life cycle of chromaffin granules. Newly formed vesicles break away from the Golgi apparatus (1) and are packaged with either NE or EPI (2). Packaged vesicles are transported to the cell membrane for interaction with SNARE proteins (3). After a stimulus, CAs are released from the chromaffin cell (4) and the empty vesicles are transported back to the Golgi for recycling (5 & 6).

readily available for release in response to a stimulus. These vesicles are known as the readily releasable pool and are primed for secretion. Once vesicles reach the cell membrane, they become tethered by SNARE proteins[72]. The SNARE protein makes

contact with the granule through synaptobrevin, which inserts into the chromaffin granule and SNAP-25, which is anchored to the cell membrane. This connection is believed to be crucial in exocytosis by overcoming the free energy barrier between the cell membrane and the granule membrane[61]. Upon stimulation, calcium enters the cell and promotes fusion of the granule and the cell membrane, creating a small pore for neurotransmitters to escape. More potent simulation will cause the fusion pore to completely open dispelling all contents within the chromaffin granule into the blood stream[73].

1.7 Mechanisms Affecting Adrenal Chromaffin Cell Secretion

1.7.1 Nicotinic Acetylcholine Receptors

nAChRs are large protein ligand-gated channels that consist of five subunits arranged around a central membrane-spanning pore[59]. nAChRs consist of a large N-terminal domain containing the binding site for ACh, four transmembrane segments and a short C-terminal domain[59]. After activation of nAChRs, cations enter the intracellular space causing voltage-gated calcium channels to open, resulting in an influx of extracellular calcium into the cell[60]. This calcium influx is essential for exocytosis, as calcium sensors near the exocytotic sites, such as synaptotagmin1, react to the calcium resulting in catecholamine secretion[58].

The nAChRs desensitize after prolonged or repeated exposure to stimuli[74-75]. Rats exposed to nicotine for long periods of time produce an up-regulation in nAChR expression[76]. It is possible that the increased activity of the nerves innervating the adrenal medulla could have an effect on nAChR activity or expression. Such alterations would have a direct effect on the efficiency and frequency of catecholamine secretion, which makes these receptors possible targets for further investigation.

1.7.2 Catecholamine Metabolism

Catecholamine synthesis occurs within individual chromaffin cells. Catecholamines undergo two basic metabolic fates (Figure 1-5). The first is via monoamine oxidase (MAO). This pathway converts norepinephrine into 3,4-dihydroxyphenylglycol (DHPG)[77]. Approximately 80% of circulating DHPG at rest is due to metabolism of NE that leaks from sympathetic nerves[78]. Adrenal chromaffin cells are different from sympathetic nerves in terms of how catecholamines are metabolized. Chromaffin cells contain not just MAO, but also catechol-*O*-methyltransferase (COMT). In fact, the COMT that is present in the cells is the membrane-bound form that has a higher affinity for catecholamines than does the soluble form found in other regions of the body[79-81]. When NE and EPI are metabolized by COMT, the metabolites, normetanephrine (NMN) and metanephrine (MN) are generated, respectively[77]. NMN and MN produced can diffuse into the blood stream. In fact, the COMT pathway is favored so highly in adrenal chromaffin cells that

93% of circulating MN levels and 25 to 40% of circulating NMN levels within the blood are derived from catecholamine metabolism inside chromaffin cells[77].

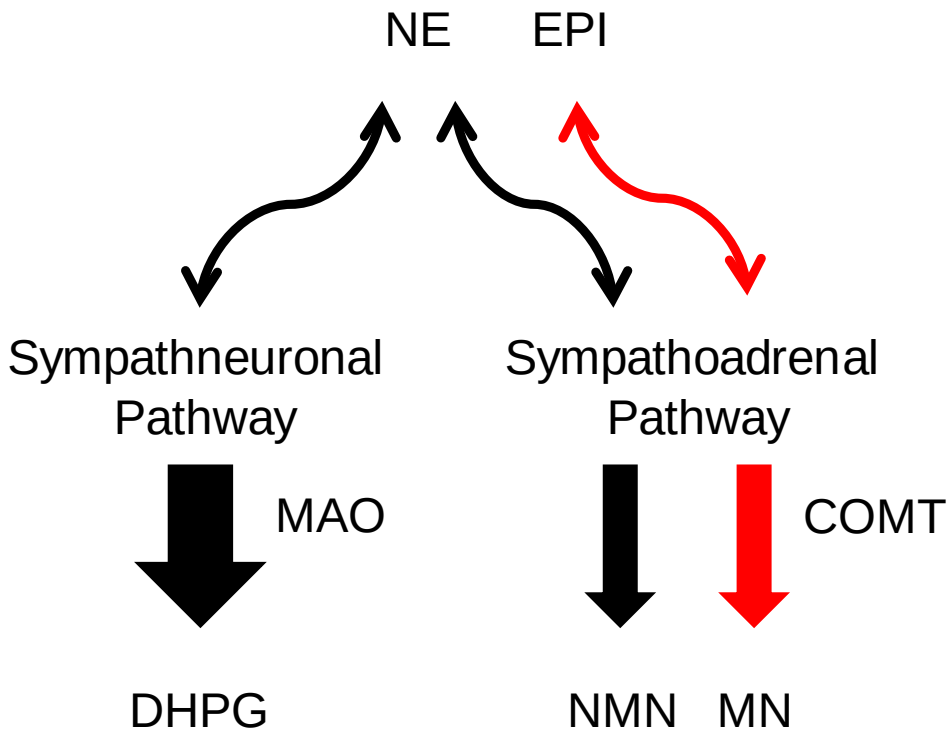

Figure 1-5. Overview of catecholamine metabolism differences between sympathetic neurons and adrenal chromaffin cells. In sympathetic neurons, monoamine oxidase (MAO) degrades norepinephrine (NE) to 3,4-dihydroxyphenylglycol (DHPG). In adrenal chromaffin cells, however, catechol-O-methyltransferase metabolizes NE and EPI to normetanephrine (NMN) and metanephrine (MN), respectively.

These metabolites are of particular interest in catecholamine secreting adrenal tumors known as pheochromocytomas. Metabolite levels are often used as a screening tool for diagnosis of pheochromocytomas[82]. In fact, a quick literature search reveals that the majority of research into MN or NMN surrounds identification of these tumors. Previous research has shown that perfused adrenal glands from spontaneously hypertensive rats release more NE and EPI than glands from normotensive rats[83]. It is

possible that these differences may be somehow be related to a dysfunction in catecholamine metabolism within adrenal chromaffin cells, resulting in excess NE and EPI levels for secretion.

1.7.3 Calcium and Exocytosis

Calcium is an essential part of the exocytosis and its importance was first demonstrated in cat adrenal glands stimulated by ACh[84]. Knight *et al.* first demonstrated the requirement of calcium for exocytosis in bovine chromaffin cells[85]. Another key finding was the necessity of calcium and ATP-dependent priming to prompt vesicle exocytosis[86]. Investigation of calcium's role during exocytosis has yielded insights into the different pools of secretory vesicles[87-89]. Though calcium promotes secretion, the relationship between calcium and exocytosis is not linear in the sense that a two-fold increase in [Ca^{2+}] will not yield a two-fold increase secretion[90]. It has been demonstrated in frog neuromuscular junctions that doubling the concentration of extracellular Ca^{2+} produced a 16-fold increase in acetylcholine secretion[91].

The innate relationship between calcium and exocytosis is evident. This leads to the possibility that calcium handling in DOCA-salt hypertension may be altered. In rat chromaffin cells, there is a variety of calcium channels located on the cell membrane. The breakdown of calcium channels present on rat chromaffin cells is as follows: L-type (50%), N-type (25%), P/Q-type (15 %) and R-type (10%)[58]. Calcium channel blockers

have been found to enhance the protective effects of angiotensin receptor blockers in salt-sensitive hypertension[92]. Calcium activity can be monitored using the fluorescence probe, fluo-4 AM. Investigating calcium flux into cells from normotensive and hypertensive test animals could provide further insight regarding the mechanisms of exocytosis in the DOCA-salt animal model.

1.7.4 Potassium Channel Function

Potassium channels are a family of ion channels that set the resting membrane potential of a cell and return the cell membrane potential to a resting state following depolarization[93]. Rat chromaffin cells have been found to express big potassium, small potassium, ATP-sensitive and voltage-gated potassium channels[94-97]. Once a cell body, such as a neuron or chromaffin cell, receives an electrical or chemical stimulus, sodium and calcium channels open allowing ions to travel across the cell membrane and into the cell[98]. Increasing intracellular sodium and calcium leads to an increase in the cell membrane resting potential, which for rat chromaffin cells at equilibrium is near -50 mV[98]. As the cell membrane potential increases, it will reach a threshold causing depolarization which promotes vesicle fusion and secretion[99]. Following the depolarization, potassium channels are responsible for restoring the cell membrane potential to its resting value by removing positively charged potassium ions from the cell. Briefly, after the cell membrane has been depolarized potassium channels will open. This causes a net flux of potassium to exit the cell. Once a threshold value has

been obtained for the cell membrane, ion channels promoting the entrance of inward positive charge will close leaving only potassium channels open. Potassium channels will continue to move potassium ions out of the cell until the resting membrane potential once again set. Alterations or impairments in potassium channel function or expression could lead to a prolonged depolarization resulting in increased secretory firing.

Recent work has shown that blood pressure in big potassium (BK) channel knock-out mice, specifically the BKβ1-KO, is sensitive to dietary potassium levels and can cause an increase in blood pressure due to increased salt and water handling[100]. These findings parallel the physiological mechanisms associated with the DOCA-salt hypertension model. Work by Sausbier *et al.* also yielded similar results by determining that small arteries in BKα-KO mice had increased vascular tone and decreased vasodialation. These alterations were accompanied by higher levels of aldosterone, further linking vascular tone to adrenal gland function[101]. These links between potassium channel expression and vascular function provide the foundation for the hypothesis that altered potassium channel function may be present in adrenal chromaffin cells also.

Alterations in either potassium channel function or expression could lead to a delayed time course for repolarization of the cell. In other words, the cell would stay depolarized longer. Delaying repolarization would create a longer time-course for catecholamine secretion if potassium channels are impaired. In fact, it has been shown in spontaneously hypertensive rats that there is a higher frequency for catecholamine

secretion from hypertensive chromaffin cells versus normotensive cells[102]. This could, in part, be due to impaired potassium channel function.

1.7.5 The Involvement of Superoxide in DOCA-salt Hypertension

Superoxide, also known as hyperoxide or O_2^-, is produced naturally within the body[103]. The production of superoxide starts with two oxygen molecules interacting with nicotinamide adenine dinucleotide phosphate-oxidase (NADPH-oxidase). This reaction forms two molecules of superoxide, a hydrogen ion and a $NADP^+$ cation[104]. The enzyme, Superoxide dismutase, clears excess superoxide following production[105]. In a healthy body, superoxide can act as a signaling molecule. Increased superoxide concentrations, either by increased production or decreased removal, result in cellular damage[106].

Oxidative stress has been implicated in a number of diseases including obesity, diabetes and hypertension[107-108]. Previous work has shown that there is increased production of superoxide in the vascular walls of various animal models of hypertension, including spontaneously hypertensive and DOCA-salt hypertensive rats[109-111]. Work by Cuzzocrea *et al.* demonstrated that introducing a superoxide dismutase mimetic causes a reduction in the mean arterial blood pressure of spontaneously hypertensive rats[112]. Our group has also studied the effects of superoxide in the DOCA-salt

hypertension model. Work by Dr. Hua Dong demonstrated that the impairment found in the prejunctional α_2-AR found on sympathetic neurons could be reversed when animals were given chronic treatment of apocynin, an NADPH-oxidase inhibitor and tempol, a reactive oxygen species scavenger[33]. Our group has also found evidence that superoxide is associated with the impairment of the norepinephrine transport clearance efficiency (unpublished data). A goal of this dissertation was to further investigate the potential role of reactive oxygen species on the frequency and kinetics of individual secretory events from adrenal chromaffin cells.

1.8 DOCA-salt Model of Hypertension

There are several hypertension animal models used in research including spontaneously hypertensive, Dahl-salt sensitive and DOCA–salt models[113]. The work reported in this dissertation used the DOCA-salt model[114]. DOCA-salt animals are made hypertensive by the synthetic mineralcorticoid DOCA chronically. This model is ideal for investigating the pathophysiology of heightened sympathetic nerve activity, and oxidative and inflammatory stress in the cardiovascular system[115]. A unique characteristic of DOCA-salt hypertension is that blockade of angiotensin receptors does not have any effects on blood pressure values[116]. This is because DOCA-salt hypertension is characterized as a low-renin and increased blood volume form of hypertension. DOCA-salt rats mimic most of the changes seen in chronic cardiovascular remodeling in humans including hypertension, hypertrophy, fibrosis,

electrical conduction abnormalities and vascular hypertrophy and dysfunction[115]. This model was selected for our research because it exhibits heightened SNS activity and oxidative stress (elevated O_2^-). As mentioned above, our group is interested in sympathetic nerve-mediated control of vascular tone and how these control mechanisms are altered in hypertension. DOCA-salt treatment reliably induces the development of salt-sensitive hypertension in rodents and has a gradual onset. Finally, current research indicates excessive mineralcorticoid action contributes to a larger number of cases of clinical hypertension than generally appreciated[117].

1.9 Monitoring Catecholamine Secretion from Adrenal Chromaffin Cells

1.9.1 Electrochemical Methods

Historically, intracellular electrophysiological techniques have been used to investigate ion channel function during exocytosis[118]. These techniques are ideal for monitoring how ion channels function during the exocytotic process. Electrophysiological techniques have yielded a wealth of information, including the discovery of new types of calcium and potassium channels associated with exocytosis[119]. However, these techniques do not yield direct information about the time course and quantal size of individual exocytotic events. Over the past 20 years, electrochemical methods, including amperometry and fast-scan cyclic voltammetry, have (Figure 1-6) become an important tool for the investigation of exocytosis[38, 120-121].

Ideally, one would like to measure dynamic changes in neurotransmitter concentration in a single neuroeffector junction. However, this is not possible due to the small size (nm). Carbon fibers are typically used for these measurements for their relatively small probe size (1-10 μm is common) and their biocompatibility. Use of these small recording microelectrodes enables one to dynamically measure changes in neurotransmitter concentrations in the extracellular fluid surrounding neurons or secretory cells. Electrochemical measurements also offer good sensitivity for electroactive neurotransmitters, high temporal resolution (μs) and good response reproducibility if the microelectrode preparation is well controlled. Additionally, electrochemical measurements offer some selectivity for the neurotransmitter being detected by virtue of the formal redox potential of the molecule. In other words, if different neurotransmitters undergo redox chemistry at different potentials, then this can be used as a means to identify the molecule being detected.

NE and EPI are part of the catecholamine family. This family of molecules contains an oxidizable hydroquinone group via a reversible 2-electron/2-proton redox reaction. By taking advantage of the electroactive nature of these molecules, one can monitor real-time secretion via electrochemical detection if a sufficient voltage is applied for oxidation.

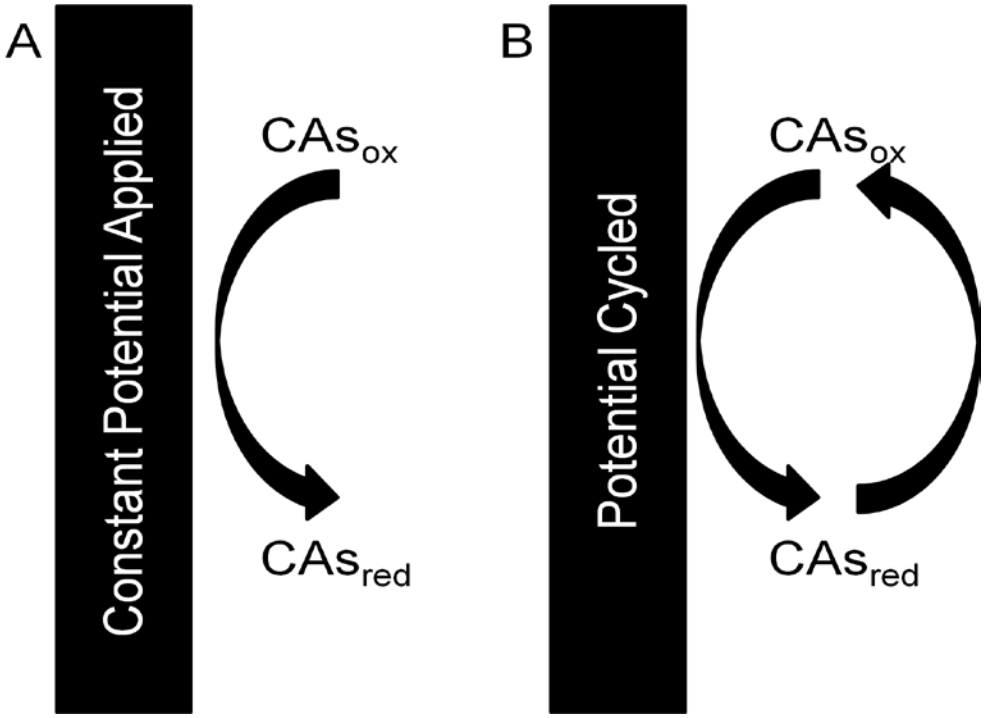

Figure 1-6. Differences between continuous amperometry and FSCV. The current measured in amperometric measurements is often diffusion limited (A). Either and oxidation or reduction reaction is used for analyte monitoring. There is no recycling of the molecule between oxidation states and a depletion layer extends from the electrode surface out into the solution. For this reason, amperometry is an excellent technique for monitoring rapid transient changes in neurochemicals of known identity. In FSCV, the analyte is cycled between the oxidized and reduced states of the molecule (B). If the scan rate is relatively fast, then no significant depletion layer develops near the electrode.

1.9.1.1 Continuous Amperometry

Continuous amperometry is an electrochemical technique in which a constant potential is applied to a working electrode. Amperometric measurements utilize a reference electrode, counter electrode and microscale working electrode. The current response is monitored as a function of time. Dynamic changes in current are reflective of transient changes in analyte concentration near the electrode. For a redox reaction under pure diffusion control, the time-dependent current response is given by the

Cottrell equation (Equation 1-1) where the variables are n (number of electrons transferred), F (Faraday's constant), A (electrode area), D_o (diffusion coefficient), C_o (analyte concentration), t (time in s).

$$i(t) = \frac{nFAD_o^{1/2}C_o^*}{\pi^{1/2}t^{1/2}}$$

Equation 1-1

Amperometry is a useful analytical tool due to its high temporal resolution (μs) and low limits of detection (fM) which allows for the detection of small amounts of catecholamines released over millisecond time spans during exocytosis from chromaffin cells[38]. The technique has been employed for *in vitro* work to investigate a variety of biological questions. For example, amperometry was a critical tool for initial investigation of exocytosis in model systems[38, 40-41]. These studies provided the first evidence of different modes of exocytosis, including the kiss-and-run theory which provided insight into how vesicles merge with the cell membrane and then secrete their contents[122]. Amperometry has also been used to investigate neurotransmission in a number of different tissues including blood vessels, chromaffin cells, neurons in the brain, and many more[50-51, 123-127].

1.9.1.2 Fast-Scan Cyclic Voltammetry

Fast-scan cyclic voltammetry (FSCV) is a potential sweep method in contrast to amperometry which is a fixed potential method. By recording a cyclic voltammogram, molecules can be identified based on their half-wave potential. As mentioned,

chromaffin cells can secrete both NE and EPI. A technique such as amperometry oxidizes (or reduces) any molecules that have a half-wave potential below the potential being applied. Amperometry is useful for investigation of secretory kinetics due to its high temporal (μs) and spatial (μm) resolution. Amperometry is not an ideal technique for identifying the molecules secreted during an exocytotic event. Signal detected via amperometry can be a combination of the oxidation of multiple molecules, such as NE and EPI. In order to identify the contents of exocytotic events, voltammetry at high scan rates can be used, which is commonly referred to as FSCV. FSCV provides good temporal resolution (ms) with the same spatial resolution as amperometry. However, the key difference between the two techniques is that by scanning the potential NE and EPI can be differentiated based on their molecular structure. Both molecules have an oxidizable quinone structure, however only epinephrine has a secondary amine structure. These two structures are oxidized at different potentials, with the quinone being oxidized near 0.600 V and the secondary amine being oxidized near 1.425 V (both cases vs. Ag/AgCl, Figure 1-7). Oxidation of the quinone and secondary amine give rise to two distinct oxidation waves in a voltammetric measurement. Many groups have used FSCV to identify and quantify electroactive molecules secreted from cells and nerves. For example, Wightman *et al.* provided initial evidence for profiling bovine chromaffin cells and determined that cells were differentiated into primarily NE or EPI secreting cells[41, 121]. Ewing *et al* used FSCV to probe single PC12 cell exocytosis using microelectrode arrays[128-129]. The Mathews group has also used fast-scan voltammetry to characterize dopamine receptors in the mouse striatum[130]. Fast-scan

voltammetry provides real-time identification for secretory events from normotensive and hypertensive chromaffin cells, which will provide a profile on any alterations that might occur in the secretion ratio in DOCA-salt hypertension.

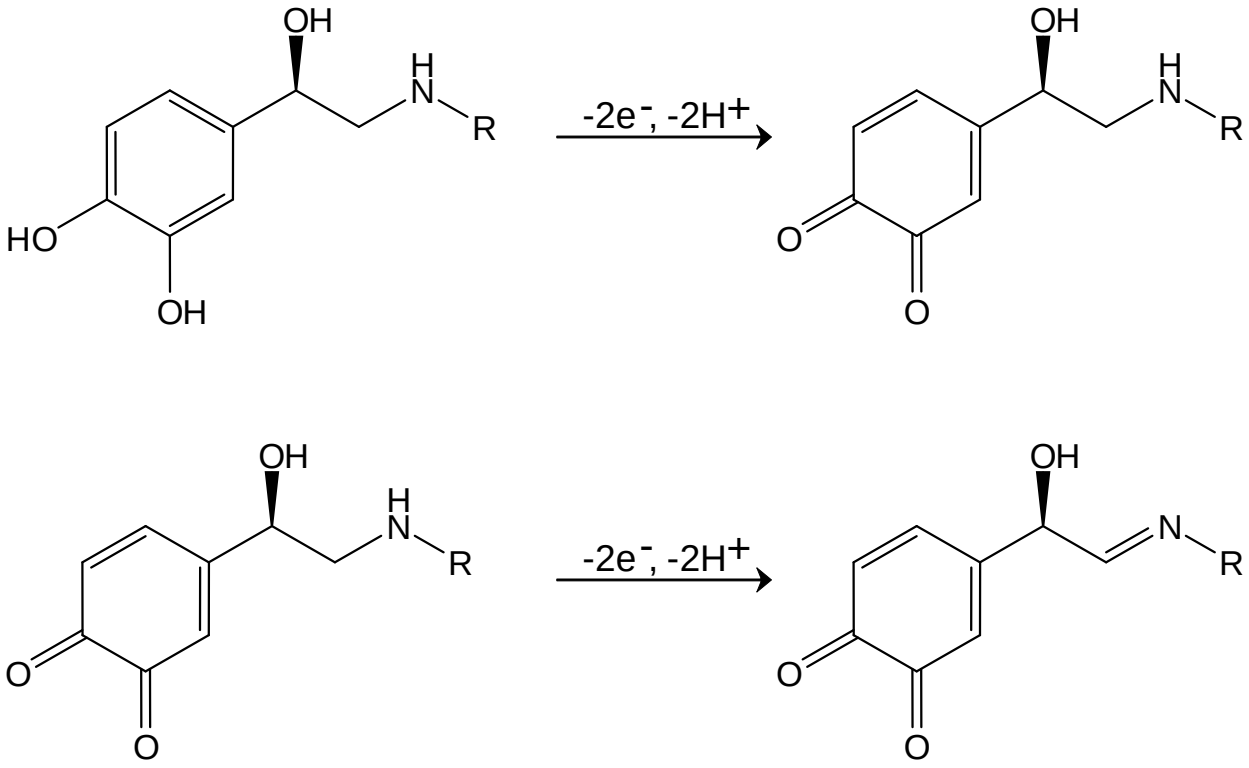

Figure 1-7. Oxidation mechanisms for identification of NE and EPI. Oxidation of NE (R=H) and EPI (R=CH_3) to their quinone form is a two electron process that occurs near 0.6 V vs. Ag/AgCl (A). Only EPI has a secondary amine that can also be oxidized through a two electron process resulting in the formation of a non-reversible imine (B). Presence or absence of the amine oxidation allows for the identification of secretory events as resulting from release of NE or EPI[121].

1.9.2 High performance liquid chromatography

One of the oldest techniques for identifying neurotransmitters released chromaffin cells in urine or blood samples is high performance liquid chromatography (HPLC). HPLC works by separating molecules based on their polarity and size. Initial work used urine, blood or tissue samples to determine the levels neurotransmitters and

their metabolites[83, 131-132]. HPLC has low limits of detection and can separate a wide variety of molecules. However, the lack of real-time analysis makes HPLC a poor option for investigating the kinetics of neurotransmission in adrenal tissue. HPLC does allow for quantification of tissue levels for NE and EPI, which is why it will be used for determining how DOCA-salt hypertension affects full tissue levels in adrenal medulla of normotensive and hypertensive rats.

1.10 Microelectrode Materials and Construction

1.10.1 Carbon Fiber Materials and Fabrication

Graphitic carbon has been vigorously studied due to its low cost, wide potential window, relatively inert electrochemistry, and electrocatalytic activity for a variety of redox reactions[133]. Of specific interest to this dissertation are carbon fibers. Some carbon fibers possess a microstructure consisting of radially aligned graphite sheets which are very disorganized[134-135] (Figure 1-8 A). Disorganization leads to surface oxides being present on the surface of the majority of carbon surfaces[133]. These surface oxides can lead to an adsorptive effect for positively charged analytes. For *in vitro* measurements of NE and EPI, which are cationic neurotransmitters, oxide functional groups promote adsorbtion[136-138]. Oxide functional groups prefer the disordered edge plane of graphitic carbon which implies a highly disorganized electrode material would greatly benefit catecholamine detection[133].

Previous group work has investigated two types of carbon fiber for norepinephrine detection, which are the T-650 and the P-55 carbon fibers produced by CYTEC industries[33]. This group investigated the effects of various agonist and antagonists on norepinephrine detection for the two fiber types. No other characterization was performed however, which will be necessary for detecting the small amount of catecholamines (attomole levels). Thus, the requirement for a highly disorganized carbon structure is needed in order to promote a high percentage of absorption onto the electrode surface.

To accomplish this goal, electrodes will be fabricated similarly to Wightman *et al* in a disk-shaped mannar[139]. The disk-shape leads to an electrode surface with high signal to background, which is ideal for discerning individual secretory events from one another. Raman spectroscopy and electrochemistry was used to characterize the two fiber types and to provide a set of quality-control values for identifying superb electrodes to be used for *in vitro* studies. Raman spectroscopic characterization of carbon materials is well known[133, 140]. The organization of the carbon microstructure, in the simplest definition, can be determined by the intensity of Raman bands found at 1360 cm^{-1} and 1582 cm^{-1} respectively. The 1360 cm^{-1} is associated with the breakdown of symmetry in the graphite lattice, where the 1582cm^{-1} is associated with the stretching of the graphite lattice. For these reasons the 1360cm^{-1} is often referred to as the “D” (disorganized) band and the 1582cm^{-1} is known as the “G” (graphite) band. The ratio of

these two peaks can be used as a measure of lattice organization[140]. Electrochemical investigation using voltammetry can provide insight into the electron-transfer kinetics and relative cleanliness of the electrode surface. By using two surface sensitive redox systems, potassium ferrocyanide and norepinephrine, limiting currents and half-wave potentials can be obtained which will provide quality-control values for determining if electrode fabrication was successful or not.

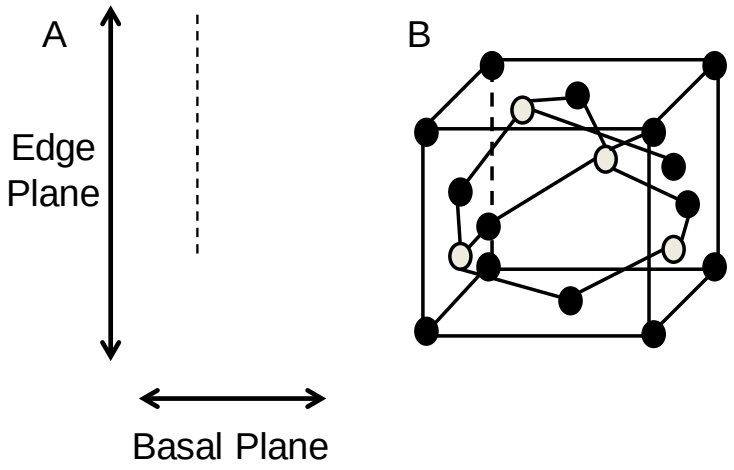

Figure 1-8. Lattice shapes for sp^2 and sp^3 carbon. Graphite forms overlapping sheets (A), which are layered in a radial structure for carbon fiber electrodes. Surface oxides form preferentially along the edge plane of graphite. A basic diamond lattice is shown which describes the first (black spheres) and displaced (grey spheres) lattices.

1.10.2 Diamond Film Enhancement Using a Novel Nucleation Process

Another carbon material often used for electrochemistry is boron-doped diamond (BDD). BDD microelectrodes are formed by depositing films onto a metal wire substrate. Diamond electrodes offer exceptional microstructural stability over a wide range of potentials, are electrically conductive and exhibit a low background current[141]. Furthermore, molecular adsorption, particularly polar molecules, is generally weak on

the hydrogen-terminated diamond surface. Compared to carbon fibers, diamond generally offers improvements in response reproducibility, limit of detection and response stability. The electron-transfer kinetics for a number of redox systems are similar for diamond and activated carbon fiber microelectrodes. However, the kinetics for NE and EPI oxidation are more sluggish on diamond as compared to carbon fibers[33]. Diamond is a unique carbon substance that is comprised of a sp^3 bonded carbon lattice (Figure 1-8 B). In the past 20 years, synthetically made diamond films have become a material of high interest[142] and have been utilized to measure sympathetic neuroeffector transmission at arteries and veins[35, 126] along with nitric oxide release in guinea pig illeium[143]. Within our group, we have created BDD electrodes for use *in vitro*[141, 144]. The electrodes were fabricated by depositing thin diamond films onto platinum wires using chemical vapor deposition (CVD)[145]. Diamond is an ideal electrode material for biological use due to its low background signal, high chemical stability and minimal adsorption of biological species[141]. This protocol has led to a number of discoveries regarding neurotransmitter function in DOCA-salt hypertension[35, 126], however the key drawback of BDD electrode fabrication is the lengthy time required. Tachibana *et al.* found that diamond grows heteroepitaxially on platinum substrates[146]. To increase the growth rate in our group's fabrication protocol, platinum substrates are sonicated in a diamond seeding solution. These diamond seeds provide initial deposition sites for film growth. Even with this seeding however,

continuous diamond film coverage requires 8-10 h of deposition time. It has been shown diamond growth rate can be increased by first depositing an amorphous carbon film onto a substrate prior to seeding[147]. Adding this initial step should reduce the growth time required to deposit a continuous film on our platinum wires. Further investigation will determine if films grown in this manner have ideal characteristics for *in vitro* biological work.

1.11 Research Objective and Specific Aims

Sympathetic nerve control of vascular tone is altered in DOCA-salt hypertension[37, 126, 148-150]. Previous work from our group showed that (i) there is greater NE availability at sympathetic neuroeffector junctions in this model of hypertension due, in part, to impaired prejunctional α_2-AR and NET function, and (ii) that this impairment is due, in part, to oxidative stress and inflammation[33, 36]. What could not be determined in the prior work is if vesicular storage and exocytosis is altered.

To this end, research was conducted using a model system, adrenal medullary chromaffin cells, to determine if the neurotransmitter release mechanism in sympathetic nerves is altered in the DOCA-salt model of hypertension. Electrochemical measurements were made to study the exocytosis mechanism using single adrenal chromaffin cells isolated from Sham and DOCA-salt hypertensive rats. **It was hypothesized that a greater number of secretory events with more rapid release**

kinetics would be found for chromaffin cells isolated from DOCA-salt rats than from cells isolated from Sham controls. It was also hypothesized that the impairments in exocytosis are linked to oxidative stress and inflammation. The work consisted of four aims:

Specific Aim 1: Fabricate and characterize carbon-fiber disk electrodes and BDD electrodes deposited using a novel nucleation process to be used in the single cell measurements.

1a. Work out the protocols for preparing reproducibly behaved carbon-fiber disk electrodes for use in the single cell measurements. **1b.** To characterize the material properties and electrochemical performance of the disk electrodes. **1c.** To implement a novel nucleation process to improve the initial nucleation density for depositing boron-doped diamond thin films on sharpened Pt wires. These microelectrodes are most practical for measurements at *in vitro* blood vessel preparations.

Specific Aim 2: To measure catecholamine secretion from single Sham and DOCA-salt chromaffin cells isolated in culture and to determine if altered catecholamine release is related to impaired potassium channel function.

2a. To use continuous amperometry to monitor individual secretory events and secretion profiles from Sham and DOCA-salt chromaffin cells evoked by a chemical stimulus. **2b.** To determine if the release frequency and kinetics are altered in DOCA-salt chromaffin cells. **2c.** To measure catecholamines (NE and EPI) and their respective metabolite levels in adrenal glands using HPLC to determine if there are any

changes in whole tissue levels (*i.e*., metabolism) in DOCA-salt hypertension. **2d.** To use pharmaceutical approaches to determine the types of potassium channels expressed by these chromaffin cells and to identify which subtype might be impaired.

Specific Aim 3: To determine in the altered catecholamine release in DOCA-salt cells is linked to oxidative stress and inflammation and or to altered calcium handling.

3a. To compare and contrast calcium handling in Sham and DOCA-salt chromaffin cells using fluorescence spectroscopy with calcium-sensitive fluorescent probe, fluo-4. **3b.** To probe for oxidative stress effects at the chromaffin cell level by administering the NADPH oxidase inhibitor, apocynin, to Sham and DOCA-salt rats over a 4-week period. Prior work showed that administering this drug over a 4-week period lowers blood pressure and super oxide levels in sympathetic nerve terminals of DOCA-salt rats.

Specific Aim 4: To use fast-scan cyclic voltammetry to determine if there is any difference in the ratio of NE to EPI released from DOCA-salt chromaffin cells.

4a. To use fast-scan cyclic voltammetry to qualitatively identify NE and EPI – containing vesicles and to quantify the ratio of these neurotransmitters released from DOCA-salt cells as compared to Sham controls.

Chapter 2

Experimental Section

2.1 Carbon Fiber Electrode Characterization

2.1.1 Raman Spectroscopy

Raman spectroscopy was used to probe the carbon fiber microstructure. Raman spectra were obtained using a Raman 2000 instrument (Chromex, Albuquerque, NM), equipped with a 50-mW Nd:YAG laser (532 nm line). The laser beam was focused to a spot approximately 5 μm diameter, which results in an estimated power density of *ca*. 150 kW/cm^2. Spectra were obtained using a 10 s integration time. The spectrometer was calibrated using 2-acetyloxybenzoic acid (aspirin). Figure 2-1 shows a Raman spectrum of the T-650 carbon fiber used for the electrochemical recordings. Two peaks are observed, one at 1380 cm^{-1} and another at 1582 cm^{-1}. The peak at 1360 cm^{-1}, also known as the "D" (disorder) band, is attributed to a breakdown in the symmetry in the graphite lattice and the resulting effect on Raman selection rules[133, 140]. This peak is due to the less ordered carbon within the microstructure. On the other hand, the peak at 1582 cm^{-1}, also known as the "G" (graphite) band, is due to the single crystal E_{2a} phonon from graphite lattice[140]. These two peaks are characteristic of a disordered microstructure with a high fraction of exposed graphitic edge plane, such as carbon fiber[133]. An ideal electrode for catecholamine detection will have a high level of

disordered carbon, as these edge plane sites serve as sites for catecholamine adsorption, which promotes electron transfer[138, 151].

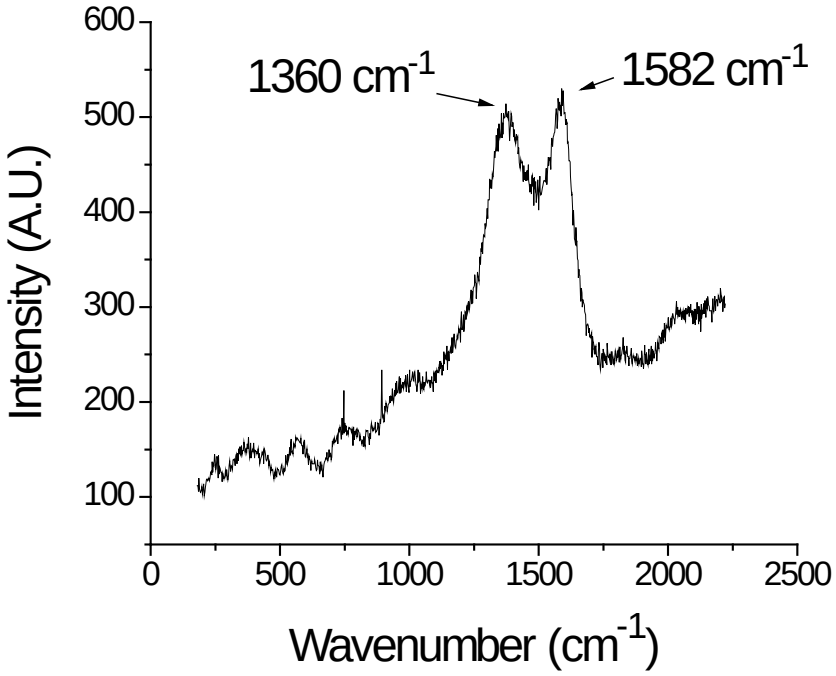

Figure 2-1. Raman spectrum of a T-650 carbon fiber. Two peaks are found from the T-650 carbon fiber seen at 1360 cm^{-1} (D band) and 1582 cm^{-1} (G band).

2.1.2 Scanning Electron Microscopy

Scanning electron microscopy (SEM) was used to probe the morphology and shape of the polished electrodes. Images were obtained using a JEOL 6400V electron microscope equipped with a LaB_6 emitter (Tokyo, Japan). Electrode tips were carefully removed using a fine pair of scissors and attached to a specimen stub via carbon tape (SPI Supplies, West Chester, PA). Carbon ink (SPI Supplies, West Chester, PA) was used to make electrical connection between the glass capillary and the substrate stage.

As shown in Figure 2-2, polished electrodes have an elliptical shape. The image was taken at a 4,300x magnification, 10 kV SEI (secondary electron imaging) and a WD (distance from lens to sample surface) of 9.3 mm.

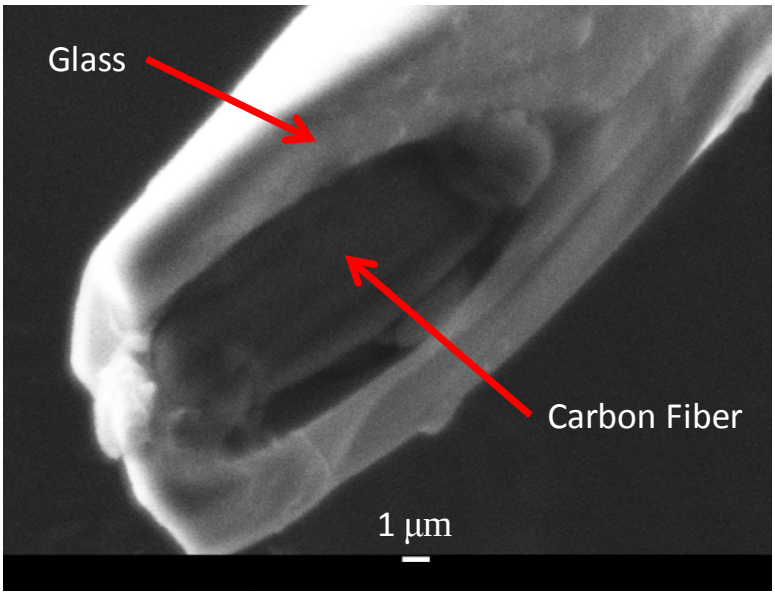

Figure 2-2. Scanning electron micrograph of a polished carbon fiber disk microelectrode. The image is a polished carbon fiber disk electrode after exposure to fast-scan voltammetric experiments. It can be seen that there is a gap between the carbon fiber and the glass capillary, most likely due to etching of the carbon fiber during the high scan rate and applied potential. The image was obtained under the following conditions: 4,300x magnification, 10 kV SEI and a WD of 9.3 mm.

Unfortunately, SEM was not a high priority for characterizing carbon fiber electrodes early in the research process. SEM images were only obtained to determine the effects of FSCV on the construction integrity. The images verify the oval shape of polished electrodes. The carbon etching (i.e. corrosion) results at the positive potentials used in the FSCV experiments.

2.1.3 Electrochemical Characterization

Cyclic voltammetry was used to determine the surface area for individual microelectrodes, to check for cracks in the epoxy seal and to ascertain the level of surface cleanliness. The physical, chemical and electronic properties of an electrode can all influence the electrode reaction kinetics and mechanisms for a redox system. All voltammograms were obtained using CHI potentiostats (CHInstruments, Inc., Austin, TX). A three electrode system was employed consisting of a carbon fiber working electrode, a platinum counter electrode and an in-house fabricated Ag/AgCl reference electrode, potassium ferrocyanide ($K_4Fe(CN)_6$) and NE were used as test probes for the electrochemical characterization. Both molecules undergo electron transfer through a so-called inner-sphere pathway[133]. Inner-sphere electron transfer is often referred to as surface sensitive redox systems. In other words, inner-sphere redox system's electron transfer rates depend of the condition of the surface (microstructure, debris, etc…). The key differences between the two redox probes is that $Fe(CN)_6^{-3/-4}$ does not require adsorption to the electrode surface as where NE does[133]. Therefore, surface cleanliness is an important parameter affecting the electron transfer rate[152]. Figure 2-3 shows the cyclic voltammograms for polished carbon fiber microelectrodes in the presence of 100 μM $K_4Fe(CN)_6$ (A) and NE (B), respectively. These voltammograms were recorded at 100 mV/s. Both voltammograms exhibit a limiting current. The sigmoidal curves indicate that steady-state mass transport rates are achieved for both compounds. The half-wave potentials, $E_{1/2}$, are 138 mV and 270 mV, respectively. The

curves' shape, in particular the $E_{1/2}$ values, indicate that the microelectrodes are clean and exhibit relatively rapid electron-transfer kinetics for both dissolved redox species.

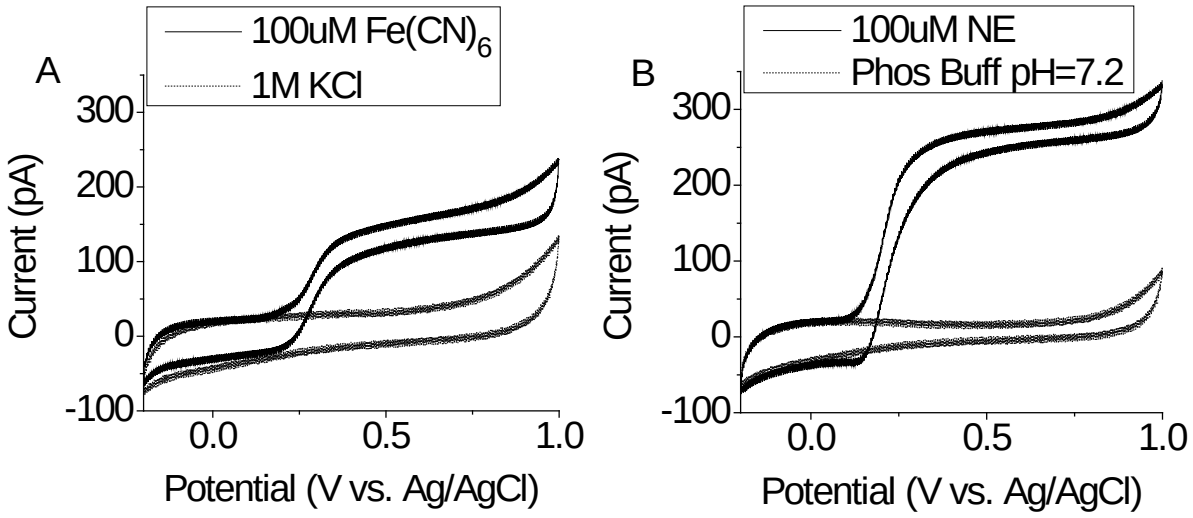

Figure 2-3. Cyclic voltammograms for carbon-fiber microelectrodes exposed to for ferrocyanide and norepinephrine. Cyclic voltammograms are shown for 100 μM ferrocyanide (A) and NE (B). Both voltammograms have a mass-transfer limited current at higher potentials. This indicates that the electrode's current response is limited by the rate at which molecules diffuse to the electrode surface.

The $E_{1/2}$ for $K_4Fe(CN)_6$ is near 275 mV and for NE is near 190 mV, which are both in agreement with previous work done in our group for this carbon fiber[33, 153].

2.2 Sham and DOCA-salt Rat Preparation and Surgery

All biological experiments were performed using male Sprague-Dawley rats, 250-275 g (Charles River Laboratories, MI). All protocols were approved by the Michigan State University Committee on Animal Use and Care. Rats were housed 2-3 per cage in a temperature- and humidity-controlled room. They were exposed to a daily 12-h light/dark cycle and given free access to standard laboratory rat chow (8640 Rodent

Diet; Harlan/Teklad) and water. Briefly, the rats were anesthetized and underwent a uninephrectomy to remove their left kidney. Sham animals were stitched up and placed back in their cages. DOCA-salt rats were prepared by implanting a DOCA-salt pellet subcutaneously, producing a dose of 200 mg/kg (body weight). Animals were allowed to recover for four weeks before experiments. At the time of experiment, the animals were euthanized with a lethal pentobarbital injection (100 mg/kg, i.p.) and the adrenal glands were removed through the abdomen via laparotomy. The gland was immediately placed into cold HEPES buffer for dissection. The adrenal medulla was dissociated, as more fully described in section 2.5, and single cells were deposited on to coverslips for microscopy or electrochemical investigation. The full surgical procedures and post-operative treatments have been described in detail elsewhere[34-35, 149].

2.3 Superoxide Measurements

For investigation into the affects of superoxide on adrenal chromaffin cell function, rats were prepared as described in section 2.2. Sham and DOCA-salt rats were split into two groups each. For Sham rats, one group received tap water supplemented with 2 mM apocynin and the other received only tap water. Apocynin inhibits the superoxide generating enzyme NADPH oxidase. The same protocol was implemented for DOCA-salt rats, where one group received high salt-water supplemented with 2 mM apocynin and the other was left on just high salt water. Treatment began two days following surgery and continued until sacrifice four weeks later. Blood pressures for rats were recorded the week of experiments.

2.4 Cell Isolation

For chromaffin cell isolation, coverslips that were to be used for cell plating were autoclaved. Autoclaved coverslips were placed in small petri dishes (3 coverslips per petri dish, 2 petri dishes total). Each petri dish was filled with 3 mL of poly-D-lysine for cell adhesion and placed under UV light for 10 min. After UV light exposure, the petri dishes were placed in an incubator set at 37 $^{\circ}$C with a 5% CO_2/O_2 atmosphere content for 30 min. The poly-D-lysine was then removed from the dishes and replaced with 3 mL of Locke's buffer (154 mM NaCl, 3.6 mM KCl, 5.6 mM $NaHCO_3$, 5.6 mM glucose, and 10 mM Hepes buffer, pH 7.2), which had been previously filtered through a Millipore disposable vacuum filtration system. The Locke's buffer was then swirled in the petri dishes for 2-3 min and then removed. Coverslips were covered and left at room temperature until the day of surgery. Coverslips were prepared in batches large enough for two weeks worth of cell isolations.

Male Sprague Dawley rats were anesthetized with 50 mg/kg pentobarbital. A laparotomy was used to gain entrance into the stomach cavity. Both adrenal glands were located and removed, and placed in an ice-cold Locke's buffer. The adrenal glands were then placed into a large dish and pinned in place inside a sylgard elastomer. The fat and connective tissue were then carefully removed. The cortex was carefully trimmed away to reveal the adrenal medulla. The adrenal medulla was then placed in a vial containing 6 mL Locke's buffer containing 12 mg collagenase type I and 24 mg Bovine Serum Albumin. Exposure to collagenase is a critical step in the cell culture procedure. Care must be taken to keep the exposure time and physical

agitation constant. This solution is then placed in a 37 °C water bath for approximately 29 min. After 10 and 24 min respectively, careful and gentle agitation was applied to the medulla through flame-etched glass pipettes. The medulla was gently moved in and out of the pipette in order to help break the tissue apart. After 29 min, the vial was centrifuged for 5 min at 120 g. The collagenase solution was then removed and replaced with warm (37 °C) Locke's buffer. The vial was placed back in the centrifuge for another 5 min at 120 g. This step was repeated a second time. After the second centrifuge in Locke's buffer, the solution was removed and replaced with warm (37 °C) Dulbecco's Modified Eagle Medium (DMEM) solution supplemented with 5% Fetal Bovine Serum, 50 IU/mL penicillin and 50 µg/mL streptomycin. The vial was then placed on a cyclone briefly to re-suspend the cells in solution. The cell suspension was transferred to a 1 mL plastic pipette. Two to three drops were placed on each coverslip, which was then placed back in the incubator for 30 min. After 30 min, the petri dishes were removed and filled with 3 mL of warm DMEM and placed back in the incubator for 2-3 h.

2.5 High Performance Liquid Chromatography

High performance liquid chromatography was used to determine catecholamine and metabolite levels from adrenal medulla isolated from Sham and DOCA-salt rats. After removing both adrenal glands from an animal, the adrenal medulla was isolated by carefully trimming away the cortex of the gland. The medulla was snap frozen at -80 °C until time for measurement (< 2 weeks). The frozen medulla (2 medulla were used for

each rat) were weighed and placed into 0.1 M perchloric acid. For both Sham and DOCA samples, the tissue was homogenized using an OMNI TH-01 homogenizer with a 5 mm blade. This was followed by centrifugation at 13,520 *g* for 10 min at 4 ^{o}C. The resulting supernatant was then collected and passed through a 30 kD filter and re-centrifuged. The centrifugate was analyzed immediately afterward by HPLC-EC (electrochemical detection) for catecholamine and metabolite levels. 10 µL of the supernatant was directly injected onto a reversed-phase column for separation using an autosampler. The analysis was accomplished using a commercial HPLC system (ESA Biosciences, Chelmsford, MA) that consisted of a solvent delivery module (model 584), an autosampler (model 542) with sample cooling to 4 $^{\circ}$C and a coulometric detector (Coulochem III). The detector was equipped with a 5021A conditioning cell (electrode I) and a 5011A high-sensitivity analytical cell (electrode II and III). An HR-80 (C18, 3 µm particle size, 80 mm length X 4.6 mm ID) reversed-phase column (ESA Biosciences) was used for the separation. The mobile phase was a commercial Cat-A-Phase II (ESA Biosciences) that consisted of a proprietary mixture of acetonitrile, methanol, phosphate buffer and an ion-pairing agent (pH 3.2). The separation was performed at 35 $^{\circ}$C using a mobile phase flow rate of 1.1 mL/min. Quantification was achieved using external standards and creating a calibration curve for analytes of interest. No internal standard was used due to the fact that there was no extraction performed on the medulla tissue. HPLC data are presented as the mass of the molecule detected (µg) normalized to the mass of the frozen adrenal medulla (g).

2.6 Microscopy

2.6.1 Dopamine-Beta-Hydroxylase and Vesicular Monoamine Transporter Staining

For all microscopy experiments, coverslips plated with isolated adrenal chromaffin cells were used as described in section 2.4. Initial work focused on verifying that the isolated cells were catecholamine-containing cells from the adrenal gland. Cover slips, plated with cells, were placed in staining trays containing 1 mL of phosphate buffered saline (PBS) to wash away cell culture media. The PBS was then immediately replaced with 1 mL of Zamboni fixative (15% picric acid, 5.5% formaldehyde, 79.5% PBS) and cells were fixed at room temperature for 20 min. The fixative was washed away with fresh PBS and was replaced with 300 μL of blocking serum (5% goat serum in 95% Triton PBS (1% Triton-X, 99% PBS)). Blocking serum was left for 1 h at room temperature with primary antibodies (1:200 dilution) raised against a rabbit polyclonal dopamine-β-hydroxylase (DβH, SC-15318, Santa Cruz Biotechnology) or a mouse monoclonal vesicular monoamine transporter (VMAT1, SC-166391, Santa Cruz Biotechnology). Cells were incubated with the primary antibody overnight at 4 °C. The following day, the cover slips were washed at 5 min intervals with PBS. Cells were then incubated with a secondary antibody for 1 h. The secondary antibody for DβH staining was goat anti-rabbit IgG conjugated to fluorescein isothiocyanate (FITC, Jackson ImmunoResearch, West Grove, PA) at a final dilution of 1:40 (v/v). Goat anti-mouse Cy3 (Cyanine Dye 3, Jackson ImmunoResearch, West Grove, PA) was used to localize VMAT1 at a final dilution of 1:200 (v/v). Cover slips were then washed at 5 min intervals, removed from the staining wells and placed on

glass slides. Images were obtained using laser scanning confocal microscope (TCS SL Leica Microsystems, Bannockburn, IL). The excitation wavelength for FITC was 488 nm and 550 nm for Cy3. Emission wavelengths for FITC and Cy3 are 525 nm and 568 nm, respectively. The fluorescence intensity was analyzed offline using Image-Pro Plus 2 software (Media Cybernetics, Inc. Bethesda, MD). Figure 2-4 shows confocal microscopic images of DβH (A) and VMAT (B) and as an overlaid image (C).

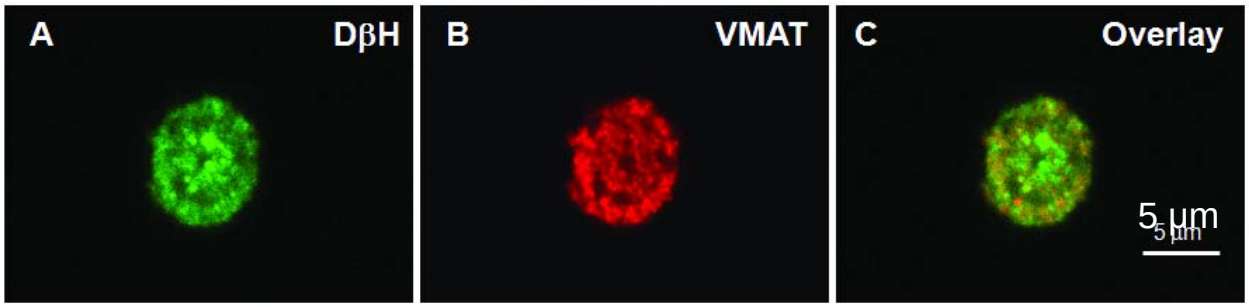

Figure 2-4. Fluorescence microscopy of isolated chromaffin cells. Dopamine beta-hydroxylase (DβH, A) and the vesicular monoamine transporter (VMAT, B) were stained for immunocytochemical imaging. DβH is the precursor for NE synthesis and VMAT is the transporter responsible for packaging catecholamines into chromaffin vesicles. An overlay of the DβH and VMAT staining is shown in C. The presence of DβH and VMAT in the isolated cells provides evidence that cells have machinery for catecholamine synthesis and packaging, suggesting they are adrenal chromaffin cells.

2.6.2 Calcium Imaging

Chromaffin cells were plated onto coverslips as previously described. After allowing cells to adhere for 2-h, coverslips were placed in a 35 mm petri dish containing 2 mL of OPTI-MEM 1 + GlutaMax-1 (Gibco 51985), 2 µL of fluo-4 AM (Invitrogen F14201) and 10 µL of Pluronic F-127 (Invitrogen P6866). Cells were incubated in the fluo-4 AM solution at 37 ^{o}C with 5% CO_2/O_2 for 30 min. After incubation, coverslips were placed into a flow bath mounted on a scanning laser confocal microscope, the same one used for the DβH and VMAT studies. HEPES buffer (150 mM NaCl, 5 mM

KCl, 2 mM $CaCl_2$, 1 mM $MgCl_2$, 10 mM Hepes and 12 mM Glucose) was flowed through the bath using an automated flow control.

To stimulate calcium flux into the cells, 1 mM acetylcholine (ACh) or 70 mM K^+, both in HEPES solution, were flowed through the bath. Fluo-4 AM fluorescence was captured at 488 nm using a "xyt" collection mode for 60 frames over a 4 min time span. After the first 5 frames, which were used as the background, ACh or K^+ were flowed through for 30-40 frames and then switched back to HEPES buffer to start washing out the stimulant. A fluorescence profile over time was created by normalizing the signal intensity to the first 5 frames of each experiment.

2.6.3. Dihydroethidium Staining

Dihydroethidium (DHE) was used to stain for super oxide (O_2^-). Similar to the other staining protocols, chromaffin cells were plated onto coverslips. Coverslips were placed into wells of a 24-well plate. Two coverslips from Sham and DOCA animal controls and two coverslips from a Sham/DOCA animals treated with apocynin were used for each experiment. All four wells were filled with 2.5 mL of Krebs-Ringer-Hepes (KRH) buffer (130 mM NaCl, 1.3 mM KCl, 2.2 mM $CaCl_2$, 1.2 mM $MgSO_4$, 1.2 mM KH_2PO_4, 1.0 mM HEPES, 0.09 mM Glucose). Two of the wells also contained 5 µL of DHE (10^{-3} M). 2 coverslips from the non-drug treated and treated animal were run in parallel. A cartoon depicting the set-up is shown below in Figure 2-5.

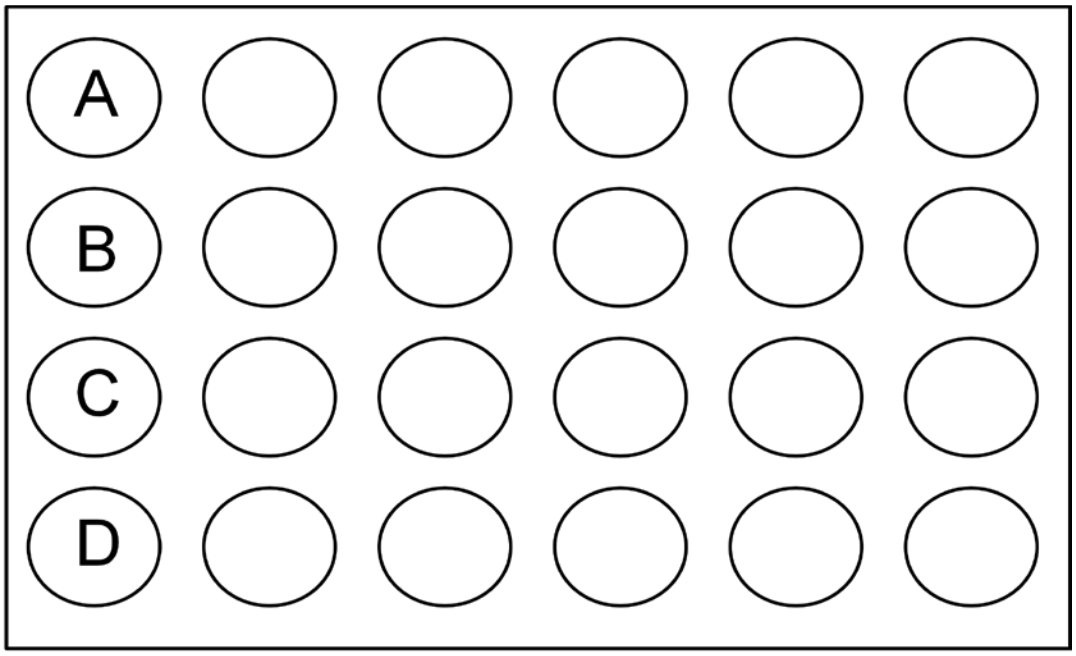

A = Sham/DOCA
B = Sham/DOCA with DHE
C = Sham/DOCA treated with apocynin
D = Sham/DOCA treated with apocynin with DHE

Figure 2-5. Dihydroethidium staining protocol. Coverslips with adhered chromaffin cells were placed into wells containing Krebs-Ringer-Hepes buffer (A & C) or buffer and the superoxide probe dihydroethidium (DHE) (B & D).

Coverslips were left in the wells containing KRH buffer (both non-DHE and DHE containing buffer) for 30 min at 37 ^{o}C and 5% CO_2/O_2. After incubation, the coverslips were mounted on microscope slides with a small drop of fluoromount G. Fluoromount G is used to reduce fluorochrome quenching during microscopy. Slides were placed under the same confocal microscope used for the other imaging studies. Images were taken for both non-apocynin treated and apocynin treated cells on the same day without changing any experimental conditions between the groups. This allowed for the normalization of the apocynin treated cells to the non-apocynin treated group.

2.7 *In Vitro* Electrochemical Measurements

2.7.1 Amperometry

All continuous amperometric experiments were set-up in the same general manner. To start, coverslips were placed in a homemade flow cell which had HEPES buffer (150 mM NaCl, 5 mM KCl, 2 mM $CaCl_2$, 1 mM $MgCl_2$, 10 mM HEPES and 12 mM Glucose) perfused through it. An Ag/AgCl (ESA Biosciences Inc, 66-EE009) reference electrode and a platinum wire counter electrode were placed inside the flow cell to complete the three-electrode circuit. Cells were found visually through an Olympus inverted microscope. After visual inspection to find a viable cell, a small glass capillary (containing a chemical stimulant), previously pulled on a capillary puller, and a carbon-fiber microelectrode were positioned for experimentation through the use of two micromanipulators[154]. The glass capillary was used as a delivery system for the stimulating drug, acetylcholine or high-potassium, using a pressurized N_2 burst that was controlled by external hardware (picospritzer II, General Wave Corporation). The capillary was positioned near the cell approximately 20-30 µm away. A pressurized pulse of nitrogen gas expels the stimulant onto the cell. This delivery system controlled the length of time and pressure used to apply the drug (hence the concentration or amount of drug delivered). The volume of stimulant was not determined; however a single capillary was used through a set of experiments to maintain consistency. The

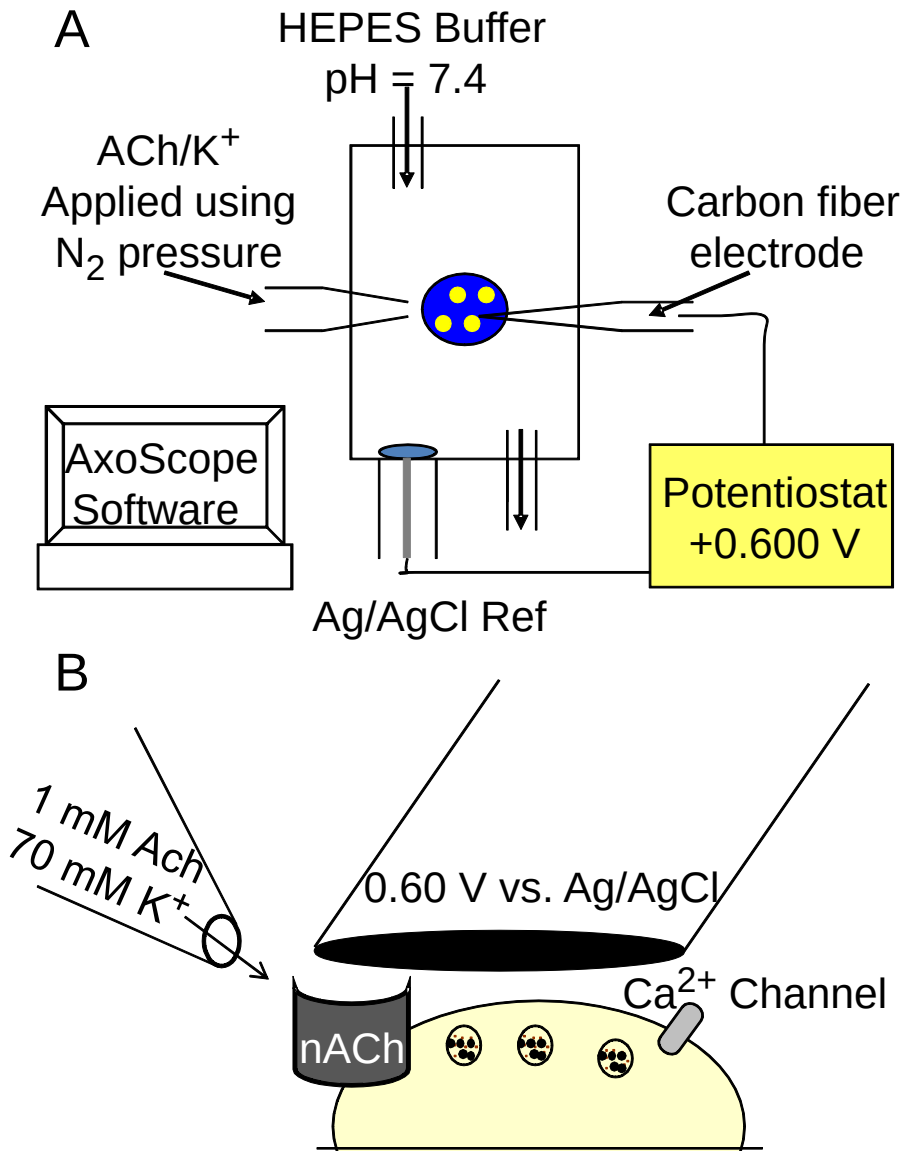

Figure 2-6. Cartoon depicting the electrochemical set-up for *in vitro* measurements. (A): Chromaffin cells are placed into a flow bath containing HEPES buffer (pH = 7.4). A carbon fiber electrode (0.600 V vs. Ag/AgCl) is placed in contact with a chromaffin cell and the electrical cell is completed using a platinum wire as the counter electrode and a Ag/AgCl reference electrode. Cell secretion is stimulated using acetylcholine or high potassium and secretion is monitored as an oxidation current offline via AxoScope software. (B): A magnified view of the electrode near a chromaffin cell. Acetylcholine or high potassium is delivered to the cell via a pressurized nitrogen burst.

recording microelectrode was connected to a potentiostat (Omni-90, Cypress Systems) poised at an anodic potential of 0.60 V versus the Ag/AgCl reference electrode. A 60 Hz filter was connected between the potentiostat and the DC amplifier in order to remove electrical noise. Data were presented on a Dell personal computer using Axoscope software. Figure 2-6 A shows a representation of the experimental set-up and Figure 2-6 B provides a zoomed in view near the cell.

The catecholamines released were measured as an oxidation current versus time. As catecholamines are secreted from the chromaffin cells, a resulting current "spike" occurs in the oxidation current-time profile. These spikes can yield a variety of information including the amount of catecholamines released per event and the kinetics of the release event. This information was used to determine if changes secretion occur in DOCA-salt hypertension. An example of the current spikes is found in Figure 2-7 along with the different criteria used for kinetic and quantal release assessment.

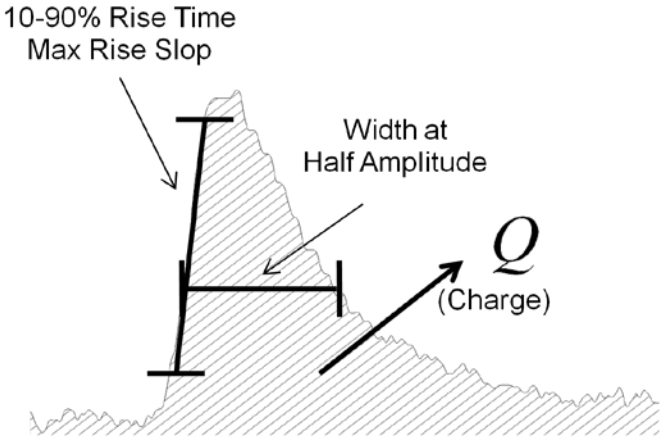

Figure 2-7. Individual current spike analysis representing an individual secretory event. The spikes were analyzed for the max rise slope and rise time between 10-90% of the generated oxidation current, half-width and quantal charge (Q).

2.7.1.1 Control Measurements and Initial Investigation of DOCA-salt hypertension

Initial measurements using chromaffin cells consisted of simply placing the electrode in contact with the cell, positioning the pulled capillary containing either ACh or K^+, and applying a 2 s burst of 1 mM ACh. In order to determine if the signal that was being detected was real, hexamethonium and calcium-free buffer were used as controls.

Hexamethonium is a nAChR antagonist. It works be binding to the nAChR, thus blocking ACh from activating the receptor[155]. Thus, in the presence of hexamethonium, secretion should be attenuated. Experiments were performed using Sham cells, in which a group of cells was stimulated with 1 mM ACh and another group was stimulated using 1 mM ACh in the presence of 100 µM hexamethonium. Calcium-free buffer was also used for initial control experiments. External calcium is needed for catecholamine secretion. Removing calcium from the physiological buffer should block any secretion that might occur from stimulation.

2.7.1.2 DOCA-salt Hypertension Affects on Adrenal Chromaffin Cell Secretion: Frequency and Kinetics

To probe how DOCA-salt hypertension affects the secretion patterns from adrenal chromaffin cells, continuous amperometry was used to monitor secretion evoked by 1 mM ACh or 70 mM K^+. Acetylcholine is the physiological stimulant released by pre-ganglionic sympathetic nerves innervating the adrenal medulla[59]. We

used this drug to initially investigate the differences between healthy control chromaffin cells and hypertensive cells. Differences found between Sham and DOCA cells could be attributed to altered catecholamine release or a change in the nAChR expression or activity. To rule out the latter possibility, high potassium was used to evoke catecholamine release. Potassium stimulates secretion by directly depolarizing the cell without the use of the nAChR[58].

2.7.1.3 Potassium Channel Function

After a cell undergoes depolarization and begins to secrete catecholamines, potassium channels are responsible for re-setting the membrane potential[156]. This process repolarizes the cell and effectively shuts-down secretion. For the potassium channel studies, we used paxilline (BK channel blocker, 0.5 μM)[95], 4-aminopyridine (voltage-gated K^+ channel blocker, 1 mM)[97], apamin (SK channel blocker, 0.1 μM)[96], glibenclamide (ATP-sensitive K^+ channel blocker, 50 μM)[94] and NS 1619 (BK channel activator, 100 nM). The effects of the K^+ channel agonist and antagonists were evaluated by measuring the S2/S1 ratio for which S2 is the oxidation current evoked by the second ACh application in the presence of the drug relative to S1 which is the oxidation current measured initially in the absence of drug. In each experiment, after the initial recording (S1), a potassium channel drug would be applied through the flow bath for 20 min. Following the 20 min application, a second recording was performed to analyze receptor function in the presence on an antagonist.

2.7.1.4 Reactive Oxygen Species Effects on Chromaffin Cell Secretion

Previous work by our group showed that reactive oxygen species (ROS) are involved in the impairment of auto-receptors located on sympathetic nerves innervating mesenteric smooth muscle cells[36]. Since adrenal chromaffin cells are heavily innervated by sympathetic neurons, it is possible their function is also impaired by reactive oxygen species. Methods for how the apocynin was administered to the animal and surgical preparations can be found in sections 2.2 and 2.3, respectively. An apocynin treated and non-apocynin treated animal were sacrificed in pairs. This resulted in two Sham or DOCA animals, a non-treated and treated rat, being sacrificed on the same day. The animals were randomized so that on half the days a control animal was sacrificed and tested first, and on the other half an apocynin-treated animal was sacrificed and tested. This served to remove experimental bias form the results. After the cells were plated onto their coverslips and allowed time to adhere, coverslips were placed in the flow bath and set-up in a similar manner to the initial investigation of chromaffin cells outlined in 2.7. Four cells were investigated for each animal using 1 mM ACh, with a carbon-fiber electrode being used for each new animal.

2.7.2 Fast-Scan Voltammetry

FSCV was used to expand our findings from the amperometric studies. Specifically, the method was used to determine if the NE/EPI secretion ratio was altered in DOCA-salt Amperometry is a fantastic tool for investigating temporal and quantal changes in secretion between Sham and DOCA cells. However, amperometry provides little specificity, as all molecules that are oxidizable at the applied potential will

contribute to the detected current. As mentioned, the applied potential used for our amperometric studies was 0.600 V vs. Ag/AgCl. At this potential, the quinone on both NE and EPI (molecules shown in Figure 2-8 A & B) can be oxidized in a two-electron reaction. Only EPI (Figure 2-8 A) has a secondary amine structure that is oxidized around 1.425 V vs. Ag/AgCl[121]. NE is not oxidizable at this potential.

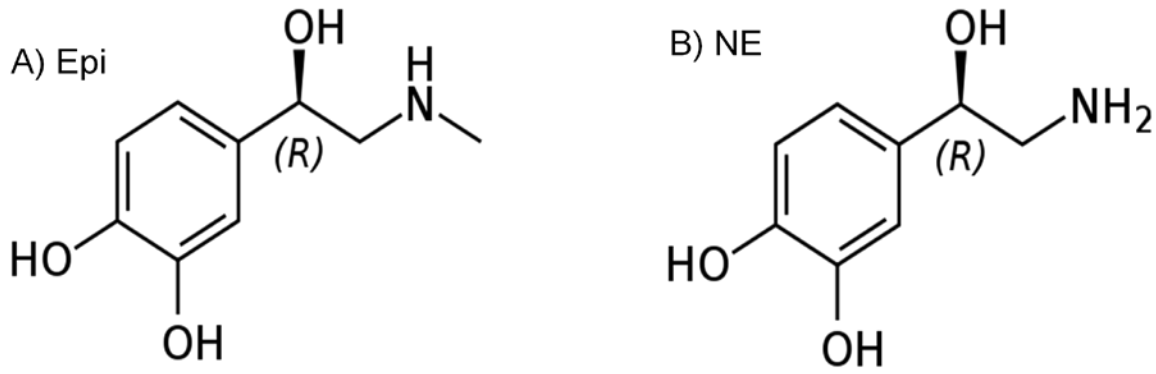

Figure 2-8. Molecular structure of epinephrine and norepinephrine. Both EPI and NE contain a quinone group which is oxidizable near 0.600 V vs. Ag/AgCl under fast-scan voltammetry conditions. Only EPI contains a secondary amine which is oxidizable at higher potentials near 1.425 V vs. Ag/AgCl.

Electrodes were prepared for FSCV as detailed in section 3.2.1. Cover slips with plated cells were placed in a flow cell containing Tris-HCl buffer (150 mM NaCl, 4.2 mM KCl, 2 mM $CaCl_2$, 0.7 mM $MgCl_2$, 50 mM Tris-HCl and 11.2 mM glucose) flowing at 2-3 mL/min. The flow cell was positioned on the stage of an inverted microscope for monitoring the electrode positioning. High K^+ (70 mM) was used to evoke catecholamine release via a pressurized burst of N_2 gas for 2 s (Picospritzer II, General Wave Corporation). Catecholamine secretion was recorded using a computer running

TH-1 FSCV software (ESA Inc). FSCV was run at 600 V/s from 0.1 V – 1.5 V vs. Ag/AgCl at a frequency of 60 Hz for a total time of 30 s. The signal was filtered through a two-pole Bessel filter at 2 kHz.

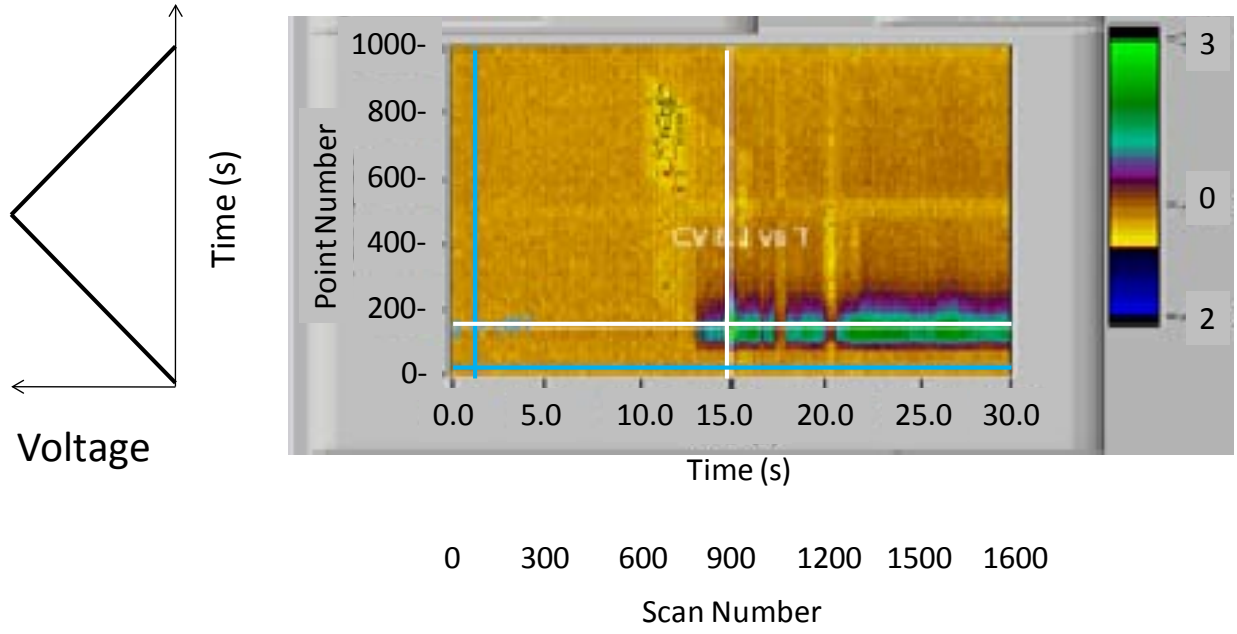

Figure 2-9. 3D color-plot obtained via TH-1 software. Current-time traces and individual cyclic voltammograms are obtained by selecting a potential (y-axis) and scan number (x-axis) of interest (white cursor). Next, a background potential and cyclic voltammogram are selected (blue cursor) to be subtracted from your signal of interest. The software generates current-time traces for an individual potential and cyclic voltammograms for a given scan number.

The TH-1 software creates current-time (i-t) traces for a particular potential, along with the ability to select cyclic voltammograms (CVs) for a given time point. These data are generated in a separate panel of the software in their background subtracted form. Background subtraction is achieved by manually selecting a cyclic voltammogram (or range) and potential within the 3D color-plot created after the completion of an experimental run (Fig. 2-9). The background selected must be at a time point before

cell stimulation and catecholamine secretion. By doing this, all the voltammograms at a given potential (i.e. – 0.600 V vs. Ag/AgCl) will be normalized to the control signal, which leaves the user with an i-t trace that is due to oxidation of the quinone on catecholamines. Individual voltammograms can then be selected from the 3D color plot and used to identify an event as either NE or EPI. Manually selecting the background introduces bias, because the point selected as the background can influence the amplitude of the signal generated thus leading to mislabeling current signals as NE or EPI.

To remove this bias, an average i-t trace was created for the quinone and amine peaks. The quinone i-t trace was generated by taking the average of i-t traces between 600 ± 50 mV, and the amine i-t trace was generated using the average between 1425 ± 25 mV. These averages were put through a MatLab peak finding algorithm. The algorithm converted the data into the second derivative of the input signal. In the second derivative form, the signal will have a value of zero when the slope of the first derivative (original data) is zero (Figure 2-10). Peaks are selected if the second derivative signal has a slope of 0.03 for 5 consecutive data points and then the time point where the second derivative crosses the y-axis at zero is marked as an oxidation event.

If peaks were observed at the same time point for both the 600 and 1425 mV average these peaks were identified as EPI, if peaks were only observed at 600 mV

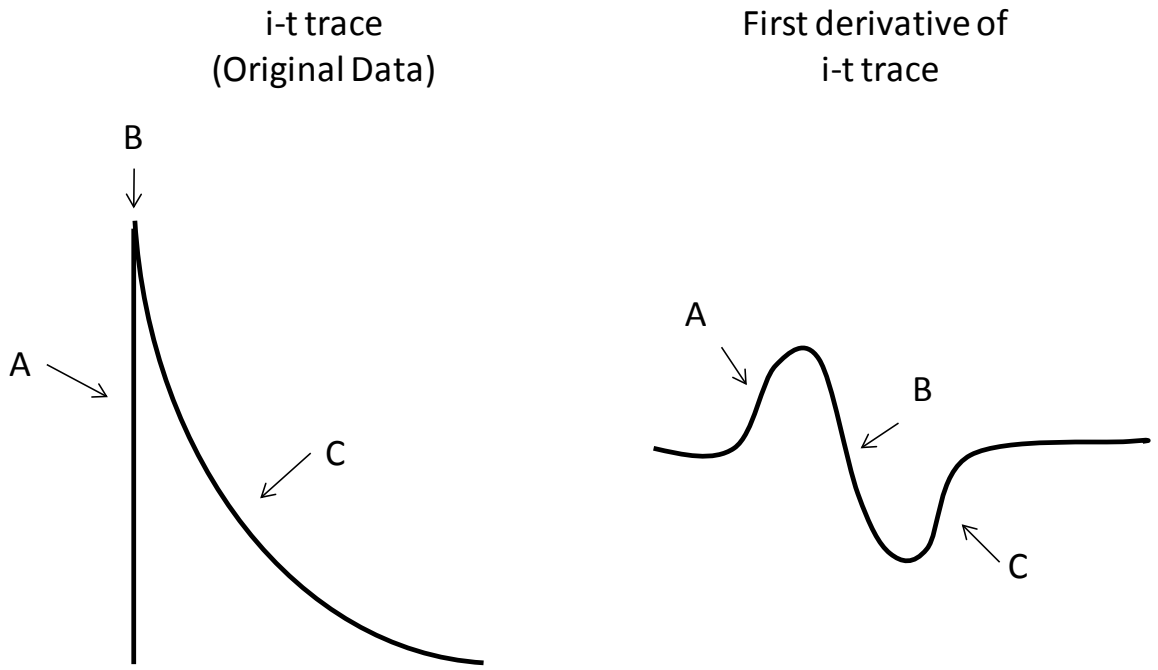

Figure 2-10. Data treatment for MatLab identification of individual peaks. Current-time traces generated from FSCV experiments contain peaks associated with vesicular secretion. Within individual peaks there is a rising (A), peak (B) and falling (C) part. For peak identification, a MatLab algorithm converts the current-time signal into its second derivative that still contains the original rising (A), peak (B) and falling (C) part of the oxidation spike. In the second derivative the current initially increases along the rising part of the spike (A) and then crosses the zero line at the oxidation peak (B). By setting a minimum slope for the rising part of the second derivative, peaks can be discriminated and identified at points where the second derivative crosses the zero line.

then they were identified as NE. Using the TH-1 software, we validated the MatLab analysis using voltammograms to identify peaks as either NE or EPI for several randomly selected cells.

2.8 Statistical Analysis

HPLC data are reported as a mean ± S.E.M. with "n" values indicating the number of animals used for the study. Amperometric recordings were made at a sampling rate of 10 kHz and filtered using a low-pass Gaussian filter with a 1 kHz time

constant. Individual oxidation currents (spikes) were analyzed using a threshold event detection routine. A threshold limit of twice the background current was used as an event discriminator. Spikes were not used in the analysis if there was any evidence of superimposed events, the current did not return to baseline, the signal was twice the background signal and only positive deflecting spikes were investigated. The quantitative and kinetic parameters analyzed for each spike were the total charge (Q), the full width at half maximum ($t_{1/2}$), the rise time (10-90%) and the number of exocytotic events. Data are reported as a mean ± S.E.M. with "n" indicating the number of cells or the number of individual release events from a cell. Statistical differences between groups were determined using a Student's t-test for paired or unpaired data as appropriate. One-way analysis of variance and Dunnett's multiple comparison tests were used to analyze data from the K^+ channel antagonist studies. A Chi^2-test of association was used to determine any changes in NE and EPI release in the FSCV studies. A one-way ANOVA followed by a Tukey's honestly significant difference test and Kruskal-Wallis followed by Dunn's test was used to analyze the water intake for Sham and DOCA animals respectively. A student's *t* test was used for interpretation of the frequency, kinetic and microscopy data for the reactive oxygen species work. Differences were considered significant when $p<0.05$.

Chapter 3

Carbon Fiber Microelectrode Fabrication and Characterization for In Vitro Electrochemical Measurements

3.1 Introduction

Electrochemical methods, such as amperometry and voltammetry, have been used over many decades for the *in vitro* and *in vivo* investigation of neurotransmitter release. A number of neurotransmitters are electrochemically active, including NE and EPI, meaning that they can be detected as an oxidation current at an appropriate recording electrode[40-41, 51-52, 126, 130, 157]. Two electrode materials commonly used for these measurements are carbon fiber and BDD. Both electrodes are responsive to catecholamine oxidation; however, each offers unique advantages and disadvantages.

Carbon fiber microelectrodes provide superb sensitivity for catecholamine oxidation as well as good spatial and temporal resolution in measurements because of the micrometer dimensions. The sensitivity arises, in part, from catecholamine adsorption onto the carbon fiber surface. Adsorbed catecholamines self-catalyze the oxidation of diffusing catecholamines[138]. This process is shown in Figure 3-1. When used in tissue or other complex environments, carbon fiber microelectrodes often have limited response stability due to strong molecular adsorption by matrix components or by biomolecules or reaction products. Generally speaking, they are not re-usable

without some kind of surface reconditioning[158]. Depending on the microelectrode geometry, easy surface pretreatment may not be possible (i.e., microcylinder).

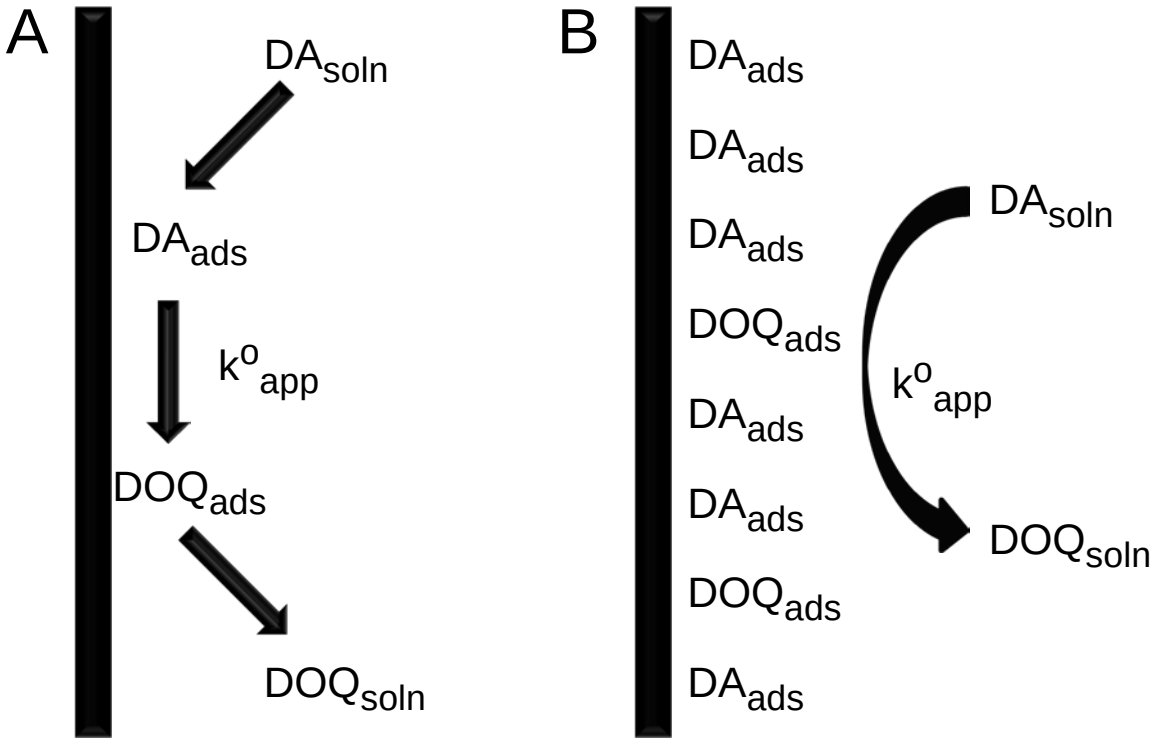

Figure 3-1. Mechanism of catecholamine oxidation at a graphitic carbon electrode. Catecholamines diffuse to and adsorb onto the electrode surface (A). Catecholamines in the solution transfer electrons to the electrode surface through the adsorbed catecholamines (B). Adapted with permission from *Self-catalysis by catechols and quinones during heterogeneous electron transfer at carbon electrodes*. Copyright (2000) Journal of the American Chemical Society.

Carbon fiber microelectrodes have been utilized in the peripheral nervous system to measure sympathetic neuroeffector transmission at the adventitial surface of mesenteric arteries and veins and rat tail arteries[33, 37, 120, 123, 153, 159-160]. A microcylinder geometry is used in these measurements. This architecture is useful for measuring local changes in NE concentration, by release from innervating sympathetic nerves, at the blood vessel surface. For single cell measurements, a disk-shape

geometry is more appropriate to decrease the background current arising from the "extra" electrode area. The fabrication of carbon fiber microdisk electrodes has been described previously by other groups[40-41, 121, 161-162]. In this chapter, a protocol is described for preparing carbon fiber microdisk electrodes for use in catecholamine secretion measurements from single chromaffin cells isolated in culture.

One drawback of carbon fibers is their susceptibility to undesirable molecular adsorption (*i.e*., fouling). Undesirable adsorption makes the electrode material susceptible to biofouling during *in vitro* electrochemical measurements. One electrode material that is significantly more resistant to adsorption/fouling is BDD. BDD microelectrodes are formed by depositing films onto a metal wire substrate[35, 125-126, 163]. Diamond electrodes offer exceptional microstructural stability over a wide range of potentials, are electrically conductive and exhibit a low background current[141]. Furthermore, molecular adsorption, particularly polar molecules, is generally weak on the hydrogen-terminated diamond surface. Compared to carbon fibers, diamond generally offers improvements in response reproducibility, limit of detection and response stability. The electron-transfer kinetics for a number of redox systems is similar for diamond and activated carbon fiber microelectrodes. However, the kinetics for NE and EPI oxidation are more sluggish on diamond than on carbon fibers[33]. While conical-shaped diamond microelectrodes have been utilized to measure sympathetic neuroeffector transmission at arteries and veins[35, 126], it is difficult to fabricate diamond

electrodes into the disk geometry needed for single cell measurements. Another drawback to using diamond electrodes is the time required for film deposition and microelectrode preparation. The lengthy deposition time is due to the relatively low initial nucleation density that exists on non-diamond substrates. Substrate surfaces are typically seeded with nanodiamond particles to increase the initial nucleation density. When coating some metal substrates, like Pt wires, achieving a high nucleation density buy ultrasonic seeding can be a challenge. Another option for increasing the initial nucleation density is to deposit a thin film of amorphous carbon prior to seeding the surface with naonometer-sized particles of diamond. This method is known as the "Rotter" method. This method promotes a more uniform diamond coating than just directly seeding the platinum wire itself[164]. By applying the Rotter method, it was hypothesized that our group's established diamond electrode fabrication process[145] could be accomplished faster while retaining the ability to readily detect catecholamines.

This chapter describes the fabrication and characterization of carbon fiber and BDD microelectrodes used in this research. The electrodes were characterized using electrochemistry, Raman spectroscopy and scanning electron microscopy.

3.2 Protocols

3.2.1 Carbon Fiber Disk-Shaped Electrode Fabrication

Recording microelectrodes were constructed according to the protocol described by Wightman *et al.*[161] The protocol is outlined in Figure 3-2. A carbon fiber (T-650

CYTEC Industries) is inserted into a single barrel borosilicate glass capillary (1.2 mm o.d., 0.68 mm i.d., 10.2 cm length). The capillary was filled with acetone prior to fiber insertion in order to decrease static forces. A carbon fiber was inserted into the capillary using forceps. After insertion, the bottom of the capillary was touched gently against a Kimwipe to remove any residual acetone. The capillary was then placed into a capillary puller (P-30 Sutter Instruments) so that the center of the capillary was inside the heating coil. The heat and pull forces were both set to a value of 980 and the trip

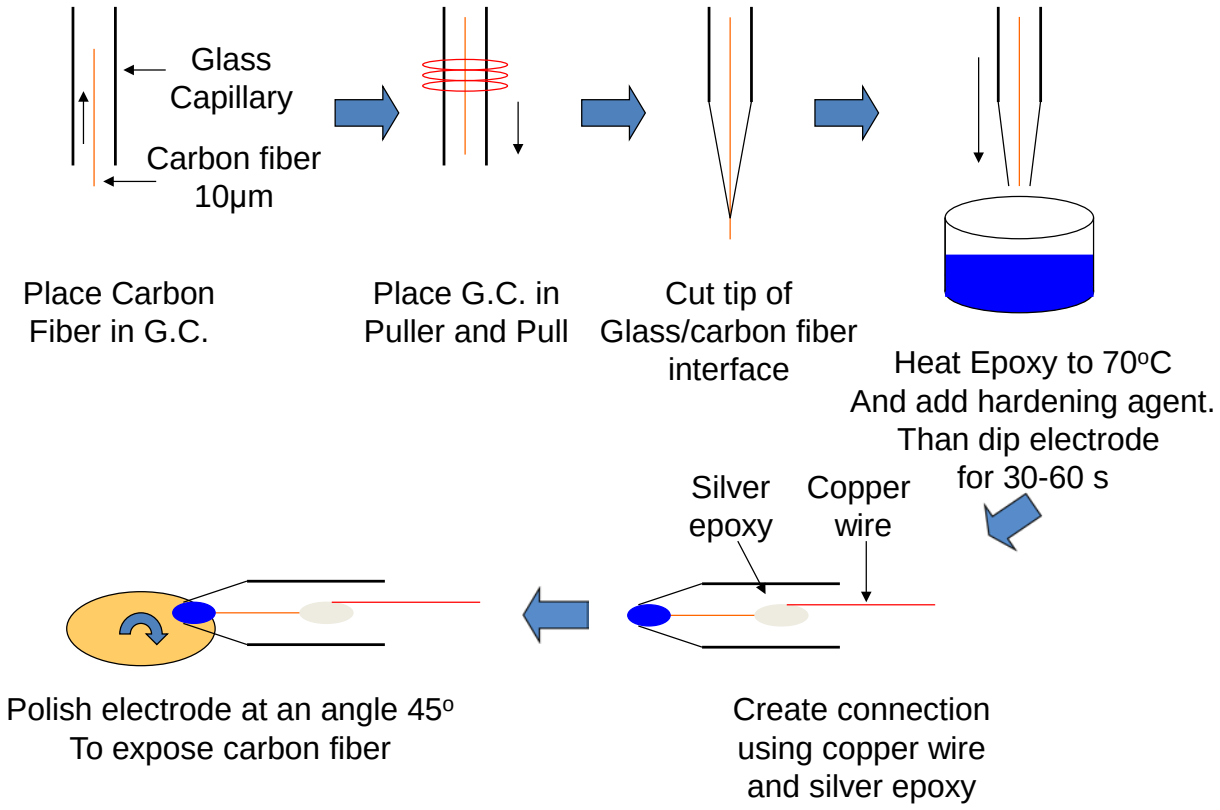

Figure 3-2. Schematic depiction of the basic steps in the fabrication of carbon fiber disk microelectrodes. Carbon fibers are placed inside glass capillaries and then put into a capillary puller. After drawing the glass down to make a seal with the fiber, the tip is trimmed slightly and the capillary is placed (tip-first) into a heated epoxy resin briefly. Capillaries are cured and electrical connection is accomplished via a copper wire with a

small amount of silver epoxy. Finally, electrodes are polished using a diamond wheel to produce disk-shape at the surface.

point for the solenoid was set to 4.25 μm. The capillary was pulled and the exposed carbon fiber was trimmed with a pair of fine scissors before removal from the puller. The electrodes were then placed under a stereomicroscope, and the tip was cut flush with the capillary using a pair of fine scissors. Next, an epoxy resin (Epon 828) was heated to 70 °C and mixed with 14% (w/w) of the hardening agent, *m*-phenylenediamine. The electrode was dipped into the mixture for approximately 30-60 s in order to allow for the heated epoxy to fill the capillary tip via capillary forces. The epoxy-filled capillary was placed horizontally into a homemade holder and allowed to sit/cure overnight. The electrode then received a final heat treatment at 80 °C for 2 h. Electrodes prepared in this manner were ideal for continuous amperometric measurements.

The protocol for making electrodes used in fast-scan cyclic voltammetry was slightly different. Instead of curing for 2 h, electrodes were initially exposed to an 8 h cure at 100 °C. Without removing the electrodes, the temperature was increased to 150 °C and applied overnight. This extra curing time is crucial for fully curing the epoxy and minimizing carbon electrode corrosion/degradation during the potential excursions required for the voltammetric measurements.

Following curing, a copper wire containing silver epoxy on the tip was gently inserted into the back end of the capillary until the copper wire attached to the carbon

fiber. This creates an electrical contact point for electrochemical experiments. The back end of the capillary was then filled with superglue epoxy to impart some mechanical stability to the wire. The electrode was then placed in a holder at a 45° angle for polishing on a diamond polishing plate (104 C or D, Sutter Instruments) for 5 min. Next, the electrode received a second polishing in 3 μm diameter alumina slurry for 3 min. The polishing procedure produces electrodes with similar areas, providing higher response reproducibility between batches. Next, electrodes were immersed in deionized water and ultrasonicated for 20 min to remove polishing debris. Following sonication, electrodes were briefly polarized in order to create a disorganized electrode surface that is consistent from one electrode to another[165]. The polarization protocol I used was to cycle each electrode from -0.4 – 1.3 V (vs. Ag/AgCl) in phosphate buffer (pH = 7.2) for approximately 1 min at a scan rate of 5 V/s. Following polarization electrodes were tested in a solution of potassium ferrocyanide or norepinephrine. The theoretical area of each electrode fabricated using this method should be that of an elliptical disk, which is shown in Equation 3-1.

$$A = \pi ab$$

Equation 3-2

where the area A is equal to pi π, multiplied by the radius of the minor length a and the major length b. When polished at a 45° angle, the major length should be 1.41 times longer than the minor length which was found using Equation 3-2:

$$Length = \frac{r_m}{\cos(45)}$$

Equation 3-2

Therefore, for a carbon fiber electrode with a diameter of 6.8 μm, the expected minor length would be 3.4 μm and the major length would be 4.8 μm. Plugging this into Equation 3-1 yields an ideal value of 5.1 x 10^{-11} μm^2. This value was used to calculate the theoretical limiting current expected in a voltammetric measurement for a know redox system. Using the steady-state current equation (Equation 3-3),

$$i_{ss} = \frac{4nFAD_o C_o^*}{\pi r_o}$$

Equation 3-3

one can calculate the limiting current. In this equation F is Faraday's constant, n is the number of electrons transferred in the oxidation/reduction reaction for a given molecule, A is the electrode area, D is the diffusion coefficient, C is the concentration and r is the electrode radius (radius units are cm^2). When NE was measured using cyclic voltammetry at a concentration of 100 μM, a carbon fiber radius of 3.4 μm (T-650 carbon fiber, Cytec) and a scan rate of 100 mV/s, one obtains a value of 2.8 x 10^{-10} A for the theoretical current. Microelectrodes exhibiting a limiting current close to this value were judged to be ideal for biological measurements.

3.2.2 Boron-Doped Diamond Deposition

Platinum wires (76 μm diameter, Sigma Aldrich) were cut into 1.3 cm lengths. Each wire was then electrochemically etched in 1 M KOH to form a conically-shaped tip. The etching was performed by lowering the end of a wire into the KOH solution and applying a 12 V AC relative to four carbon counter electrodes positioned equidistant from the Pt wire. The voltage was applied using a variable autotransformer (Staco Energy Products, Dayton, OH). The wire was etched until visible bubble evolution ceased (ca. 30 s). This process was then applied to the other end of the wire. The sharpened wires were then ultrasonically cleaned in clean acetone for 30 min while suspended vertically in the solvent in order to avoid tip damage[126, 145, 153, 163]. The clean wires were then positioned horizontally on the reactor stage of a microwave CVD system (1.5 kW, formally AsTex Inc., now Seki Technotron, Japan). The wires were then exposed to a 2% CH_4/H_2 source gas mixture (4 sccm CH_4 and 196 sccm H_2) for 30 min at 600 W and 45 Torr. The total gas flow was 200 sccm. At the end of this period, the plasma was extinguished and the wires were cooled to room temperature under reduced pressure with the plasma extinguished (*i.e.*, no cool down in atomic hydrogen). The wires were then removed from the reactor and each was seeded with nanoscale diamond particles by ultrasonication in a diamond powder (3–6 nm diameter, Nanostructured and Amorphous Materials Inc., Los Alamos, NM)/ethanol suspension for 30 min. Each wire was suspended vertically during the seeding to avoid damage to the tip ends. This process embeds diamond particles into the relatively soft amorphous carbon layer and these particles, as well as sites on the carbon layer itself, serve as the initial nucleation zones for ultra-nano crystalline diamond growth (see Fig. 3-3).

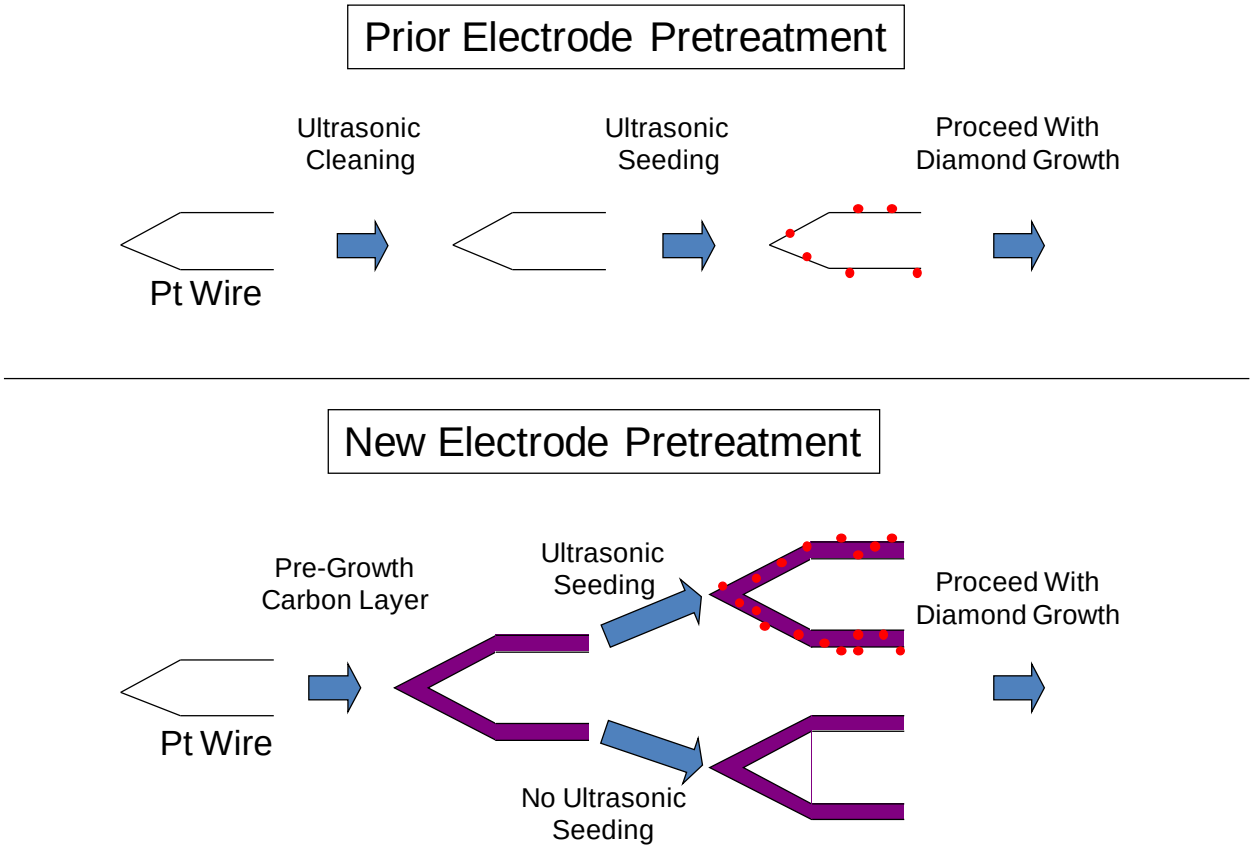

Figure 3-3. Diagrams illustrating the steps involved in conventionally (top) seeding the Pt wires for diamond growth and the steps associated with the NNP treatment.

The seeded wires were then placed back into the CVD reactor, mounted horizontally on the quartz stage and coated with boron-doped microcrystalline diamond. The diamond film was deposited from a 0.5% CH_4/H_2 source gas mixture with B_2H_6 added for boron-doping. The total gas flow was 200 sccm (197 sccm H_2, 1 sccm CH_4, and 2 sccm B_2H_6). The microwave power and system pressure were 600 watts and 45 Torr, respectively. To study the effect of deposition time on the film properties, the wires were coated over the pre-growth carbon layer for 2, 4 and 6 h periods. At the end

of the deposition period, the CH_4 and B_2H_6 gas flows were stopped and the wires remained exposed to H_2 plasma. Over a 30 min period, the plasma power and pressure were slowly reduced to cool the films to a temperature below ca. 400 °C in the presence of atomic hydrogen. The wires were then cooled to room temperature under reduced pressure prior to removal from the deposition chamber.

3.3 Results

3.3.1. Carbon Fiber and Diamond Film Evaluation by Raman Spectroscopy

Two types of pan-based carbon fibers were used in our studies, T-650 and P-55 (CYTEC Industries), to determine the ideal fiber for catecholamine measurements. Generally speaking, the more microstructurally disordered the carbon fiber is, the greater the molecular adsorption will be (*e.g.*, catecholamines), and the greater the oxidation current response will be for a given analyte concentration in solution. To determine the fiber type best for the single cell measurements, Raman spectroscopy was used to assess the microstructure. Figure 3-4 shows spectra for a P-55 (A) and a T-650 (B) carbon fiber. Each spectrum consists of two peaks near 1360 cm^{-1} and 1582 cm^{-1}. The 1360 cm^{-1} peak (D peak) is due to a breakdown in symmetry in the graphite lattice that produces scattering along the graphene edge plane sites, whereas the 1582 cm^{-1} peak (G peak) is attributed to the E_{2g} phonon peak associated with the graphite lattice[133]. For the P-55 fiber, the D peak has a much lower intensity than the G peak[140]. The D/G ratio for the P-55 fiber as seen in Figure 3-4 is 0.46. The ratio of the

D and G peak intensities can provide insight into the organization of the fiber microstructure[133, 140]. An increase in the D peak intensity is reflective of an increase in the amount of "microstructurally disordered" carbon in the fiber l and a decrease in the nominal crystallite size. The higher D/G intensity ratio for the P-55 fiber suggests that this fiber has a more disordered microstructure with a relatively high fraction of edge plane exposed. The T-650 fiber, which has a D/G ratio of 0.97, is more microstructurally ordered. The T-650 spectrum also shows a broadening of the G peak, which is found as disorder in the graphite lattice increases[140]. Based on the higher D/G ratio, the T-650 fibers were selected for use in the single cell electrochemical measurements.

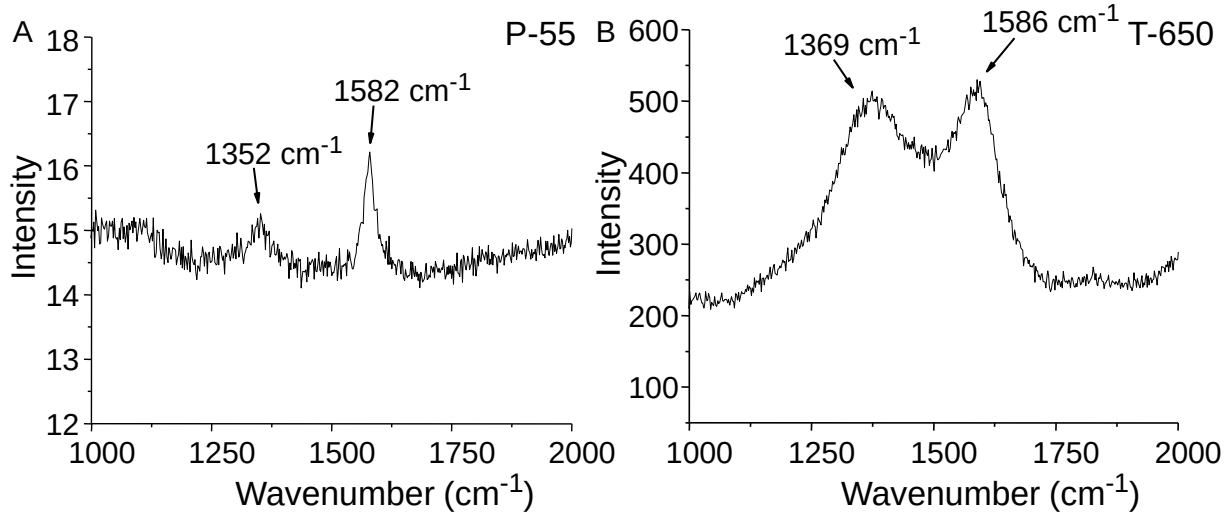

Figure 3-4. Raman spectra for P-55 and T-650 carbon fibers. Spectra were obtained using a 50-mW Nd:YAG laser (532 nm line) at 150 kW/cm^2 and an integration time of 10 s.

Figure 3-5 A-D shows Raman spectra for the pre-growth carbon layer as well as for diamond films deposited over the pre-growth layer for 2, 4 and 6h periods. The

spectrum for the pre-growth layer looks like that typically seen for ultrananocrystalline diamond deposited from Ar-rich source gas mixture (Fig. 3-5 A)[166-171]. There are four peaks, a relatively weak one at 1193 cm^{-1}, a strong one at 1333 cm^{-1} and moderately intense ones at 1493 and 1570 cm^{-1}. The peak at 1333 cm^{-1} is ascribed to the first-order phonon for cubic diamond. The full width at half maximum (FWHM) of this peak is 137 cm^{-1}. The large FWHM, compared to 2-4 cm^{-1} seen for single crystal diamond, indicates that carbon layer is nanocrystalline in morphology with a large number of phonon scattering centers, such as grain boundaries. This is completely consistent with the nanocrystalline morphology revealed in the SEM images (section 3.3.2). The peak at 1570 cm^{-1} is ascribed to the G-band well known for sp^2-bonded carbon. This peak arises from the in-plane stretching modes of the sp^2-bonded carbon in the grain boundaries of the nanocrystalline diamond that comprise the pre-growth carbon layer. The peaks at 1193 cm^{-1} and 1493 cm^{-1} are attributable to C-H bonds of the sp^2-bonded carbon domains[166-170, 172]. Birrell *et al.* showed that the intensity of these peaks correlates with the amounts of hydrogen used during the growth[168]. Furthermore, they showed that these peaks are absent in the spectrum using UV-Raman. The reduction in peak intensity with decreasing excitation wavelength is consistent with the assignment of these peaks to sp^2 carbon, although the exact nature of these bonds is yet unknown. Clearly, the pre-growth carbon layer is composed of small grains of diamond with a high volume of grain boundaries. The grain boundaries are composed

of sp^2-bonded carbon. Additionally, the presence of the 1570 cm^{-1} is consistent with the presence of a more amorphous sp^2-bonded carbon layer at the interface between the Pt and the diamond nanocrystallites. For these reasons, the visible Raman spectrum is dominated by the scattering of the sp^2-bonded carbon as the scattering cross section is 50x greater for sp^2 than for sp^3-bonded carbon[173-174].

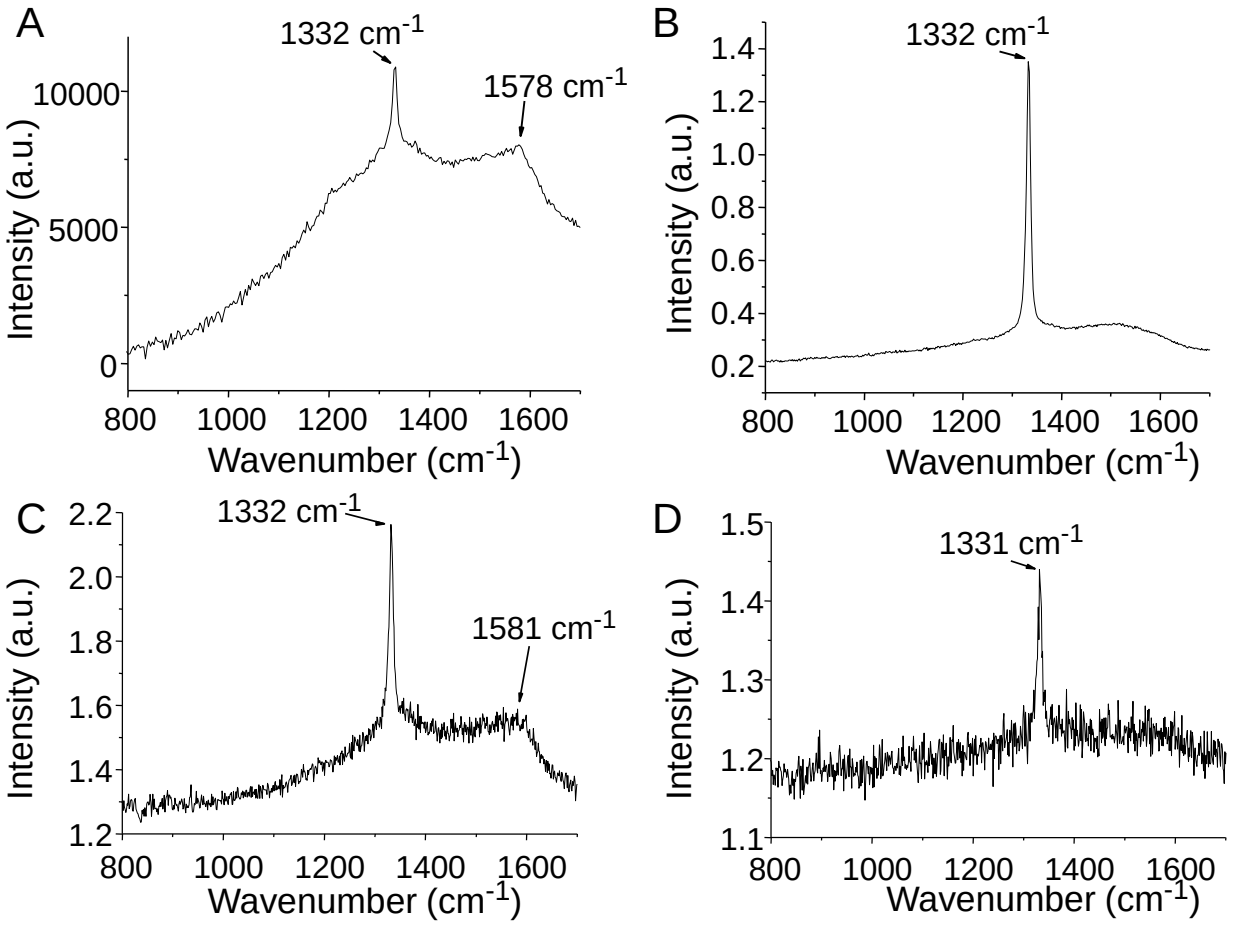

Figure 3-5. Raman spectra of the NNP layer (A) and BDD films deposited for 2, 4 and 6 h (B-D) on the NNP layer. Spectra were obtained using a 50-mW Nd:YAG laser (532 nm line) at 150 kW/cm^2 and an integration time of 10 s.

Spectra for the diamond films grown over the pre-growth layer are shown in Fig. 3-5 B-D. These spectra were recorded using a different integration time and spot size than were used to record Fig. 3-5 A so direct comparison to the spectral intensities is not possible. The spectra are all similarly shaped with an intense peak at 1333 cm^{-1} and a weaker but broad peak at 1560 cm^{-1}. The intensity of the diamond phonon peak (1333 cm^{-1}) relative to the intensity of the sp^2-bonded carbon peak (1560 cm^{-1}) increases with the deposition time. This is due to a thicker film with a larger crystallite size that results with increasing deposition time.

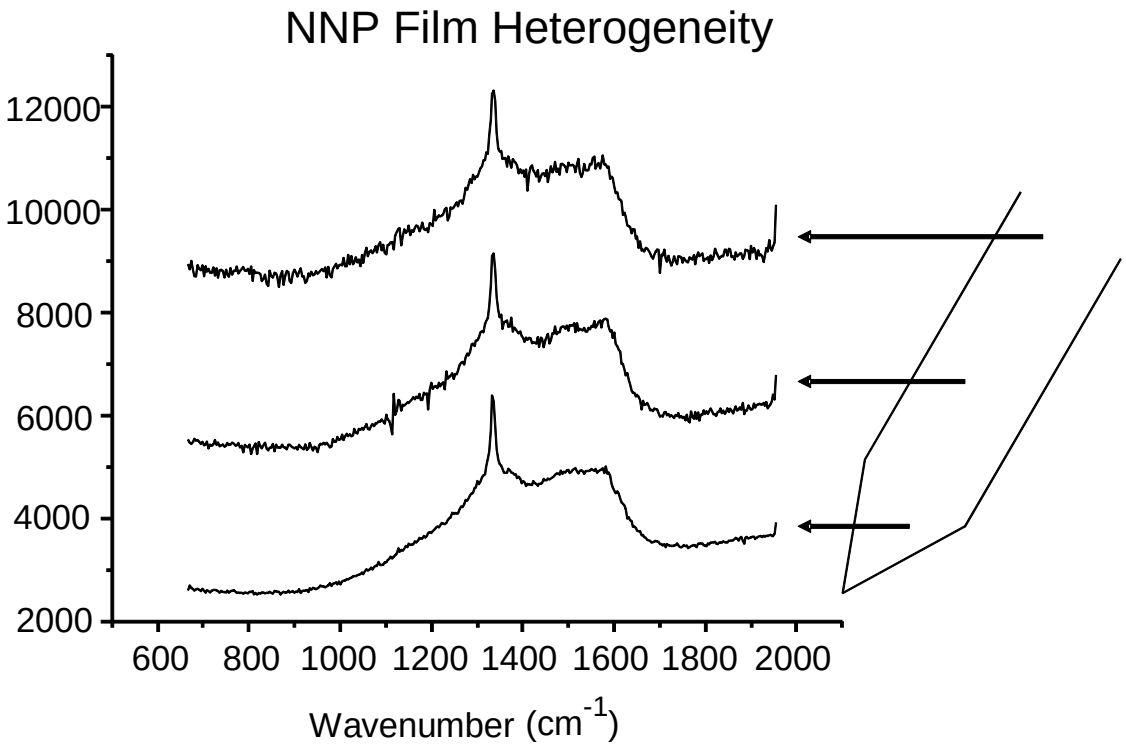

Figure 3-6. Visible Raman spectra recorded at different points along a sharpened Pt wire coated with the pre-growth carbon layer.

Figure 3-6 shows a series of Raman spectra recorded along the length of a wire coated only with the pre-growth carbon layer. The spectra are quite similar in shape at the different wire positions. This suggests that the microstructure of the pre-growth carbon layer is uniform along the length of the wire. The intense diamond phonon peak is seen at 1332 cm^{-1} along with the broad scattering intensity in the 1500-1580 cm^{-1} region due to the sp^2-bonded carbon that exists at the grain boundaries and the interface between the Pt and the diamond nanocrystals. The 1190 and 1490 cm^{-1} peaks are not as well resolved in these spectra as they are in Fig 3-5 A.

3.3.2. Scanning Electron Microscopy of BDD Films Grown on an NNP layer

Figure 3-7 A-C shows scanning electron micrographs of the pre-growth carbon layer on a sharpened Pt wire. The images presented in Figure 3-7 A and B reveal that the cone tip is more of less uniformly coated with a carbon film while the image in Figure 3-7 C shows the side of the cone is only partially covered. This is a typical observation. The interesting finding is that at the 2% CH_4/H_2 source gas ratio used to deposit the pre-growth carbon layer in our CVD reactor, the carbon film is predominantly composed of nanoscopic crystals of diamond 100-500 nm in diameter. Higher magnification images of the (Figure 3-7 B) tip and (Figure 3-7 C) cone reveal the faceted nanocrystalline morphology. The thickness of this layer is on the order of 1 µm, based on cross sectional SEM image analysis (Figure 3-8). In summary, three key findings are (i) diamond can readily nucleate on Pt as the pre-growth layer is essentially

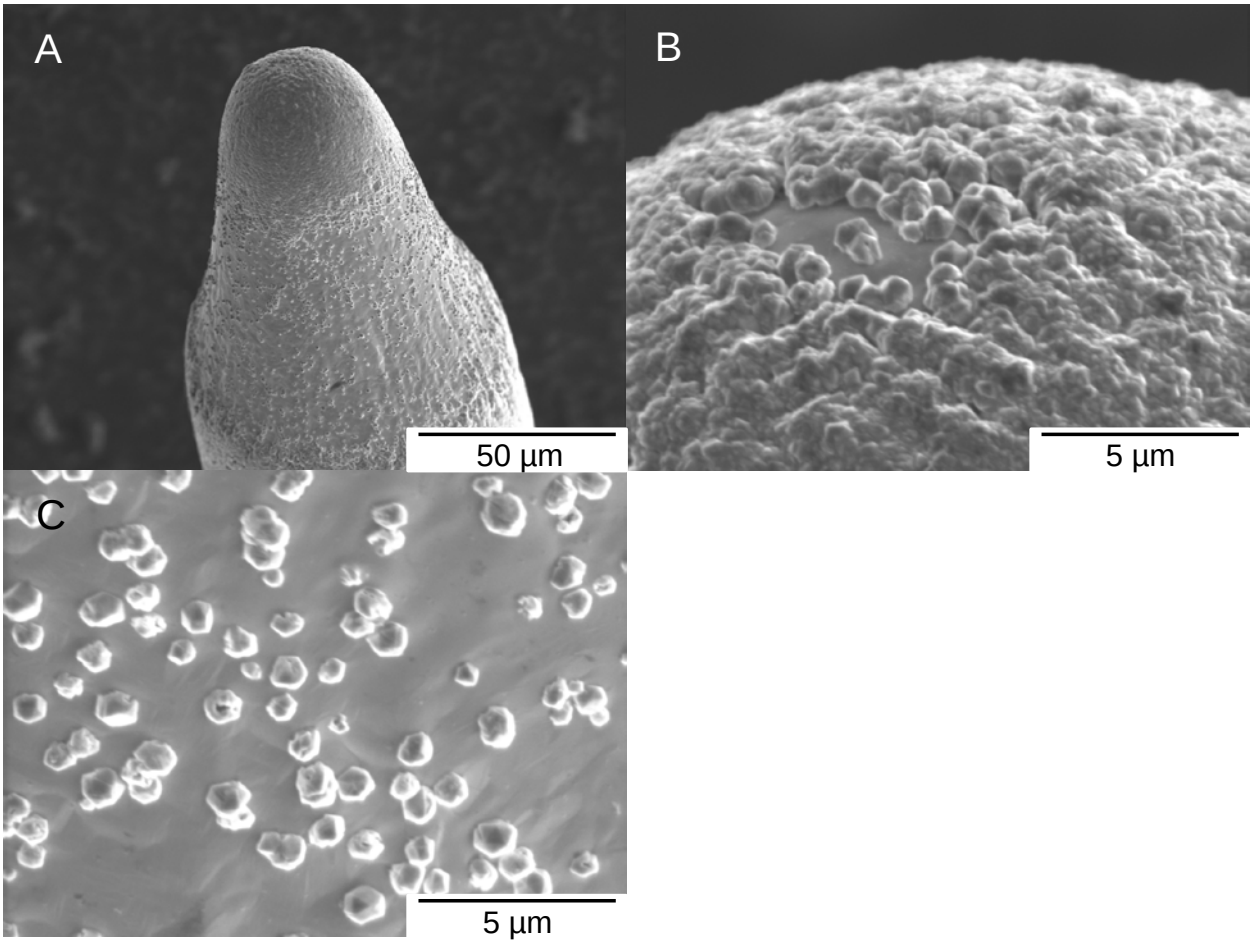

Figure 3-7. SEM images of the pre-growth carbon layer on an etched Pt wire. Images shown are for (A) the entire microelectrode, (B) the tip region and (C) the cone. The pre-growth carbon layer was deposited for 30 min using 2% CH_4/H_2 at 600 W and 45 Torr.

nanocrystalline diamond, and (ii) the pre-growth carbon layer thickness is near 1 µm on Pt instead of the typical tens-of-nanometer thickness on the other substrates as reported by Rotter[164], and (iii) the pre-growth carbon layer does not uniformly form over the Pt wire.

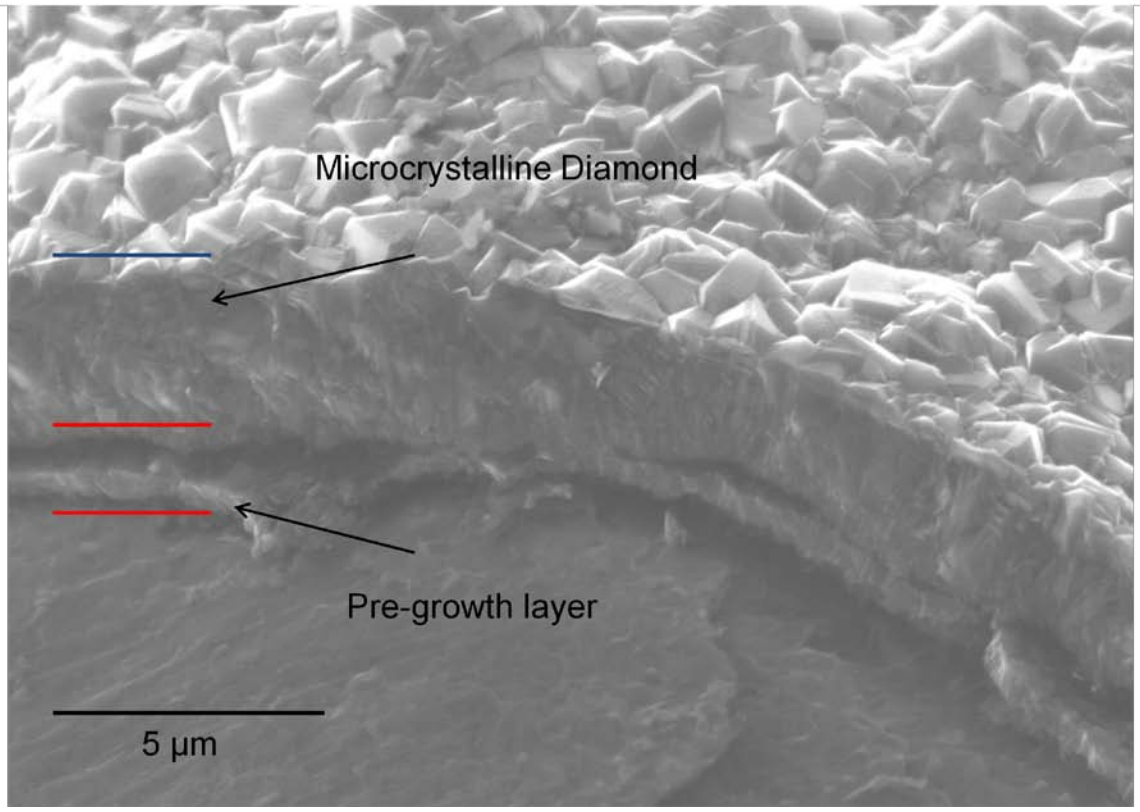

Figure 3-8. SEM cross-section of a 4 h diamond film deposited on the carbon pre-growth layer. The thickness of the pre-growth layer is approximately 1 µm.

Figure 3-9 A-C shows SEM images of wires of coated with boron-doped diamond films grown over the pre-growth carbon layer for 2, 4 and 6 h periods. Figures 3-10 A-C and 3-11 A-C show higher magnification images of the tips and cones, respectively. Clearly, the diamond film is not continuous after the 2 h growth (Figure 3-9 A). The tip of the wire looks to be covered with a continuous faceted film (Figure 3-10 A), but the cone is only partially coated with diamond (Figure 3-9 A and 3-11 A). The films deposited for 4 and 6 h do, however, appear continuous (Figures 3-9 C, 3-10 C, and 3-11 C). Well faceted crystallites, micrometers in dimension, are seen for both films with a crystallite diameter that increases with growth time (Figure 3-11 A-C). This is indicative of a van

der Drift growth mechanism. The number of secondary growths appears to be minimal for these two films. The aspect ratio of the conically-shaped microelectrode is nicely visualized in Figure 3-9 B, which reveals a tip diameter of 10 µm and a cone height of 115 µm.

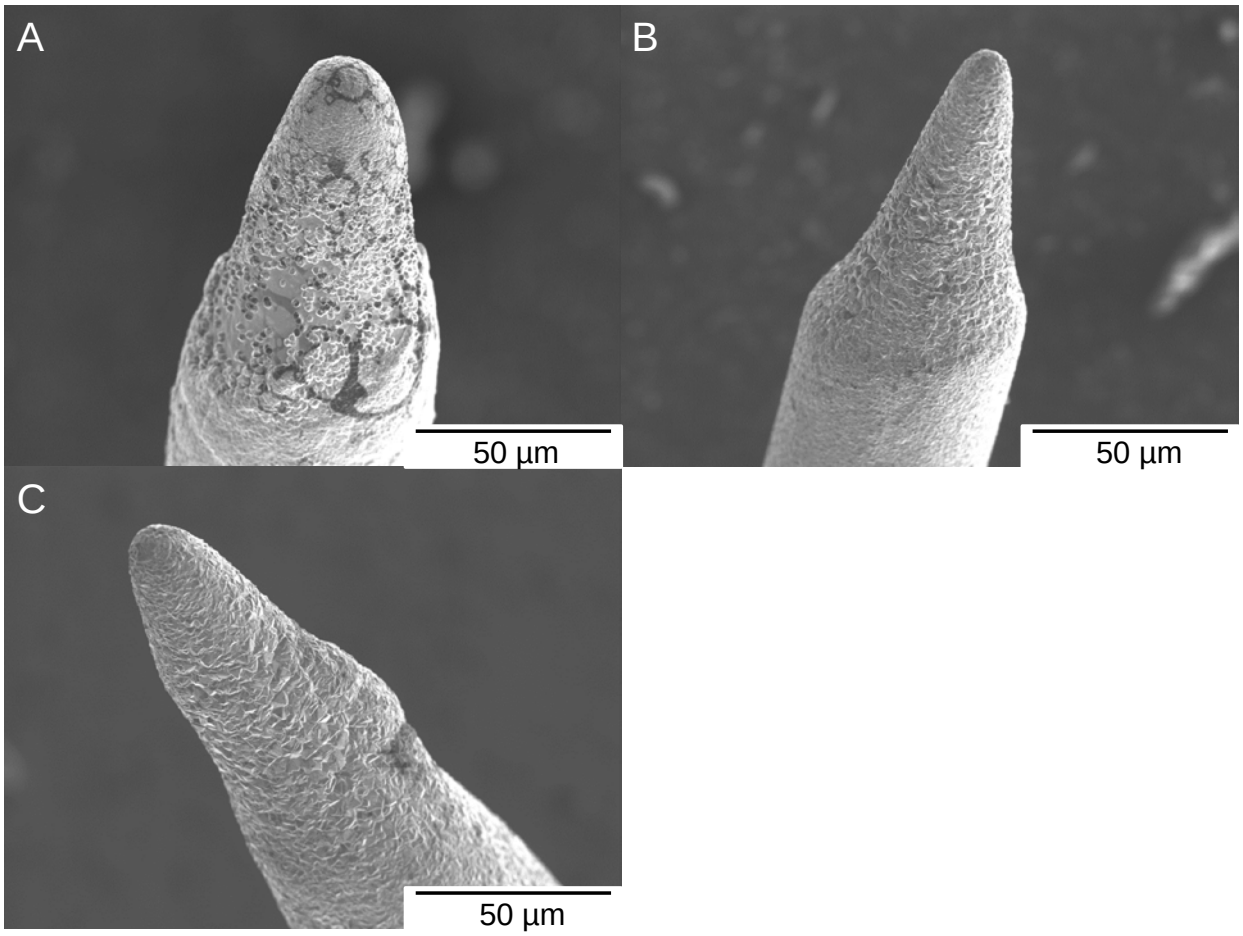

Figure 3-9. SEM images of boron-doped diamond films grown the pre-growth for (A) 2, (B) 4 and (C) 6 h. The diamond films were deposited using a 0.5 CH_4/H_2 at 600 W and 45 Torr.

Additionally SEM images are presented in Figure 3-12 A-D for the pre-growth carbon layer and diamond films grown over the pre-growth layer for 2, 4 and 6 h periods

of time. These provide additional evidence for the distinct morphological differences between the carbon coatings. Interestingly, the image of the pre-growth carbon layer (Figure 3-12 A) reveals a thick (~1 µm), high surface area, and discontinuous coating.

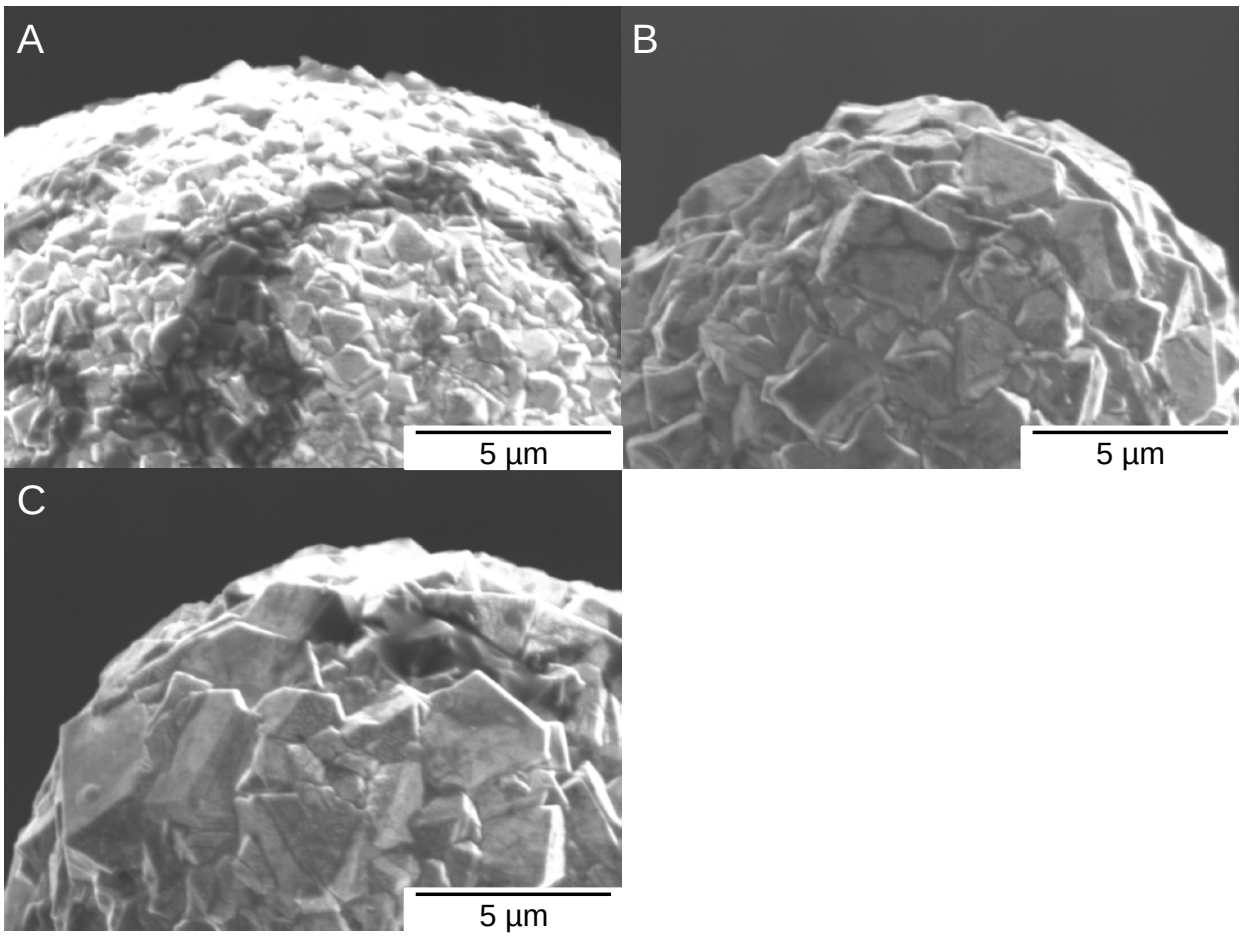

Figure 3-10. SEM images of boron-doped diamond films grown over the pre-growth carbon layer for (A) 2, (B) 4 and (C) 6 h. The images shown are for the tip region of each electrode. The diamond films were deposited using 0.5% CH_4/H_2 at 600 W and 45 Torr.

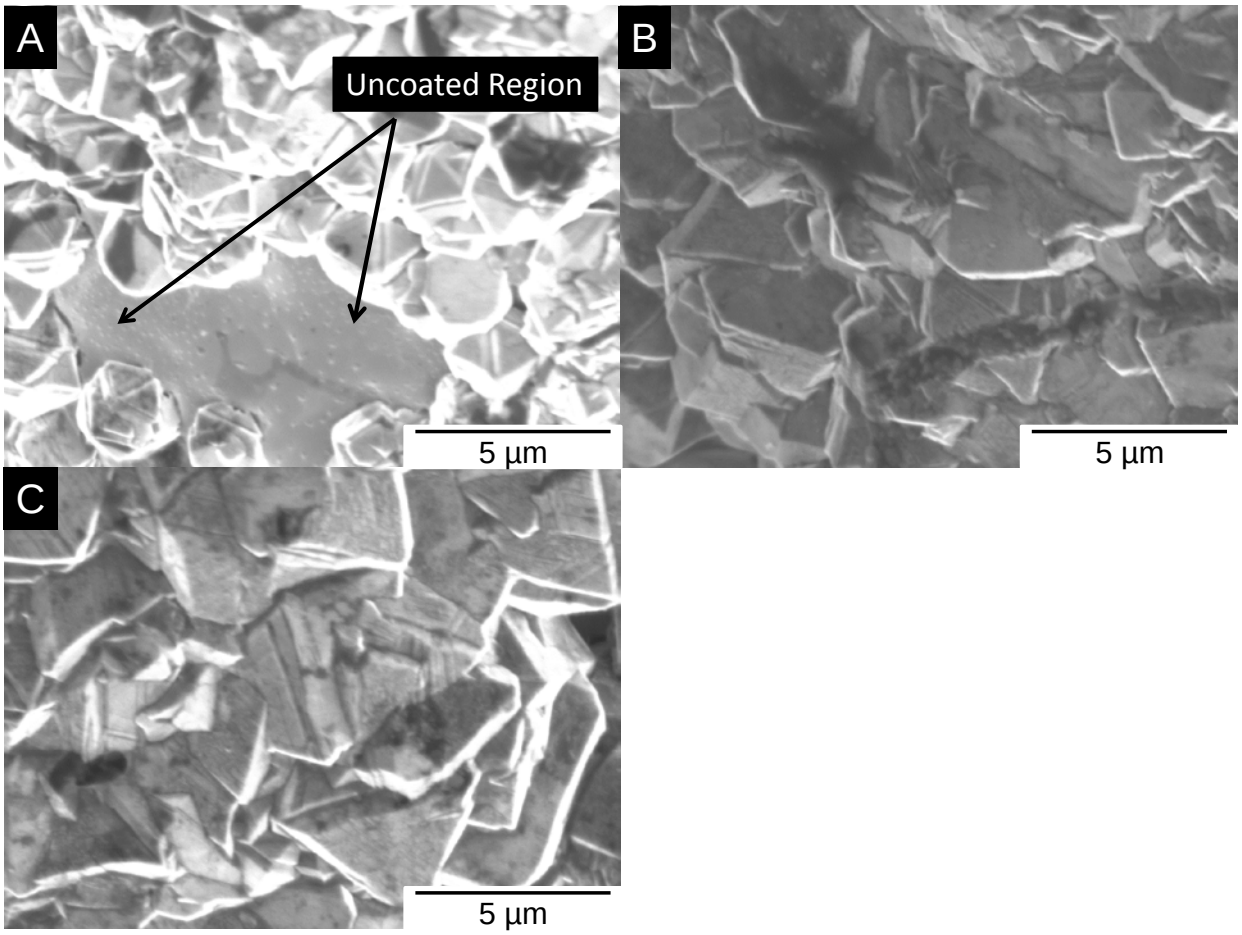

Figure 3-11. SEM images of boron-doped diamond films grown over the pre-growth carbon layer for (A) 2, (B) 4 and (C) 6 h. The images shown are for the cone region of each electrode. The diamond films were deposited using a 0.5% CH_4/H_2 at 600 W and 45 Torr.

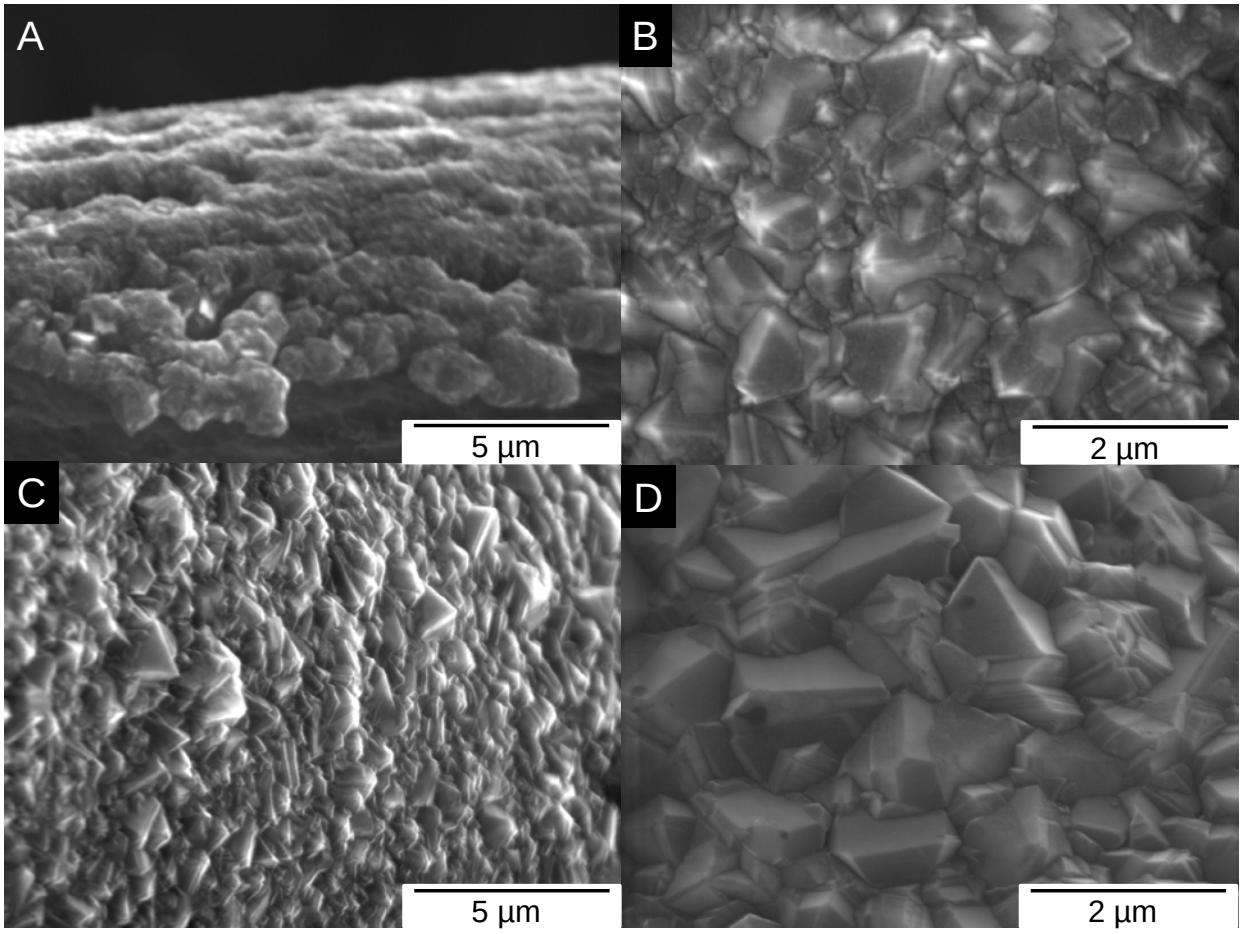

Figure 3-12. SEM images of (A) the pre-growth carbon layer and boron-doped films grown over the pre-growth carbon layer for (B) 2, (C) 4 and (D) 6 h.

3.3.3. Electrochemical Characterization of Carbon Fiber and BDD Electrodes

3.3.3.1 Caron Fiber

Cyclic voltammetry (CV) and amperometry were used to investigate the electrochemical activity of the carbon fibers. Three redox systems were used to probe the activity: $Ru(NH_3)_6^{+3/+2}$, $K_4Fe(CN)_6$ and NE. The redox reactions for each analyte are shown below.

A $Ru(NH_3)_6^{3+} + e^- \leftrightarrow Ru(NH_3)_6^{2+}$

B $Fe(CN)_6^{3-} + e^- \leftrightarrow Fe(CN)_6^{4-}$

C $NE(Hydroquinone) \leftrightarrow NE(Orthoquinone) + 2e^- + 2H^+$

Figure 3-13. Overview of redox systems used for electrochemical investigation of carbon fiber electrodes. Three systems were used including (A) ruthenium hexamine, (B) ferrocyanide and (C) norepinephrine.

The kinetics of the $Ru(NH_3)_6^{+3/+2}$ redox system on carbon electrodes are relatively insensitive to surface cleanliness and chemistry. The main factor controlling the kinetics is the density of electronic states at the formal potential of the redox system. In contrast, the kinetics for $Fe(CN)_6^{-3/-4}$ and NE are extremely sensitive to the density of electronic states as well as the surface cleanliness and chemistry[138, 145, 153, 175]. Using these three systems enable one to probe the electrical conductivity of the electrodes ($Ru(NH_3)_6^{+3/+2}$) and the surface cleanliness ($Fe(CN)_6^{-3/-4}$ and NE). Figure 3-14 shows representative cyclic voltammograms for $Ru(NH_3)_6^{+3/+2}$, $Fe(CN)_6^{-3/-4}$ and

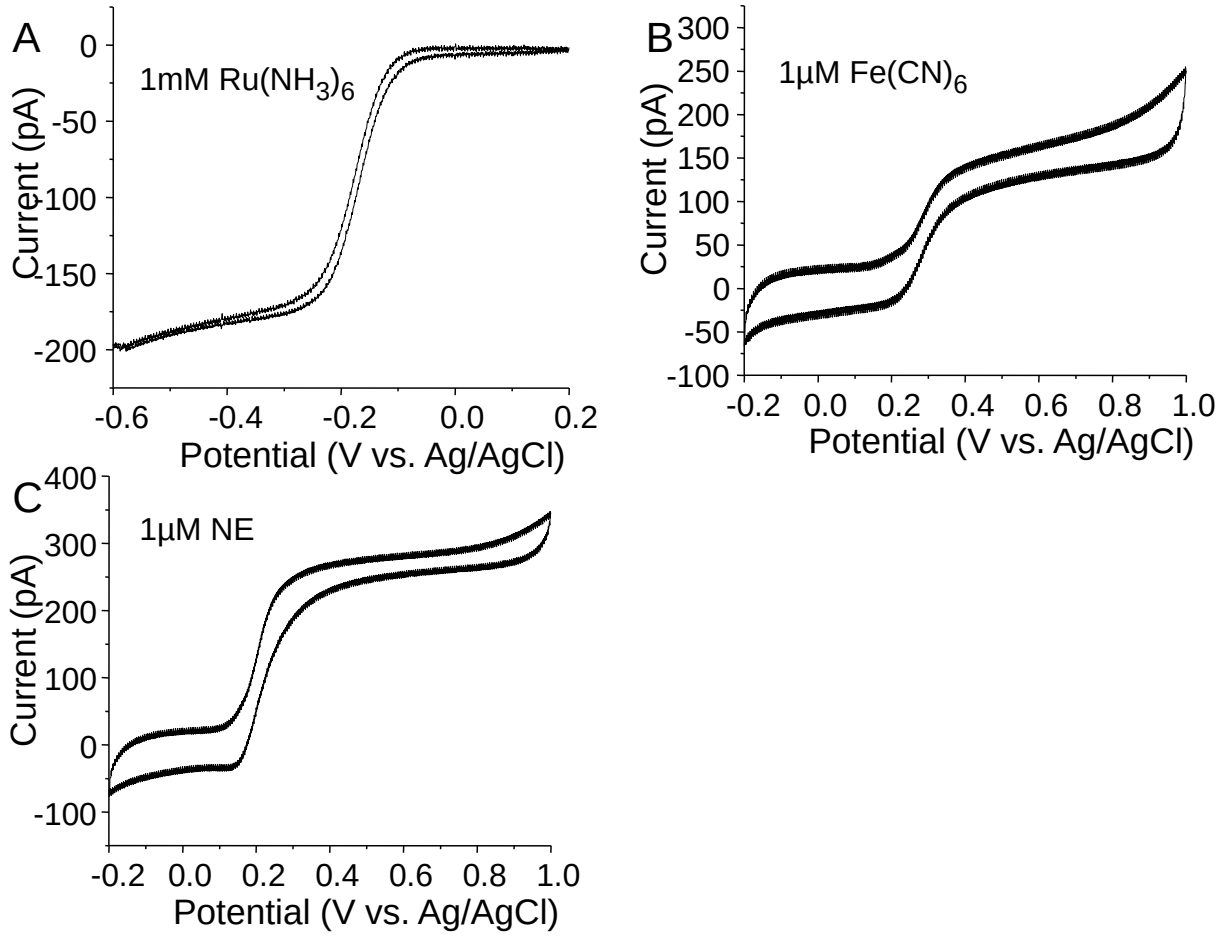

Figure 3-14. Cyclic voltammograms recorded for disk-shaped carbon fibers using (A) ruthenium hexamine, (B) ferri/ferrocyanide and (C) norepinephrine. The voltammograms were recorded at a scan rate of 100 mV/s using a Ag/AgCl reference electrode. The supporting electrolyte for ruthenium hexamine and ferrocyanide is potassium chloride. Supporting electrolyte for NE is 0.1 M potassium phosphate buffer at pH = 7.2.

NE (A, B & C, respectively) with 1M KCl used as the supporting electrolyte for $Ru(NH_3)_6^{+3/+2}$, $Fe(CN)_6^{-3/-4}$ and 0.1M Potassium Phosphate buffer at pH 7.2 for NE. It can be seen that all voltammograms have a sigmoidal appearance, which is indicative of steady-state diffusion. The half-wave potentials ($E_{1/2}$) for all three redox system are

near the values seen for freshly activated glassy carbon. This means the fibers are active and support relatively rapid electron transfer[176]. It can also be seen that the current for 100µM NE is roughly twice the current of the same concentration of $Fe(CN)_6^{-3/-4}$. This is due to the fact that NE undergoes a two-electron transfer during oxidation, while $Fe(CN)_6^{-3/-4}$ only undergoes a single electron transfer. These voltammograms also show that the electrodes have high electrical conductivity, as seen by the $Ru(NH_3)_6^{+3/+2}$. $Ru(NH_3)_6^{+3/+2}$ should have a half-wave potential roughly -100 mV vs. an Ag/AgCl reference electrode[176], and the value obtained from cyclic voltammetry is ~150 mV vs. Ag/AgCl. Voltammograms also indicate a clean electrode surface from the $Fe(CN)_6^{-3/-4}$ and NE have theoretical half-wave potentials of 160 mV[176] and 200 mV[153] vs. Ag/AgCl respectively.

The more positive half-wave potential for $Fe(CN)_6^{-3/-4}$ is most likely due to poor polishing conditions. Initial work preparing disk electrodes used both $Fe(CN)_6^{-3/-4}$ and NE as redox tools to investigate surface cleanliness. $K_4Fe(CN)_6$ was not used, as it is not a system of interest for *in vitro* experiments. It was found that the diamond wheel used for polishing away the epoxy layer around the carbon fiber becomes dull after 15-20 batches of electrodes. NE is less sensitive to minor surface imperfections due to physically adsorbing onto the electrode for electron transfer. For 29 electrodes that exhibited a half-wave potential less than 400 mV for $K_4Fe(CN)_6$, a limiting current of

138 ± 15 nA was obtained with a half-wave potential of 308 ±14 mV (reported as average ± standard error of the mean). For 49 electrodes that exhibited a half-wave potential of less than 300 mV for NE, a limiting current of 270 ± 17 nA and a half-wave potential of 223 ± 5 mV (Table 3-1) was found. These provide good criteria for discriminating electrodes that would be unfit for *in vitro* use, as the average limiting current for electrodes with half-wave potentials less than 300 mV is very similar to the ideal electrode area obtained for a perfect disk shaped electrode as calculated in earlier in this chapter.

Table 3-1. Cyclic voltammetric data for the carbon fiber microelectrodes. Values of the limiting current (i_l) and half-wave potential ($E_{1/2}$) for three different redox systems.

Redox System	Limiting Current (pA)	Half-Wave Potential (mV vs. Ag/AgCl)
$Fe(CN)_6^{-3/-4}$ (n=29)	138 ± 15	308 ± 14
NE (n=49)	270 ± 17	223 ± 5

Carbon fiber microelectrodes were also evaluated for their stability over time using amperometry. Electrodes were evaluated by being placed in the flow cell used for *in vitro* tissue work. Three electrodes were tested at random. Electrodes were poised at 0.650 V vs. Ag/AgCl and exposed to a 10 µM NE solution to obtain a baseline value. Electrodes were then exposed to a 10 µM solution of NE, EPI and ATP for varying time periods (5, 10, 30 and 60 min). 10 µM NE was once again used to assess the electrode activity before and after exposure to the potential contaminants. The results are shown

in Figure 3-15. It can be seen that there is a significant difference in the current for electrodes exposed to neurotransmitters for 60 min. To counter fouling, electrodes were held at a potential of 0.00 V vs. Ag/AgCl in between experiments.

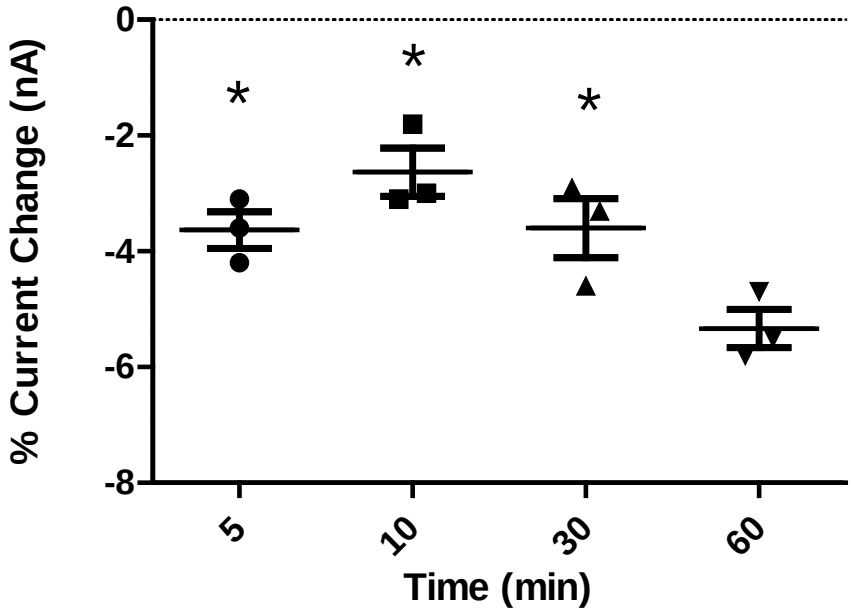

Figure 3-15. Carbon fiber electrode response over time after exposure to a solution containing 10 µM adenosine triphosphate, norepinephrine and epinephrine. * $p<0.05$ as compared to the 60 min data.

3.3.3.2 Boron-Doped Diamond

Boron-doped diamond electrodes grown via the novel nucleation procedure (NNP) method were characterized in 1M KCl and in 0.1 mM $Ru(NH_3)_6^{+3/+2}$ and $Fe(CN)_6^{-3/-4}$. Voltammograms were run in the supporting electrolyte KCl. With no redox system present in solution, the voltammetric current is related to the capacitance of the double layer $\underline{C_{dl}}$, scan rate $\underline{v}$ and area $\underline{A}$, as shown in equation 3-4.

$$i_{bkgd} = AC_{dl}\nu$$

Equation 3-3

Figure 3-16 shows the background cyclic voltammetric current-voltage curves for Pt wires coated with the pre-growth carbon layer (A) and with boron-doped diamond overlayers deposited for 2, 4 and 6 h (B-D). The curves were all recorded at 100 mV/s in 1 M KCl. Importantly, none of the curves show any evidence for exposed Pt[163]. This observation is consistent of a thin layer of amorphous sp^2 carbon. The curve for the wire with the pre-growth layer is featureless over the potential range, but the current is 10-50x greater than the current for the diamond-coated wires (B-D). The large background current results from the (i) high surface area morphology of the pre-growth layer (shown in SEM images), (ii) the exposed amorphous sp^2-bonded carbon, and (iii) the nanoscale roughness imparted to the wire during the formation of the pre-growth layer. The curves are featureless within the potential range with no evidence for any electroactive surface carbon-oxygen functional groups[177-180]. There was no B_2H_6 added during the formation of the pre-growth carbon layer; however, the carbon possesses good electrical conductivity as evidenced by the flat, relatively symmetric current-voltage curves about the zero current line. The electrical conductivity presumably arises from the sp^2 carbon domains in the grain boundaries as well as from some adventitious boron-doping that the reactor used for coating the pre-growth carbon layer is routinely used for depositing boron-doped diamond films.

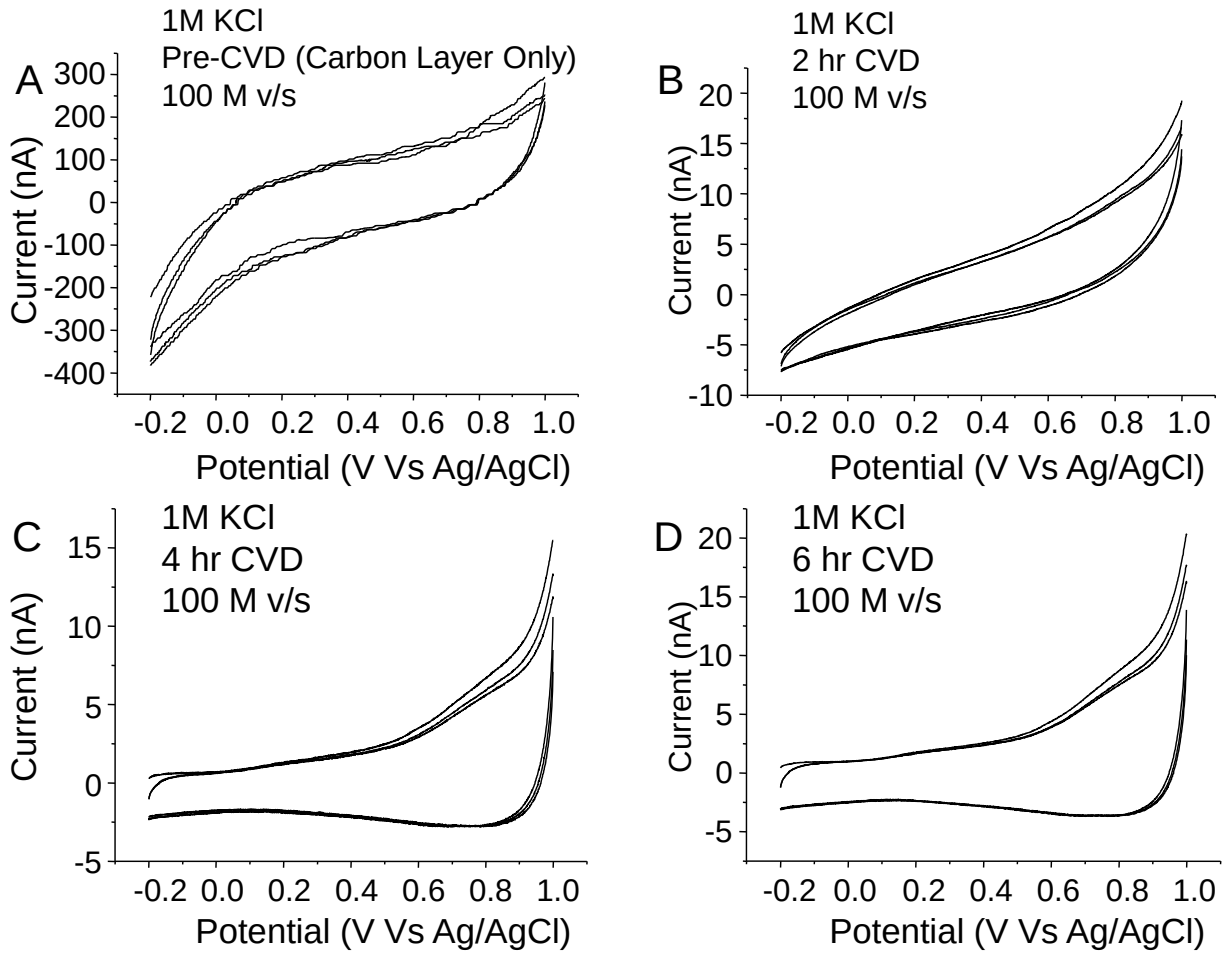

Figure 3-16. Background cyclic voltammetric *i-E* curves for wires coated with (A) the pre-growth carbon layer, and boron-doped diamond for (B) 2, (C) 4 and (C) 6 h. Electrolyte solution = 1 M KCl. Scan rate = 100 mV/s. Stable traces are shown for each electrode recorded after at least 10 cycles.

The background voltammetric current-voltage curves for the Pt wires after 2, 4 and 6 h diamond growths all have much lower background currents than the wire coated with just the pre-growth carbon layer, for reasons mentioned earlier. The curve for the 2 h film is somewhat sloped about the zero-current line consistent with there being some ohmic resistance within the film or between the film and the Pt. After the 4

and 6 h growths, the electrical resistance appears to decrease as the curves become more symmetric about the zero-current line. The curves are largely featureless except for the anodic and cathodic peaks at ca. 0.8 V just prior to the onset of Cl_2 evolution. The faradaic reactions or surface processes responsible for these peaks are unknown; however, this curve shape is typical for diamond-coated Pt wires[126, 145, 153, 163].

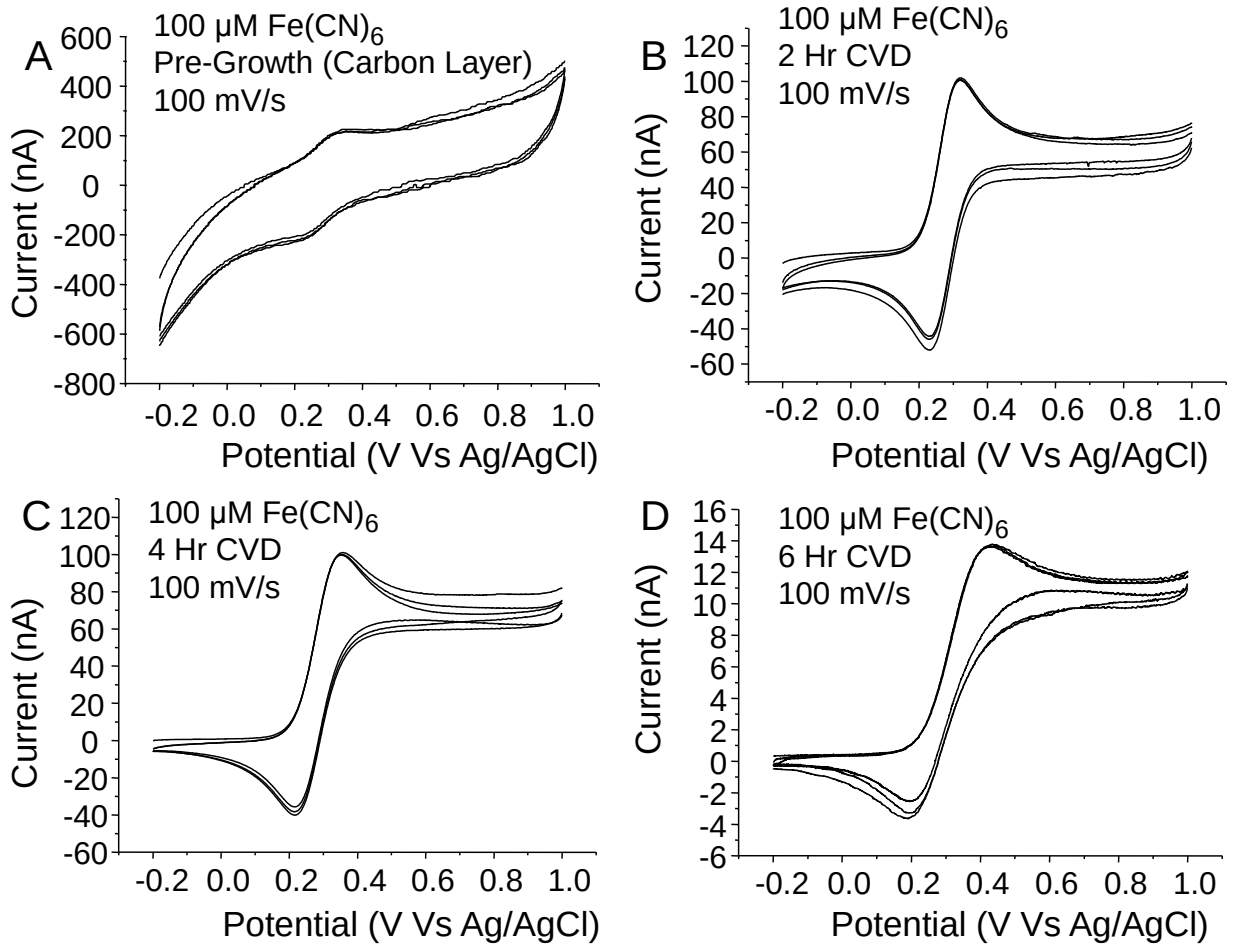

Figure 3-17. Cyclic voltammetric *i-E* curves for 0.1 mM $Fe(CN)_6^{-3/-4}$ at wires with (A) the pre-growth carbon layer, and boron-doped diamond for (B) 2, (C) 4 and (D) 6 h. Electrolyte solution = 1 M KCl. Scan rate = 100 mV/s. Stable traces are shown for each electrode recorded after at least 10 cycles.

Figure 3-17 shows cyclic voltammetric current-voltage curves for the surface-sensitive redox mediator, $Fe(CN)_6^{-3/-4}$. Total current curves are shown as no background correction was applied. The currents for each of the microelectrodes cannot be directly compared because the area of each exposed to the solution was difficult to control. Well defined oxidation and reduction peaks are seen for the pre-growth carbon electrode but they are somewhat buried within the large background current. The ΔE_p is 110 mV. By comparison, near-Nernstian behavior (ΔE_p = 60-70 mV) is typical for this redox system on clean glassy carbon and hydrogen-terminated diamond films on Si. Better defined redox peaks are seen for all three diamond-coated wires (Fig. 3-17 B-D) as the background currents for each are substantially lower. The ΔE_p values are 90 mV, 138 mV and 238 mV respectively, for the 2, 4 and 6 h growths. An interesting observation is the fact that ΔE_p (no iR correction) increases for the wires with increasing diamond deposition time (*i.e.*, more complete diamond coverage).

3.4 Discussion

The goals of this work was to establish a protocol for fabricating disk-shaped carbon fiber microelectrodes and to determine if applying a NNP to our current boron-doped diamond electrode protocol could decrease the time required for deposition of a full diamond film on our platinum wires.

The carbon fiber microelectrodes were characterized using electrochemistry, Raman spectroscopy and scanning electron microscopy. The Raman spectroscopy in

Figure 3-2 shows that the T-650 carbon-fiber has a higher ratio of edge defects than the P-55 as evidenced by the higher intensity of the 1369 cm^{-1} peak. A high fraction of edge plane is ideal for a carbon microelectrode used to detect catecholamines. It has been found that oxide groups can form at these defects which promote catecholamine oxidation[165, 181]. Thus, the T-650 would be the ideal candidate for catecholamine oxidation for biological experiments. As mentioned, the ideal electrode shape for a single cell measurement is a disk in order to maximize the signal-to-noise. Scanning electron microscope images reveal that sealed carbon-fibers, polished at a 45^{o} angle, do in fact possess an elliptical disk shape (Figure from Chapter 2). Most importantly, electrochemical testing provides a good quality control to screen electrodes for biological testing. Figure 3-11 shows voltammograms collected for three different redox systems. Testing with $Ru(NH_3)_6^{+3/+2}$, a surface insensitive molecule, showed that the electrical connectivity of our carbon-fiber electrodes is of reasonable quality. Further testing in more surface sensitive systems, including $Fe(CN)_6^{-3/-4}$ and NE, provided evidence that the polishing procedure effectively removed the epoxy from the carbon surface and produced a clean surface for electron transfer as evidenced by the average limiting current for NE. The experimental limiting current matched well with the theoretical limiting current for an elliptical disk as discussed in Chapter 2.

The conically shaped diamond electrodes are not practical for single cell secretion studies. They are useful for measurements at blood vessel surfaces, which constitutes related work in our group. The diamond films are deposited on Pt wires to

form microelectrodes. One drawback with diamond microelectrodes is the length of preparation time. Specifically, the typical time required time to deposit a continuous BDD film onto the wires using conventional substrate pretreatments is between 8-10 h. This translates into 10-12 h of total time required to set up the reactor for chemical vapor deposition and cool the wires down at the end of the growth. We hypothesized that by employing a NNP as detailed by Rotter[164], the time required for depositing a continuous diamond film could be decreased. This hypothesis is based on the theory of how diamond films nucleate and grow during the deposition process. Initial nucleation of diamond on the wires was previously accomplished via ultrasonication in a nanodiamond powder seeding solution. These "seeds" provide the initial sites at which the methane and hydrogen plasma can nucleate. Our selection of Pt as a substrate was based in large part on the work of Tachibana *et al* who demonstrated that epitaxial growth of (111)-oriented diamond is possible on (111)-oriented platinum[146]. Their work also showed a secondary growth mechanism for (111)-diamond in which the plasma directly attacks the platinum substrate. This secondary mechanism was observed during the NNP treatment of substrates, as shown in Figure 3-7 and confirmed using Raman spectroscopy shown in Figure 3-5. This spontaneous diamond formation provided a great platform for BDD microcrystalline growth, due to the high surface area and the readily available deposited diamond from the NNP layer. Scanning electron images determined that a continuous BDD film can be deposited after just 4 h of chemical vapor deposition, which is half of the time required under the previous protocol. Electrochemical testing of the BDD films grown on the NNP layer demonstrated that the NNP layer is relatively resistive, as evidenced by the nearly linear change of current

with potential around near 0.0 V. These studies also provided evidence that the NNP layer is a high surface area film, as compared with the diamond films. Turning our attention to the diamond films, the electrochemistry illustrates that after 4 h of deposition the films lose their resistive signatures, as seen by the voltammograms in only the supporting electrolyte. Investigation of $Ru(NH_3)_6$ and $K_3Fe(CN)_6$ revealed that peak splitting increased with deposition time. No follow-up studies were performed to identify the cause of this increase. However, one possible explanation is that the electron transfer rate is faster at sp^2 carbon, and the amount of sp^2 carbon decreases with longer diamond deposition. This would cause a decrease in the electron transfer rate with deposition time. The important finding from these studies is that the NNP layer greatly reduces the diamond deposition time required to create a continuous diamond film.

3.5 Conclusions

1) The work showed that carbon-fiber electrodes can be reproducibly prepared using T-650 type fibers. The polished electrodes have a disk shape, which was verified by microscopy and confirmed by electrochemical measurements. The electrodes were electrically conductive and possessed a clean surface, allowing for relatively rapid electron transfer for catecholamines, as tested using NE. Good reproducibility was observed in voltammetric measurements using the carbon fibers for $Fe(CN)_6^{-3/-4}$ and NE. Voltammetric data revealed that an

appropriate NE detection potential was 0.600 V vs. Ag/AgCl. At this potential, the NE oxidation is limited by diffusion of the analyte to the electrode surface.

2) The work also showed that improvements in the fabrication of diamond microelectrodes could be realized using the novel nucleation process pretreatment of the Pt wire substrates. The NNP layer consists of amorphous carbon and possibly some nanocrystalline diamond particles. The boron-doped overlayer readily nucleates on this “pregrowth layer” or on to this layer after ultrasonic seeding with diamond nanoparticles. The amorphous carbon is softer than the Pt and more diamond seed particles are retained on the former surface after seeding. As a consequence of the increased initial nucleation density, boron-doped diamond overlayer growth times were reduced from 8-10 h to as little as 4 h. As was the case for the carbon fibers, good reproducibility was observed in voltammetric measurements for $Fe(CN)_6^{-3/-4}$ and NE.

Chapter 4

Effects of DOCA-salt Hypertension on Catecholamine Secretion from Isolated Sham and DOCA-salt Chromaffin Cells

4.1 Introduction

Increased sympathetic drive contributes to hypertension in humans[182-184] and in several animal models of the disease[148, 185-186]. Evidence for heightened drive includes increased plasma levels of NE and hyperactive sympathetic nerve firing[27, 182, 187]. Our laboratory is investigating how the sympathetic neural control of vasomotor tone becomes altered in salt-sensitive hypertension. Neurally-controlled vasomotor tone is an important regulator of blood pressure. To date, we have found that there is differential neurogenic control of arteries and veins[35, 149] and two prejunctional control mechanisms are dysfunctional in the DOCA-salt model (rat) of hypertension[34-35, 125]: (i) the α_2-adrenergic autoreceptor and (ii) the NET.

As a consequence of the altered prejunctional control, there is increased NE availability at sympathetic neuroeffector junctions and this contributes to increased vascular contractility, hence increased blood pressure. *In vitro* electrochemical measurements made at the adventitial surface of blood vessels enable real time monitoring of NE near its sites of release and action[34-35, 120, 123-125]. NE is a

vasoconstricting neurotransmitter released from sympathetic nerves supplying arteries and veins. The action of NE is mediated by the postjunctional α_1-adrenergic receptor expressed by vascular smooth muscle cells. Activation of α_1-adrenoreceptors causes muscle contraction and elevated blood pressure.

Amperometry can also be used to monitor catecholamine release from single adrenal chromaffin cells[41, 50-53, 102, 121, 188-191]. Sympathetic neurons communicate with smooth muscle cells by Ca^{2+}-dependent exocytosis of vesicular stores of NE and other vasoconstrictor transmitters[192]. This leads to the expulsion of vesicular content into the extracellular space[190, 192-193]. Electrochemical measurements at single secretory cells have been used over the years to investigate the individual stages of exocytosis with high spatial and temporal resolution[41, 50-54, 102, 121, 188-193]. Measurements using single cells aid in the understanding of exocytosis, more so than can be accomplished through studies of intact tissues. This is because of the small size of the neuroeffector junction (~100 nm) that prohibits placement of a recording electrode in a single junction. Additionally, the coupled actions of the prejunctional α_2-autoreceptor and NET that serve to regulate of extracellular levels of NE at perivascular sympathetic nerve fibers, make it difficult to independently investigate exocytotic release of neurotransmitters.

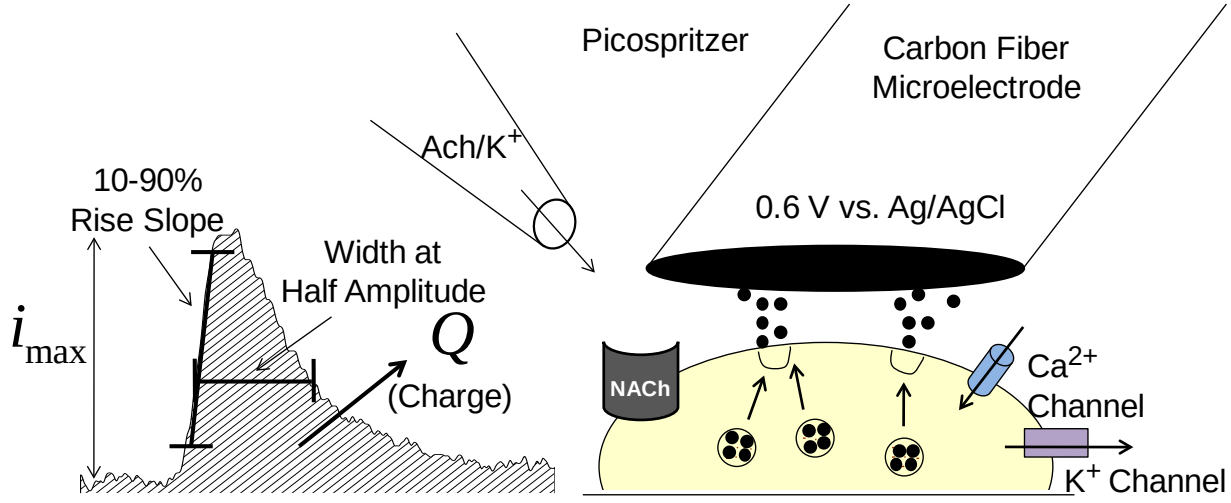

Figure 4-1. A carbon fiber microelectrode is positioned at the membrane surface of a chromaffin cell and used to detect catecholamine secretion as an oxidation current (A). A 2-s burst of ACh (1mM) or K^+ (70mM) was used to evoke catecholamine release. Secretion was monitored at 0.6 V vs. a Ag/AgCl reference electrode. A representative release event is shown to the left. Current spikes were analyzed for their 10-90% rise time and slope, the full width at half maximum, the spike area and the number of release events per stimulus.

Adrenal chromaffin cells secrete NE and EPI, and increased secretion from adrenal glands has been found in both hypertensive humans[182, 187, 194] and animals[195-196]. Circulating catecholamine levels are elevated in DOCA-salt hypertension, undoubtedly contributed to by chromaffin cells[195-196]. Chromaffin cells are a viable model for studies of the mechanisms and dynamics of exocytosis[41, 50-54, 102, 121, 188-191] (An example of the experimental set-up is provided in Figure 4-1). Since chromaffin cells do not express the α_2-adrenergic autoreceptor or NET, as do perivascular sympathetic nerves, they can be used in conjunction with electrochemical methods to study catecholamine secretion independent of autoreceptor inhibition or

transporter-mediated reuptake. Understanding how and why there is increased quantal release would lead to a better understanding of DOCA-salt hypertension as a multi-factoral disease. In addition to affecting catecholamine homeostasis, dysfunction in the adrenal gland has been linked to other pathways affecting blood pressure. For example, recent work has linked aldosteronism in BKβ1-KO mice to elevated blood pressure due to increased water retention and poor electrolyte handling[100]. The investigators in this work found that in the adrenal gland, the BKβ1 channel expression is restricted to the medulla, suggestive of a link between adrenal chromaffin cells and elevated blood pressure in aldosterone-mediated hypertension. These findings are further supported by Sausbier *et al.* who determined that small arteries in BKα-KO mice had increased vascular tone, decreased vasodialation and the animals exhibited higher levels of aldosterone, further linking vascular tone to adrenal gland function[101].

In the present work, we report on the use of single adrenal chromaffin cells, as a potential model for sympathetic nerve endings, to investigate the mechanisms of catecholamine secretion. We tested two hypotheses: (i) that catecholamine secretion from single adrenal chromaffin cells is increased in DOCA-salt hypertension and (ii) that impaired K^+ channel function contributes to the increased release.

4.2 Results

4.2.1 Electrochemical Measurement of Catecholamines from Isolated Rat Adrenal Chromaffin cells

Once the electrode fabrication was mastered, it became necessary to determine if the carbon fiber electrodes were capable of monitoring catecholamine secretion *in vitro* from isolated rat chromaffin cells. As determined in Chapter 2, isolated chromaffin cells used for experiments contained the vesicular monoamine transporter and dopamine-β-hydroxylase, which provided evidence that the cells being investigated had the mechanisms required for synthesizing and packaging catecholamines. To probe catecholamine secretion, disk-shaped carbon-fiber electrodes were prepared and positioned as described in Chapter 2 and poised at 0.600 V vs. Ag/AgCl for detection. At this potential, the catecholamine oxidation current is limited by analyte diffusion to the electrode. Initial work was performed on cells isolated from normotensive control rats and secretion was stimulated with 100 µM ACh. A representative recording is shown in Figure 4-2 A for an amperometric recording stimulated by 1mM ACh. Current spikes are representative of individual vesicle secretion[40-41]. Fig. 4-2 B shows a magnified view of a current spike. Individual spikes can be analyzed to yield information about the quantal release from each vesicle, or put another way, the number of catecholamines released during an individual secretion event. Spikes also provide kinetic information about secretion, which can be determined by analyzing the rise time, the slope of the leading edge of the current spike and the full width at half maximum, which are identified in Fig 4-2 B. To test if the signal was due to actual oxidation of a secreted catecholamine or just noise, the same experiment was repeated with the electrode held at 0.000 V vs. Ag/AgCl (Fig. 4-2 C). When the potential is lowered to 0.0 V the oxidation spikes disappear, indicating that they result from oxidation of catecholamine molecules near the cell membrane.

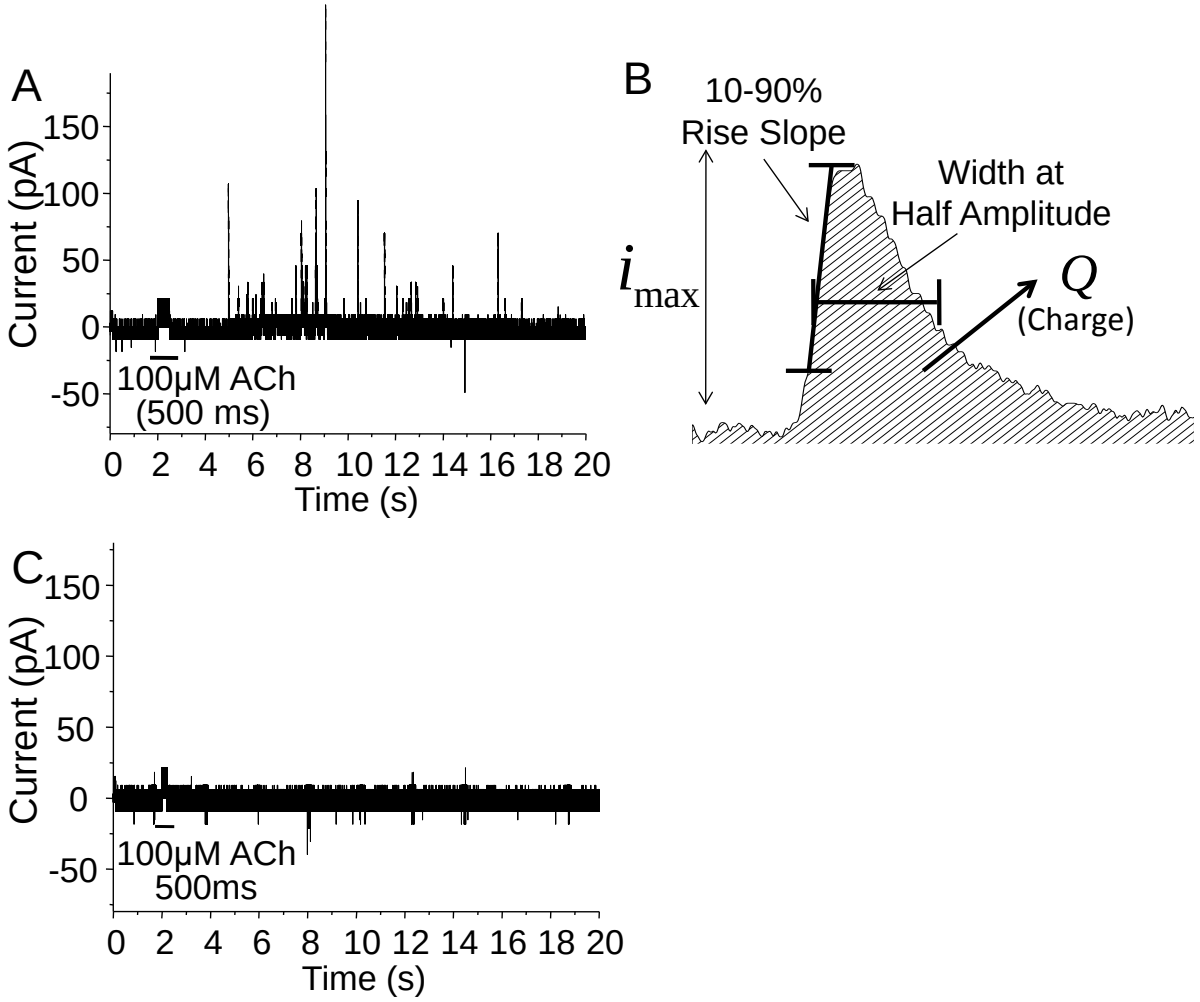

Figure 4-2. Amperometric recording from an isolated rat chromaffin cell in culture. The cell was isolated from a normotensive animal. Current-time traces are shown for 100 μM ACh stimulation and detection was monitored at an applied potential of 0.600 V (A) and 0.000 V (C) vs. Ag/AgCl. A magnified view of a current spike with an overview of kinetic data obtained from each spike provides is also shown (B).

To determine if the observed oxidation current spikes were due to vesicular secretion of catecholamines, two control measurements were performed. The first control experiment proved if calcium is required for catecholamine secretion. It is known that vesicular fusion and secretion is tightly regulated by calcium[58]. Thus, removing calcium from the physiological buffer should effectively abolish catecholamine

secretion from chromaffin cells. Figure 4-3 A shows an amperometric trace in which the calcium in the physiological buffer being perfused through the system was replaced with magnesium to maintain molality. We found that when there is no extracellular calcium present, the current spikes disappear. These data provide evidence that the oxidation spikes are dependent upon calcium entry into the cell. The second control experiment verified that the oxidation spikes are dependent on activation of the nAChR via application of acetylcholine. This was accomplished by introducing a nAChR antagonist into our physiological buffer and then attempting to stimulate secretion using acetylcholine. Figure 4-3 B provides an example of an amperometric recording with 100 µM hexamethonium, which is a known nAChR antagonist[197]. Hexamethonium greatly decreased the amount of oxidation spikes when the cell is stimulated with acetylcholine. There are some possible small oxidation spikes however they were statistically indistinguishable from the background current.

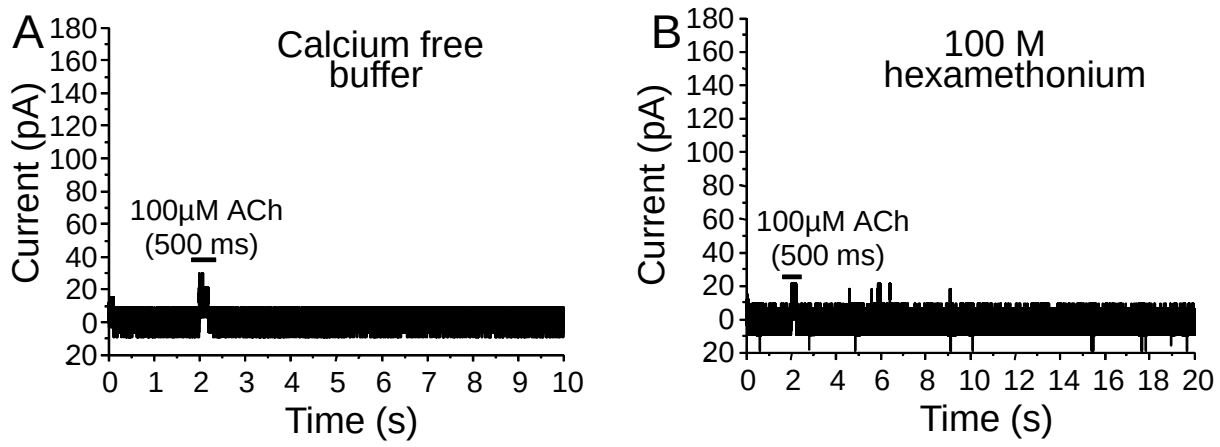

Figure 4-3. Electrochemical verification of catecholamine secretion. Current-time traces are shown for 100 µM ACh stimulation of Sham chromaffin cells in calcium-free buffer (A) and in the presence of the ACh antagonist hexamethonium (B). An applied potential of 0.600 V vs. Ag/AgCl was applied in both experiments.

These results provide evidence that the oxidation current spikes, as measured using an applied potential of 0.600 V vs. Ag/AgCl, are dependent on calcium being present in the buffer and activation of the nAChR. This evidence leads to the conclusion that the oxidation spikes being monitored are due to vesicular secretion of catecholamines from adrenal chromaffin cells.

4.2.2 Steady-state Catecholamine and Metabolite Levels in the Adrenal Medulla

Whole medulla NE and EPI levels were ~1.4 fold greater in DOCA-salt compared to Sham rats (Table 4-1). In contrast, dopamine (DA), normetanephrine

Table 4-1. Catecholamine and metabolite levels in the adrenal medulla isolated from Sham and DOCA-salt hypertensive rats (n = number of rats, two adrenal medulla were used per rat). NE: norepinephrine, EPI: epinephrine, DA: dopamine, NMN: normetanephrine, MN: metanephrine, DHPG: 3,4-dihydroxyphenylglycol.

	NE	EPI	DA	NMN	MN	DHPG
Sham (n =5)	168 ± 17	958 ± 72	6.1 ± 0.5	90 ± 31	217 ± 136	18 ± 9.7
DOCA-salt (n=5)	257 ± 34*	1302 ± 49*	6.7 ± 0.6	90 ± 14	79 ± 15	2.1 ± 0.4

Data are mean ± S.E.M µg/g tissue wet weight. (*P<0.05 *vs.* corresponding Sham value, Student's *t* test).

(NMN), metanephrine (MN) and 3,4-dihydroxyphenylglycol (DHGP) levels were all statistically similar in the two tissues. NMN and MN metabolite levels normalized to their precursor levels ($\frac{NMN}{NE}$ and $\frac{MN}{EPI}$) were used as a measure of catecholamine

metabolism. The NMN/NE ratio was 0.27 ± 0.01 in the adrenal medulla from Sham rats and 0.29 ± 0.03 (P > 0.05) in glands from DOCA-salt rats. The MN/EPI ratio was 0.05 ± 0.01 in both Sham and DOCA-salt adrenal medulla (P>0.05). These results indicate that there is no alteration of catecholamine metabolism in the adrenal medulla associated with DOCA-salt hypertension.

4.2.3 Increased Catecholamine Release from DOCA-salt Chromaffin Cells

Continuous amperometry recordings were made using an application of ACh (1 mM) to a single chromaffin cell, which evoked a burst of oxidation currents (Fig. 4-4).

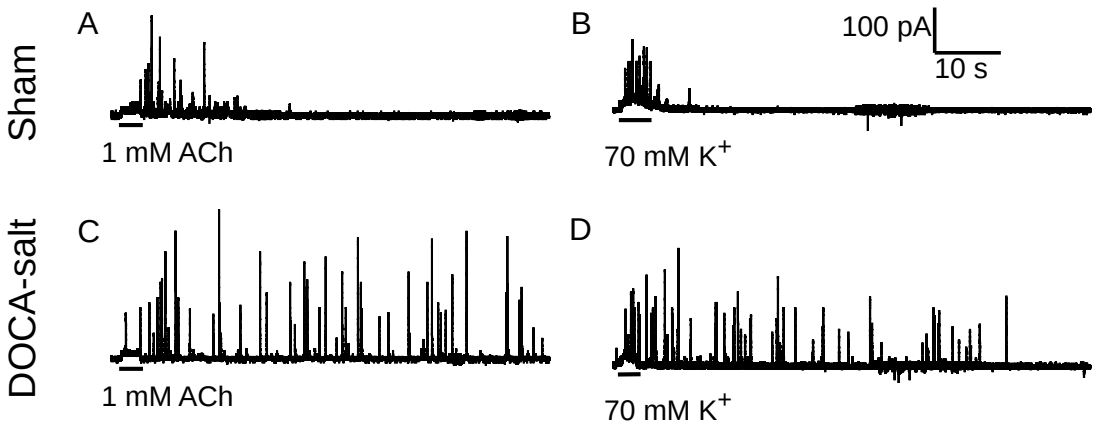

Figure 4-4. Continuous amperometric recordings from single Sham (A, B) and DOCA-salt (C, D) adrenal chromaffin cells. Current spikes arise from the electrochemical oxidation of catecholamines released from single cells with each spike representing a release event. Secretion caused by ACh (1 mM) (A, C) and high K^+ (70 mM) (B, D) is increased in DOCA-salt chromaffin cells compared to controls.

ACh elicits catecholamine secretion through activation of the nicotinic-acetylcholine receptor (nAChR), which increases intercellular Ca^{2+}, leading to exocytosis[59, 189]. Catecholamine release from cells isolated from Sham normotensive rats occurred as a

burst of secretion events lasting 10-15 s (Fig. 4-4 A). ACh also evoked bursts of oxidation spikes from DOCA-salt chromaffin cells (Fig. 4-4 C). These bursts were, however, longer in duration (30-45 s), the number of release events was 2.5 fold greater and the total charge detected over the course of a recording was 3-fold greater for DOCA-salt compared to Sham cells (Table 4-2). The increased number of spikes per stimulus seen for the DOCA-salt cells is consistent with more vesicles undergoing fusion and releasing their content.

Table 4-2. Analysis of ACh (1 mM) and K^+ (70 mM) induced catecholamine release from single adrenal chromaffin cells maintained in primary culture. Each cell was used for a single amperometric recording. Using ACh stimulation, 19 and 13 cells were used from 6 Sham and 6 DOCA rats respectively. Using high K^+ recordings, 11 and 14 cells were used from 4 Sham and 4 DOCA rats respectively.

	Events per stimulus	**Charge per/stimulus (pC)**	**Molecules oxidized/stimulus (10^8)**
Sham			
ACh (n=19)	22 ± 2.2	15 ± 2.8	0.5 ± 0.1
K^+ (n=11)	25 ± 2.1	18 ± 4.7	0.5 ± 0.1
DOCA-salt			
ACh (n=13)	49 ± 4.5*****	42 ± 9.2*****	1.2 ± 0.3*****
K^+ (n=14)	57 ± 12*****	47 ± 9.0*****	1.2 ± 0.3*****

Data are mean + S.E.M; "n" is the number of cells, which is also the number of amperometric recordings obtained (*P<0.05 *vs.* corresponding Sham value, Student's *t* test).

One possible explanation for the increased number of vesicles undergoing fusion and secretion (individual spikes) from the DOCA-salt cells could be an up-regulation in nAChR expression. To test this possibility, high extracellular K^+ (70 mM) was also used

to evoke release. Application of high K^+ evokes catecholamine secretion by directly depolarizing the cell membrane causing activation of voltage-gated Ca^{2+} channels. The data reveal that high K^+, like ACh, caused increased catecholamine secretion from DOCA-salt compared to Sham chromaffin cells (Fig. 4-4 B and D). These results suggest that the primary cause of increased secretion form DOCA-salt chromaffin cells is not due to an increased sensitivity in nAChR function. It has been shown that exocytosis can be modulated by variousstimuli[198-201]. However, due to the high concentrations of the chemical stimuli used, the release events being detected are most likely complete exocytotic events.

4.2.4 Release Kinetics

It is proposed that the individual spikes correspond to single vesicular exocytotic release events[41, 50, 53-54, 190]. In other words, we suppose that each spike corresponds to the electro-oxidation of catecholamines released from an individual vesicle. This supposition is supported by the fact that the charge per spike (Table 4-3, 0.8-1.1 pC) is similar to values reported previously for single vesicular release events (~1 pC per spike)[41, 50, 53, 190, 192]. For each spike, the integral of the current over time yields the charge. The charge can be converted to the number of molecules secreted and oxidatively detected using Faraday's Law ($Q = nFN$), where Q is charge, n is the number of electrons transferred per mole, F is Faraday's constant and N is the number of moles of catecholamines oxidized. The number of moles can be converted to the

number of molecules using Avogadro's number. Using the individual spike charge (see Table 4-3), a value of 2.5 X 10^6 molecules per vesicle is calculated for Sham secretory events evoked by both ACh and high K^+. This value is close to the 5.2 X 10^6 molecules per vesicle value reported previously for bovine adrenal chromaffin cells[41, 50, 53-54, 121, 190].

Table 4-3. Summary of the spike charge, rise time and full width at half maximum for secretory events from Sham and DOCA-salt chromaffin cells.

	Average charge/spike (pC)	Rise slope (pA/ms)	10-90% rise time (ms)	Half width (ms)
Sham				
ACh (1 mM) (n=420)	0.8 ± 0.04	50.9 ± 1.4	5.1 ± 0.2	13.1 ± 0.3
K^+ (70 mM) (n=478)	0.8 ± 0.03	57.2 ± 1.0	5.3 ± 0.1	11.6 ± 0.2
DOCA-salt				
ACh (1 mM) (n=621)	1.1 ± 0.04*****	66.1 ± 1.8*****	4.4 ± 0.1*****	10.7 ± 0.1*****
K^+ (70 mM) (n=669)	0.98 ± 0.03*****	76.6 ± 0.8*****	5.3 ± 0.1	11.7 ± 0.1

Data are mean + S.E.M; "n" is the number of single event amperometric spikes used for data analysis. The number of animals and cells used in these experiments is the same as in Table 2. (*P < 0.05 vs. corresponding Sham values, Student's *t* test)

It has been reported that a relatively constant catecholamine concentration exists in each spherically-shaped vesicle[202]. Therefore, assuming full release, the number of

catecholamine molecules reaching the electrode for detection is proportional to the vesicular volume, or radius ($Q=nFCV=nFCr^3$)[41, 54]. Figure 4-5 shows the distribution of

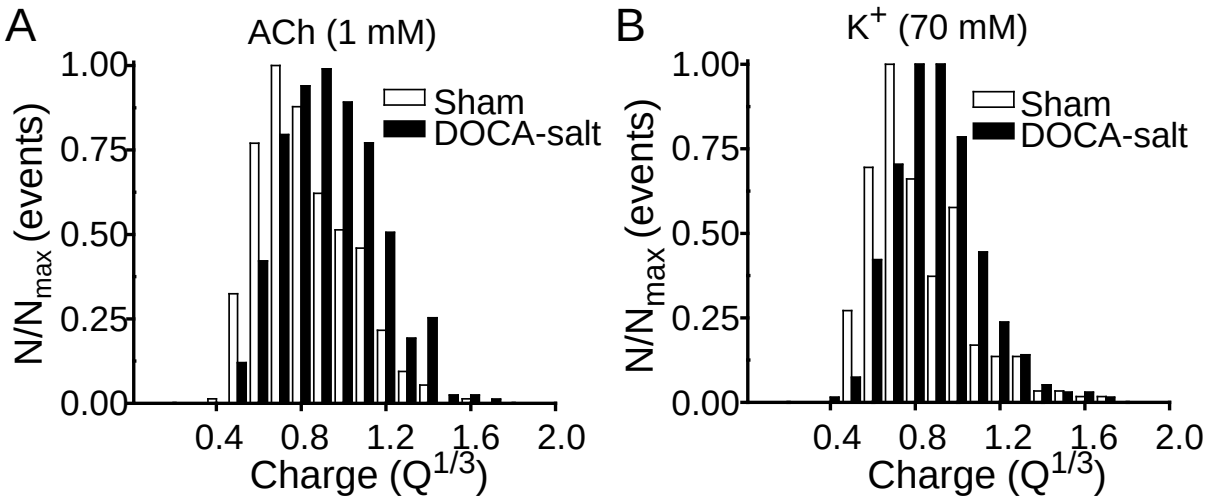

Figure 4-5. Distribution of the cubed root of the charge ($Q^{1/3}$) for individual release events from Sham and DOCA-salt cells evoked by ACh (A) and elevated K^+ (B) stimulation. Values were analyzed within 0.1$pC^{1/3}$ bins and plotted against the maximum frequency observed among individual bins. A positive shift in charge values can be seen for events from DOCA-salt cells regardless of the stimulus used. Assuming an equal concentration distribution for the two cell types, the positive shift correlates to an increase in radius for vesicles from DOCA-salt cells as compared to normotensive cells. Cubed root means were compared between Sham and DOCA data using student's *t*-test and were statistically different at $P<0.05$ (F-test was used to confirm no statistical differences between Sham and DOCA variances).

the charge ($Q^{1/3}$), which is proportional to the vesicle radius, for single secretion events from Sham and DOCA-salt cells. Values were binned into 0.1 $pC^{1/3}$ intervals and then normalized to the highest number of events within a given bin. For both ACh and high K^+ stimuli, a right-ward shift in the distribution of charge per spike is seen for DOCA-salt cells. By taking the mean of all the cubed root values, average $Q^{1/3}$ values were obtained for ACh stimulation which were 0.88 ± 0.01 and 0.99 ± 0.01 pC, respectively,

for Sham and DOCA-salt cells. These values were similar to data for high K^+ stimulation. This increased $Q^{1/3}$ value for the DOCA-salt cells is significant and consistent with an increase in the average vesicle radius.

The temporal profiles of the current spikes were analyzed to assess the kinetics of release. As mentioned in the experimental section, spikes were only analyzed if (i) they were monophasic, (ii) the peak amplitude was at least twice magnitude of the background current, (iii) the current was deflected positive and (iv) the current transient returned to the baseline. Representative recordings of oxidation currents from Sham and DOCA-salt cells are presented in Fig. 4-6 A. The nominal spike charge and the slope of the leading edge of the current spike were greater for events recorded from DOCA-salt compared to Sham cells. The current rise time (10-90%) and $t_{1/2}$ were significantly shorter for DOCA-salt compared to Sham cells (Table 4-3) when using ACh stimulation. For an unknown reason, these differences were not seen when using high K^+ stimulation. The rise time (10-90%) of a spike was used as a measure of the rate of catecholamine release. The $t_{1/2}$ was used as a measure of the rate of extrusion of chemical messengers after vesicle fusion[188]. The results suggest that rate of extrusion is more rapid in DOCA-salt compared to Sham cells. The rate-limiting step is thought to be rate of fusion pore expansion following vesicle-cell fusion[38, 50-51, 54]. The lack of K^+ effect on the $t_{1/2}$ and rise time for individual events may be due to how this stimulation recruits Ca^{2+} in the cell. It is known that the SNARE proteins responsible for tethering

the vesicle to the cell membrane and that complete exocytosis versus partial secretion is calcium dependent[61]. The differences in calcium handling could provide an explanation as to the difference between the $t_{1/2}$ values for ACh and K^+ stimulation.

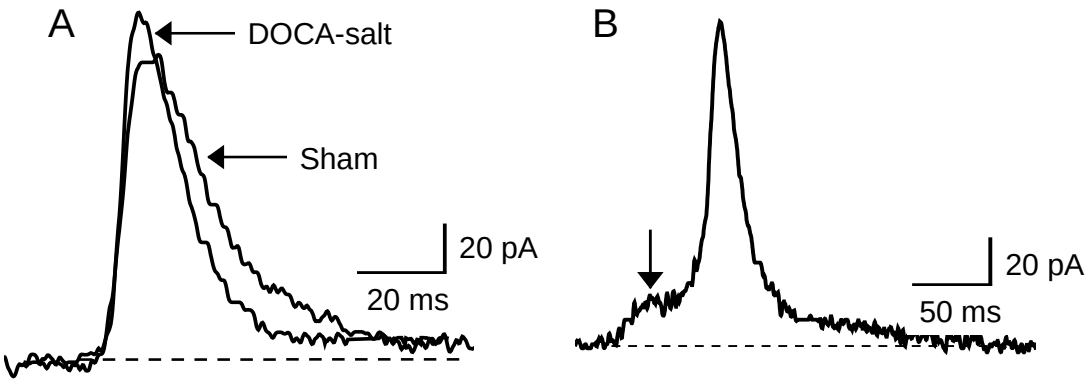

Figure 4-6. Examples of single release events recorded from cultured adrenal chromaffin cells isolated from Sham and DOCA-salt rats (A). Release events from DOCA-salt cells occur faster than release events from Sham cells based on the smaller peak width and the increased rise time. An example of a spike event with pre-foot event is shown (B). Approximately 10% of all spikes recorded from both Sham and DOCA-salt chromaffin cells exhibited this pre-foot event.

A characteristic of some of the oxidation current transients is the presence of a pre-foot event. The pre-foot event originates from the fusion of a vesicle membrane with the cell membrane and partial opening of the fusion pore. This leads to the partial release of the vesicular content[50-51, 54]. An example of a pre-foot event is shown in Fig. 4-6 B. There was no difference in the frequency of occurrence of the pre-foot events for Sham and DOCA-salt cells with approximately 10% of all current spikes exhibiting a pre-foot.

4.2.5 Impaired K^+ Channel Function in DOCA-salt Chromaffin Cells

The literature shows that in animal models of spontaneous and salt-sensitive hypertension, there is impaired K^+ channel function in nerves supplying blood vessels[203-204]. The data show that there is a greater number of catecholamine molecules secreted and that release is significantly prolonged for DOCA-salt chromaffin cells. In other words, there are a greater number of vesicles releasing their content in DOCA-salt cells per stimulus. We hypothesized that this could be due to impaired K^+ channel function[94-97, 204]. To test this, experiments were conducted in the absence and presence of different K^+ channel antagonists: paxilline (0.5 μM), 4-aminopyridine (1 mM), apamin (0.1 μM) and glibenclamide (50 μM). We also used the BK channel potassium agonist NS 1619 (100 nM). Due to vesicle depletion, control experiments showed that there is approximately a 50% reduction in the charge evoked by the second (S2) of two ACh stimuli (S1 and S2) applied to a cell. Therefore, experiments were performed in a paired manner with ACh-induced secretion from individual cells being recorded in the absence and presence of a specific K^+ channel antagonists with a 20 min delay between the first and second ACh stimulation. A summary of the results can be found in Table 4-4. Paxilline (BK antagonist) and glibenclamide (ATP-sensitive) both increased the total number of release events as well as the total charge detected (total number of catecholamine molecules oxidized) from Sham cells but not from DOCA cells. 4-AP (voltage-gated K^+ channels) and apamin (SK) did not affect catecholamine release from either cell type. NS 1619 (BK agonist) effectively decreased secretion in Sham cells (Fig. 4-7 A-D), however it had no effect on DOCA-salt secretion. Figure 4-7 (E & F) also shows two amperometric recordings from a Sham cell before and after paxilline

Table 4-4. Summary of potassium channel agonist and antagonist effects on secretion. Data is provided as the response of a second ACh stimulation (S2) normalized to an initial ACh stimulation (S1). Statistical differences for drug effects are determine versus control experiments with no drugs present.

	DOCA total charge detected	Sham total charge detected	DOCA # of release events	Sham # of release events
Control	**0.73 ± 0.07** "n" = 8	**0.60 ± 0.18** "n" = 9	**0.79 ± 0.12** "n" = 8	**0.55 ± 0.11** "n" = 9
Paxilline	**0.81 ± 0.08** "n" = 10	**2.1 ± 0.54*** "n" = 12	**0.89 ± .05** "n" = 11	**1.7 ± 0.31*** "n" = 12
NS 1619	**0.67 ± 0.16** "n" = 12	**0.28 ± 0.08*** "n" = 14	**0.81 ± 0.24** "n" = 12	**0.27 ± 0.07*** "n" = 13
Glibenclamide	**1.1 ± 0.23 "n" = 12**	**2.4 ± 0.62*** "n" = 12	**1.0 ± 0.31** "n" = 12	**2.3 ± 0.73*** "n" = 12
4-AP	**0.81 ± 0.10** "n" = 11	**1.3 ± 0.63** "n" = 12	**0.91 ± 0.11** "n" = 11	**1.3 ± 0.41** "n" = 12
Apamin	**0.80 ± 0.19** "n" = 12	**0.37 ± 0.09** "n" = 11	**0.60 ± 0.12** "n" = 12	**0.51 ± 0.11** "n" = 11

Data are mean + S.E.M; "n" is the number of cells, which is also the number of amperometric recordings obtained. (*P < 0.05 vs. control values within a given animal group, Student's *t* test).

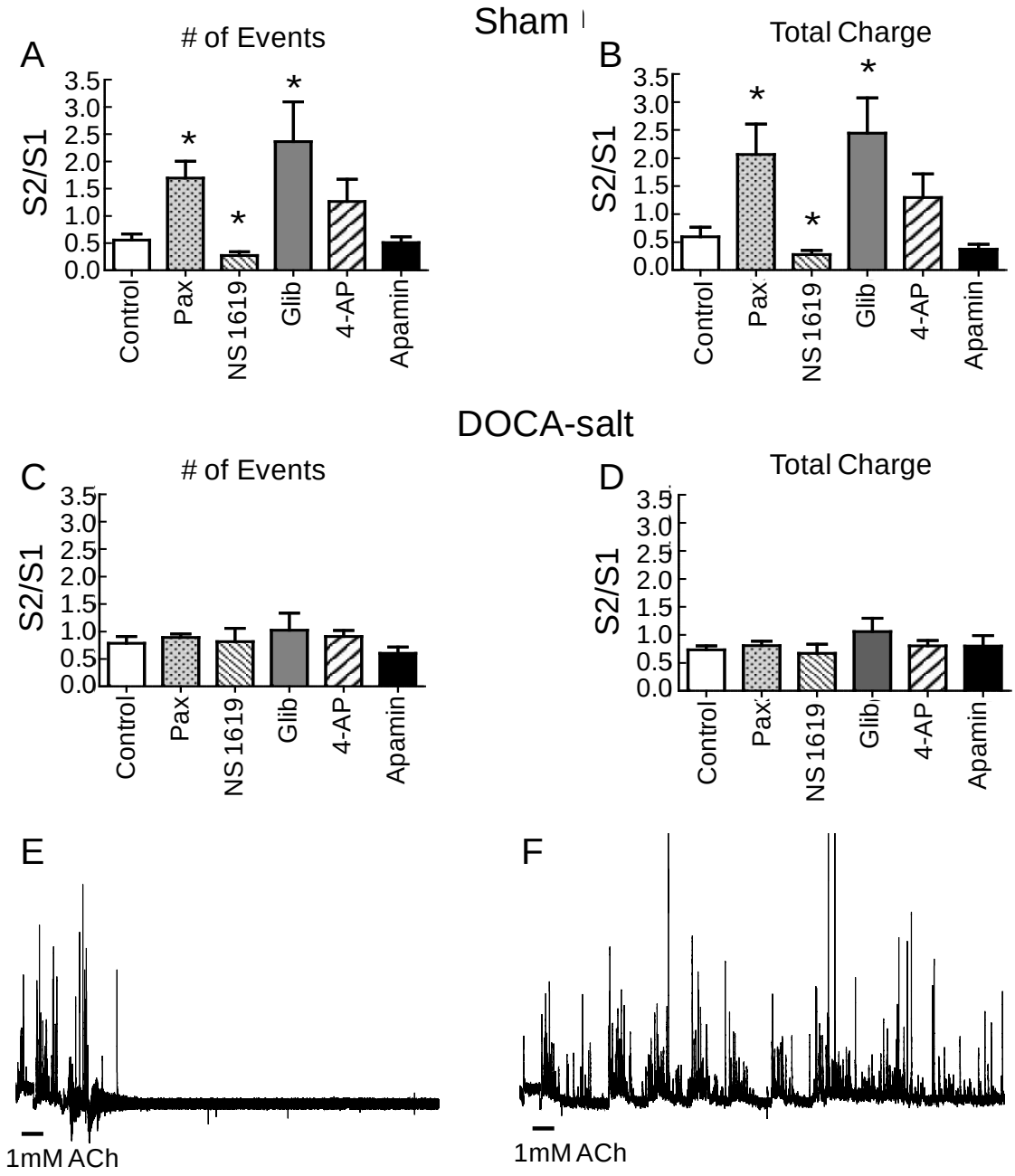

Figure 4-5. Some K^+ channel antagonists alter catecholamine release kinetics in chromaffin cells from Sham but not DOCA-salt rats. Cells were stimulated with 1mM ACh and then after a 20 min interval they were stimulated a second time with ACh. Data are the ratio of the second (S2) stimulation to the first (S1). The control bars were obtained from cells that were not treated with a K^+ channel blocker showing baseline depletion of catecholamine content. Paxilline (BK channel blocker) and glibenclamide (ATP-sensitive channel blocker) caused an increase in the number of release events and total charge detected compared to the control (A, B) ($P < 0.05$, 1-way ANOVA). To

Figure 4-5 (cont'd). check if the BK channel function properly in Sham cells, the agonist NS 1619 was also applied to cells and caused a decrease in secretion from Sham cells compared to the control (A, B) ($P < 0.05$, 1 way ANOVA). None of the drugs used affected catecholamine release from chromaffin cells from DOCA-salt rats (C, D) ($P > 0.05$). ("n" values for each antagonist represent the number of cells investigated. Sham data "n": Control – 7, Paxilline – 10, NS 1619 – 14, Glibenclamide – 10, 4-aminopyridine – 10, Apamin – 10. DOCA data "n": Control – 8, Paxilline – 10, NS 1619 – 11, Glibenclamide – 12, 4-aminopyridine – 11, Apamin – 12.). Amperometric recordings elicited from 1mM ACh before (E) and after (F) application of the BK channel antagonist Paxilline. Recordings are obtained from a chromaffin cell isolated from a Sham rat. The BK channel antagonist increases the number of release events and the duration of secretion in a similar manner to recording obtained from DOCA-salt chromaffin cells.

treatment. In the presence of paxilline, the number of release events and the duration of secretion are both increased, similar to the secretion profile from DOCA-salt cells (Fig. 4-2 C).

4.3 Discussion

Neuroendocrine chromaffin cells are part of the adrenal gland, which is innervated by the sympathetic division of the autonomic nervous system. Consequently, these cells essentially function as modified postganglionic sympathetic neurons. In our prior work studying sympathetic neuroeffector transmission to arteries and veins, we used electrochemical methods to measure NE concentrations at the adventitial surface of the blood vessel[35, 149]. In these measurements, an oxidation current is measured that reflects the extracellular NE concentration in the vicinity of the recording electrode. This concentration is contributed to by release from many nearby sympathetic varicosities. In such measurements, it is impossible to decouple the neurotransmitter release step (vesicle extrusion) from prejunctional autoinhibition, reuptake and diffusion.

Chromaffin cells serve as a viable model for sympathetic neurons and their use in these studies allowed us to investigate disease-induced alterations in catecholamine release.

In related work, Miranda-Ferreira *et al*.[102] monitored chromaffin cell secretion using continuous amperometry and found that for cells isolated from spontaneously hypertensive rats (SHR), a greater number of catecholamine molecules are released per stimulus from diseased cells as compared to controls. Their work also indicated that catecholamine secretion is altered in chromaffin cells isolated from SHR[102]. Our results in the DOCA-salt model of salt-sensitive hypertension corroborate their findings and provide new mechanistic insights as to a cause for the altered release; impaired K^+ channel function.

Whole tissue levels of NE and EPI are elevated in adrenal medulla isolated from hypertensive compared to normotensive rats, consistent with previous reports for SHR[83] and DOCA-salt rats[205]. There were, however, no differences in metabolite levels of NMN, MN and DHPG, between the two groups. These results indicate that metabolic degradation pathways for NE and EPI are not altered in medulla from DOCA-salt hypertensive rats. Therefore, a change in metabolism is not the cause for the increased number catecholamine molecules detected from DOCA-salt cells[206]. However, there is a clear build up of catecholamines in the adrenal medulla. It is believed that the majority of catecholamine metabolism occurs in the cytoplasm after leakage from vesicles or extracellular re-uptake[77]. This would suggest that the

increased catecholamine content must be building up somewhere inside the cell other than the cytoplasm, which would most likely be inside the storage vesicles.

Catecholamine release from DOCA-salt adrenal chromaffin cells was evoked by both ACh and high extracellular K^+. ACh release from preganglionic sympathetic nerves, acting at nAChRs, is the endogenous stimulant of catecholamine release from chromaffin cells[189, 207]. When cells were stimulated with ACh *in vitro,* the frequency of individual oxidation current spikes, the total number of spikes or release events, and the total number of catecholamine molecules released were significantly greater from DOCA-salt compared to Sham cells. High K^+ depolarizes chromaffin cells, independent of nAChR function, by activating L-type Ca^+ channels[119]. The fact that catecholamine release was not different between high K^+ and ACh stimulation confirms that the increased secretion is not due to altered pathways associated with nAChR activation or increased expression of this receptor.

The oxidation current spikes correspond to release from individual vesicles. Our results suggest that catecholamine-containing vesicles in DOCA-salt chromaffin cells contain a greater catecholamine molecule loading than do vesicles in Sham cells. It was also found that the rate of extrusion is more rapid from DOCA-salt cells compared to Sham cells, as evidenced by a decreased $t_{1/2}$ of the current spikes in the former for ACh stimulation[41, 50-51, 53-54, 190]. Consistent with the greater loading is the increase

in apparent vesicular radius based on the greater $Q^{1/3}$ value for the DOCA-salt cells. The increased current rise slope is indicative of a greater catecholamine concentration gradient between the sites of release and the recording electrode. This makes sense as vesicles appear to possess greater catecholamine loading in the DOCA-salt cells and would therefore be expected to release more catecholamine molecules into the extracellular space as compared to Sham controls. According to published work, which shows that adrenal chromaffin cell vesicles maintain a constant catecholamine concentration with varying vesicle size[208], it would be expected to observe an increase in the vesicle radius with a greater number of packaged catecholamines (*i.e.,* volume to accompany the increased loading). This was in fact observed. A limitation of our study, however, is that we have no microscopic evidence to confirm the suspected increase in vesicle radius.

In addition to NE and EPI, the vesicular matrix also contains chromogranin A, ATP (~120 mM), Ca^{2+} (17-30 mM) and ascorbate (~20 mM)[40, 190]. Vesicles of larger radii would have an increased membrane surface area. This could provide more points of contact with SNARE proteins located in the cellular membrane. SNARE proteins facilitate secretion by overcoming the natural repulsion energies of the vesicle and cell membrane, and promote docking and fusion[209]. It has also been shown that membrane tension and fusion pore length facilitate spontaneous fusion pore dilation[210-211]. More docking points would increase the probability of vesicle extrusion and this could be a cause for the greater number extruding vesicles (per stimulus) in DOCA-salt cells.

An additional cause for the increased secretion from DOCA-salt cells could be a greater number of vesicles available in the readily-releasable pool as chromaffin cells maintain several storage pools[54, 212]. Previously published work has shown that glucocorticoid treatment of adrenal chromaffin cells increases coupling of voltage-gated Ca^{2+} channels to the readily releasable pool of vesicles[73]. Our study was not focused on determining if the size of the vesicle pools is altered in DOCA-salt hypertension.

To better understand the cause for the prolonged release (*i.e.* increased number of vesicles undergoing exocytosis) seen for DOCA-salt cells, we tested the hypothesis that there is impaired K^+ channel function. These transmembrane channels play a crucial role in returning a depolarized cell to the resting state. Rat chromaffin cells express a diversity of Ca^{2+}-dependent K^+ channels, including voltage-independent, small-conductance, apamin-sensitive SK and two variants of voltage-dependent, large-conductance BK channels[213]. To test this hypothesis, we performed single-cell electrochemical measurements in the presence of various antagonists and an agonist to determine to role of K^+ channels in modulating catecholamine release. We hypothesized that one or more K^+ channels become impaired in this model of hypertension and this contributes to increased catecholamine secretion due to the inability of the cell to timely repolarize. We found that BK and ATP-sensitive K^+ channel function is in fact impaired in chromaffin cells from DOCA-salt rats. However, to verify

that the receptors are functional in Sham cells, we used the BK channel agonist NS 1619 and found that activating BK channels caused a decrease in secretion from Sham cells, yet had no effect on DOCA-salt cells. This impairment leads to the prolonged release from DOCA-salt cells. However, the cause for the impaired channel function is still unknown. It is possible that Ca^{2+} channels may be up-regulated in DOCA-salt hypertension causing more Ca^{2+} to enter the cell compared to healthy controls. This, however, seems unlikely based on a previous study in which no changes in Ca^{2+} handling were observed in chromaffin cells from spontaneously hypertensive rats[214]. Another possibility is oxidative stress. We have previously found that reactive oxygen species levels, mainly O_2^-, are elevated in perivascular sympathetic nerves in DOCA-salt hypertension and impaired prejunctional α_2-AR function is linked to the presence of O_2^-[36]. O_2^- may disrupt the secretory mechanism in the adrenal chromaffin cells from DOCA-salt rats.

4.4 Conclusions

1) There is increased catecholamine secretion from adrenal chromaffin cells in DOCA-salt hypertension. This leads to the increased circulating catecholamine levels known in DOCA-salt hypertension. Increased circulating catecholamines would contribute to increased vasoconstriction and blood pressure elevation.
2) These cells essentially function as modified postganglionic sympathetic neurons. The increased number of catecholamine molecules released per stimulus, the more rapid rate of extrusion and the greater number of vesicles undergoing

extrusion in DOCA-salt cells likely mimics what happens in perivascular sympathetic nerves supplying arteries and veins. Clearly, there is impaired exocytotic release of catecholamines in this model of hypertension and this likely contributes to increased vasomotor tone.

3) A cause for the greater number of vesicles undergoing extrusion and their prolonged release is impaired BK and ATP-sensitive K^+ channel function. Although measurements of release from individual sympathetic nerve varicosities are not possible, the adrenal chromaffin cell may be a suitable surrogate for further investigations of changes in catecholamine release in the sympathetic nervous system in hypertension.

Chapter 5

Causes for Increased Catecholamine Secretion from DOCA-salt Chromaffin Cells

5.1 Introduction

The *in vitro* electrochemical experiments described in Chapter 4 revealed alterations in catecholamine secretion from DOCA-salt chromaffin cells. Greater catecholamine levels were secreted per exocytotic event, as evidenced by the increased peak charge, and release were more prolonged in cells from DOCA-salt animals. The work reported in this chapter probed the causes of the impaired signaling. In Chapter 4, catecholamine metabolism, altered Ca^{2+} handling and or potassium channel dysfunction were hypothesized as possible explanations for the altered signaling in DOCA-salt chromaffin cells. HPLC analysis revealed that catecholamine metabolism is unchanged in the DOCA-salt adrenal medulla. However, as is detailed herein, impairments were discovered in BK and ATP-sensitive potassium channels in DOCA-salt chromaffin cells. These studies provided important evidence to explain the increased secretion frequency of DOCA-salt chromaffin cells.

Calcium entry into excitable cells is crucial to facilitate excocytosis[58, 61, 99]. In fact, contributions from extracellular and intracellular sources are important in adrenal chromaffin cells to promote catecholamine secretion[58, 189, 215]. Calcium is such an important factor in exocytosis that it has been considered as a possible mechanism for

alterations in secretion patterns in hypertension[214]. In chromaffin cells, calcium entry occurs after stimulation by ACh. Calcium entry helps to produce an action potential which is required to induce secretion[98]. It is possible to monitor calcium as it enters the cell by loading a cell with a fluorescent probe. The probe Fluo-4 AM was used to determine if there are any differences in Ca^{2+} handling in DOCA-salt chromaffin cells. Results from these studies are reported herein. Fluo-4 AM fluorescent intensity increases upon binding with calcium providing a convenient method for monitoring calcium flux into a cell which has been previously loaded with the dye.

Another important physiological process that has been found to disrupt sympathetic nerve signaling in DOCA-salt hypertension is superoxide production[36]. Superoxide is naturally produced via NADPH and its expression in nerves is up-regulated in this model of hypertension[9] Variations in superoxide levels have been found in a number of different diseases including Alzheimer's, diabetes and cancer[216-218]. It is possible that the secretion pattern differences observed for DOCA-salt chromaffin cells may be related to increased super oxide levels. This possibility was tested using the NADPH-oxidase inhibitor, apocynin[13]. NADPH-oxidase produces superoxide, so by inhibiting the enzyme, the negative effects associated with superoxide should be decreased. To do this, apocynin (2mM) was chronically administered to Sham and DOCA-salt animals (4 week administration) in parallel with a group of Sham and DOCA-salt animals that did not receive apocynin. This provided

information on how antioxidant treatment affected normotensive and hypertensive animals.

The results address three possible causes for the altered chromaffin cells secretion. These studies provided important information related to our working model of sympathetic neurogenic control of vascular tone in DOCA-salt hypertension.

5.2 Results

5.2.1 Calcium Flux into Sham and DOCA-salt Chromaffin Cells

Calcium flux into adrenal chromaffin cells is a critical component of exocytosis. Fluorescence studies were performed to monitor calcium entry into chromaffin cells isolated in culture. Calcium entry was evoked by stimulation with ACh (100µM) and high potassium (70 mM). Cells were isolated onto coverslips as previously described and allowed to equilibrate for 1-2 hours. As outlined in Chapter 2, cells were incubated with Fluo-4 AM for 30 min. Following incubation, cells were placed in a bath with HEPES buffer continuously flowing through. An initial background collection was performed for 10-15 s followed by stimulation with either ACh or high potassium for 2-2.5 min. Calcium influx was measured as an increase in fluorescence intensity over time.

Figure 5-1 shows the fluorescence profiles for ACh stimulation of Sham and DOCA cells. The profiles show average and standard error values for measurements of 35-40 cells from 4 Sham and 4 DOCA rats. Fluorescence intensities for individual cells were grouped together for each animal. Figure 5-1 shows the average fluorescence

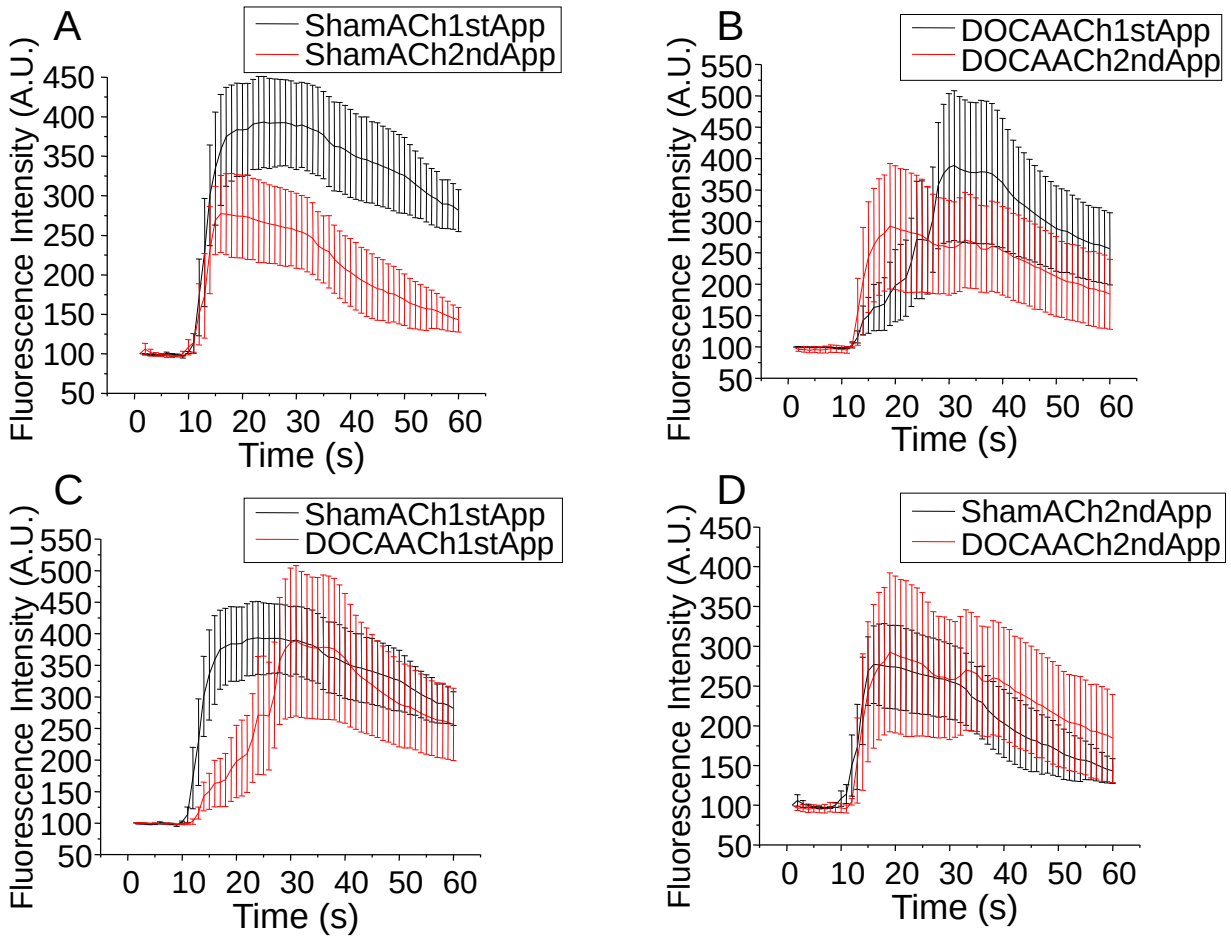

Figure 5-1. Fluo-4 AM fluorescence intensity profiles for two successive stimulations of (A) Sham and (B) DOCA-salt cells in response to 100 µM acetylcholine. The Sham and DOCA-salt cell responses are overlaid for (C) the first stimulation and (D) the second stimulation.

profiles for (A) Sham and (B) DOCA cells during a first and second application of ACh. Fluorescence intensity profiles for Sham and DOCA-salt cells after the (C) first and (D) second application of ACh are also provided. At first glance the fluorescence intensities for Sham cells after the second stimulation with ACh appear to be lower than after the first stimulation. Also, the fluorescence intensities for the first stimulation of DOCA-salt cells appear to have a slower temporal increase cells stimulated for a second time with ACh. Figure 5-2 provides the same data as Figure 5-1 using high K^+ as the secretory

stimulant rather than ACh. However, statistical comparisons did not reveal any significant differences between the fluorescence intensity profiles for Sham or DOCA-salt cells, regardless of the chemical stimulant (Figs. 5-1 & 5-2) The results indicate no difference in calcium handling for Sham and DOCA chromaffin cells ($p>0.05$ 2-way ANOVA). Therefore, the greater levels of catecholamines secreted and the prolonged secretion seen for DOCA-salt chromaffin cells appear not to be linked with alterations in calcium handling.

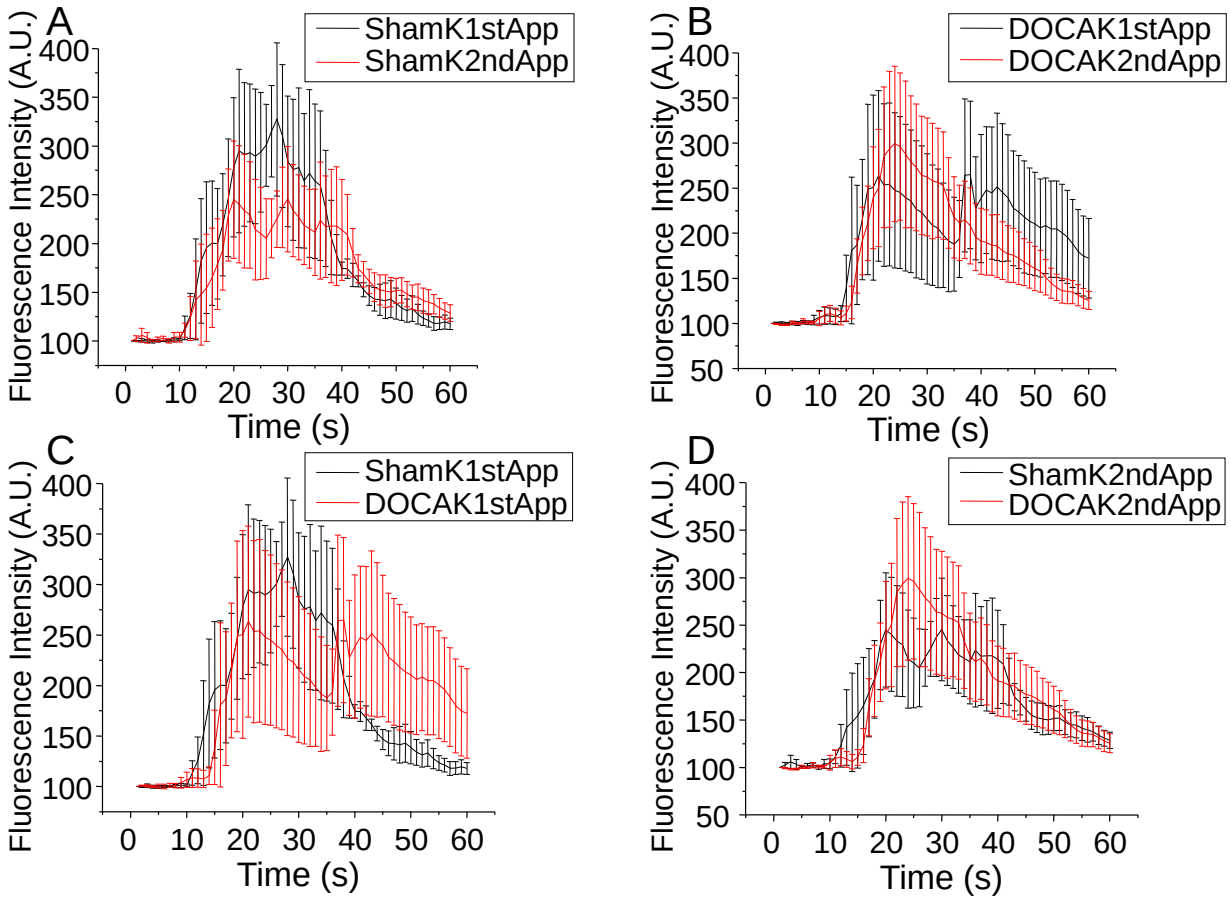

Figure 5-2. Fluo-4 AM fluorescence intensity profiles for two successive stimulations of (A) Sham and (B) DOCA-salt cells in response to 70 mM potassium. The Sham and DOCA-salt cell responses are overlaid for (C) the first stimulation and (D) the second stimulation.

5.2.2 Reactive Oxygen Species Involvement in the Pathogenesis of DOCA-salt Hypertension

Oxidative stress and inflammation are inextricably linked and are associated with spontaneous and salt-sensitive hypertension[36, 219-220]. Excess reactive oxygen species cause serious alterations to the natural biological function of various systems within the body[217, 221-222]. Previous work in our group has found links between oxidative stress and impaired sympathetic nerve function in mesenteric arteries[36]. Based on these results, we hypothesized that the altered potassium channel function in the DOCA-salt chromaffin cells may be linked to oxidative stress, specifically elevated super oxide levels. We tested this hypothesis by chronically administering 2mM apocynin to Sham and DOCA-rats (n=4 for each) over a 4-week period. In the DOCA-salt model, mean arterial pressure increases progressively over a period of several weeks and by week-four, the test animals have the fully developed disease[223]. In parallel, a group of Sham and DOCA-rats (n=4 for each) were treated identically over a four-week period but without drug administration.

Apocynin is a known inhibitor of NADPH oxidase, which generates superoxide[224]. Chronic treatment with apocynin has been shown to delay the elevation of blood pressure and restore α_2-AR function in DOCA-salt rats[223]. Thus, if oxidative stress exists in the chromaffin cells exists and NADPH oxidase is the source, then

inhibiting NADPH oxidase apocynin should cause a decrease the availability of superoxide, possibly restoring more normal potassium channel function.

After rats underwent a uninephrectomy and were implanted with a DOCA mineralcorticosteroid pellet, they were allowed 1-2 days of recovery before beginning apocynin treatment. The drug was administered ad libitium in the animals' drinking water. Water intake was monitored over the course of treatment to determine how apocynin affected water consumption. Animals were housed 2 per cage, with 2 cages of non-treated and 2 cages of treated rats (Sham and DOCA). To determine water intake, the average amount of water consumed per day was recorded, averaged, and normalized to the number of animals in the cage (mL/day-animal). Determining the water intake is critical as this parameter controlled the amount of the drug administered to each animal. The data obtained for the untreated and apocynin-treated animals were pooled into separate groups for analysis. Statistical analysis was accomplished using a simple student's *t* test. The average water intake per animal was not statistically different for Sham treated and untreated animals. DOCA-salt rats being treated with apocynin drank more water than their control counterparts that did not receive any drug (Table 5-1). In general there was a significant increase in the water consumed by the DOCA-salt animals compared to their Sham counterparts by a factor of 3-4x.

Animals also had their weight and blood pressure recorded the week of experiments (*i.e.,* the week of sacrifice). At the four-week mark, Sham untreated and apocynin-treated control rats had nominal MAP of 132 ± 4 mmHg and 136 ± 1 mmHg,

Table 5-1. Summary of mean arterial pressure, weight and water intake data for untreated and apocynin-treated Sham and DOCA-salt rats

	Blood Pressure (mmHg)	Weight (g)	Water Intake per animal per day (mL/day-animal)
Sham	131 ± 3.92	443 ± 16.03	40 ± 1.0
Sham with Apocynin	136 ± 1.47	419 ± 22.56	42 ± 1.3
DOCA	176 ± 7.86^*	376 ± 12.34*	114 ± 5.29^*
DOCA with Apocynin	186 ± 6.60^*	370 ± 9.22*	151 ± 10.4^*

*** p < 0.05 vs Sham, Student's *t* test**

^p < 0.05 vs Sham with Apocynin Treatment, Student's *t* test

and their weights were 443 ±16 g and 419 ± 23 g, respectively. There were no statistically significant differences between MAP and body weight of apocynin-treated and untreated Sham control rats. In contrast, untreated and apocynin-treated DOCA-salt rats had statistically higher MAPs than the Sham rats. DOCA-salt untreated and apocynin-treated animals had MAP of 176 ± 8 mmHg and 186 ± 7 mmHg and body weights of 376 ±12 g and 370 ± 9 g, respectively. An unexpected observation was the MAP of the apocynin-treated DOCA-salt animals was not reduced as compared to the untreated animals. Previous work in the group showed that the MAP is reduced during weeks two and three of DOCA-salt hypertension development with apocynin treatment, but these effects disappear in week four[223]. Sympathetic neuronal control mechanisms likely predominate in weeks two and three of the disease pathogenesis in this model and, therefore, apocynin treatment is most effective at lowering blood pressure during this period. At the four-week mark, there is likely significant vascular remodeling and

vessel resistance is likely the dominant factor controlling blood pressure. Apocynin treatment is rather ineffective at reducing these vascular structural alterations and, therefore, the drug has little impact on MAP. In retrospect, we should have conducted these studies using three-week rather than four-week animals. Table 5-1 presents a summary of the MAP and body weight data for untreated and apocynin-treated Sham and DOCA-salt rats

Each day, two Sham or DOCA-salt animals were sacrificed, and experiments were performed on a set of untreated and apocynin-treated chromaffin cells. The order of rat sacrifice, treated and untreated animals, was alternated every other day to account for bias that would be introduced by always sacrificing in the same order. In order to understand how superoxide levels are affected by apocynin treatment, chromaffin cells were stained with the superoxide indicator, dihydroethidium (DHE). The indicator is cell membrane permeable and upon oxidation by superoxide it binds to DNA becoming membrane-impermeable, staining its nucleus a bright fluorescent red. DHE can be used to image cells and tissues for superoxide activity[223]. Continuous amperometric measurements were performed on single cells to determine the effect of apocynin. Chromaffin cells were isolated as previously described and plated on coverslips (two coverslips containing untreated cells and two coverslips containing treated cells). Since it was impossible to run four sets of microscopic and amperometric measurements in a single day, we chose to run the Sham untreated and treated together and DOCA-salt untreated and treated together. Comparison of superoxide levels across Sham and DOCA-salt groups could not be performed due to the day-to-

day variability of the microscopy settings as apocynin treatment intensities were normalized to the non-treated fluorescent intensities obtained within the same day. When treated and untreated Sham cells were compared using a student's *t* test, the apocynin-treated cells had higher fluorescence intensity than their untreated counterparts (Table 5-2). However, there was no statistical difference between DOCA-

Table 5-2. Summary of DHE fluorescence intensities for superoxide activity in untreated and apocynin-treated Sham and DOCA-salt chromaffin cells.

	Untreated	Apocynin-Treated
SHAM 2	100 ± 9 (n=6)	80 ± 10 (n=4)
SHAM 3	100 ± 3 (n=11)	136 ± 22 (n=10)
SHAM 4	100 ± 5 (n=9)	172 ± 19* (n=16)
AVG Sham	100 ± 3	143 ± 14*
DOCA 1	100 ± 12 (n=7)	138 ± 22 (n=9)
DOCA 2	100 ± 7 (n=6)	100 ± 13 (n=7)
DOCA 3	100 ± 8 (n=11)	70 ± 5* (n=12)
DOCA 4	100 ± 11 (n=11)	63 ± 10* (n=13)
AVG DOCA	100 ± 5	88 ± 8

*** p <0.05 vs untreated data, Student's *t* test n = number of cells investigated per animal. Fluorescence intensities for each pair of data are normalized to the average fluorescence intensity obtained for untreated chromaffin cells.**

salt treated and untreated cells (Table 5-2). This suggests that apocynin treatment increases superoxide production in Sham chromaffin cells, yet has no effect on DOCA-salt cells. However, after re-examining each animal individually, it was found that only one set of Sham cells (Sham 4) had an increase in fluorescence intensity that was statistically different from data for apocynin treated cells as compared with the other Sham sets of data. Also it was found that two DOCA-salt sets of data show a decrease in fluorescent intensity that is statistically significant even though the average of all four DOCA-salt animals was showed no difference between untreated and apocynin-treated values (Table 5-2). These results are somewhat inconclusive, and lead to the data being reported, but drawing significant conclusions from it is unwise.

Continuous amperometric measurements were also made to determine the effects of antioxidant treatment on catecholamine secretion from single chromaffin cells. Plated chromaffin cells were placed in a flow bath as described in Chapter 4. Secretion was stimulated using a pressurized burst of 1mM ACh. It was found that apocynin treatment had no effect on the amount of catecholamines secreted per exocytotic event, the total number of release events per stimulus or the duration of release events in cells from Sham animals. Table 5-3 summarizes the number of release events per stimulus, the charge per release event and the total number of catecholamine molecules oxidized per stimulus, which is directly calculated from the peak charge. Apocynin treatment also had no effect on the number of release event per stimulus in cells from DOCA-salt animals, although there does appear to be a reduction in the number of events based comparison of the nominal values. Treatment does reduce the charge per stimulus and

the catecholamine molecules oxidized per stimulus to levels similar to those for cells from Sham controls.

Table 5-3. Summary of continuous amperometric data from single chromaffin cells isolated from untreated and apocynin-treated Sham and DOCA-salt animals.

	Events per stimulus	**Total Charge per stimulus (pC)**	**Total Catecholamine molecules oxidized per stimulus (10^8)**
Sham			
Untreated (n=12)	27 ± 4.2	18 ± 3.8	0.6 ± 0.1
Apocynin-Treated (n=15)	34 ± 5.2	26 ± 5.2	0.7 ± 0.2
DOCA-salt			
Untreated (n=13)	42 ± 5.0*	35 ± 4.3*	1.2 ± 0.1*
Apocynin-Treated (n=16)	34 ± 6.7	21 ± 3.8#	0.7 ± 0.1#

*** p <0.05 vs Sham cells, treated versus untreated data, Student's *t* test**
 # p <0.05 vs DOCA-salt cells, treated versus untreated data, Student's *t* test

Individual secretory events were also unchanged by apocynin treatment in Sham animals. Apocynin treatment caused a decrease in the quantal charge and half-width values for individual release events. A summary of the kinetic data is provided in Figure 5-3.

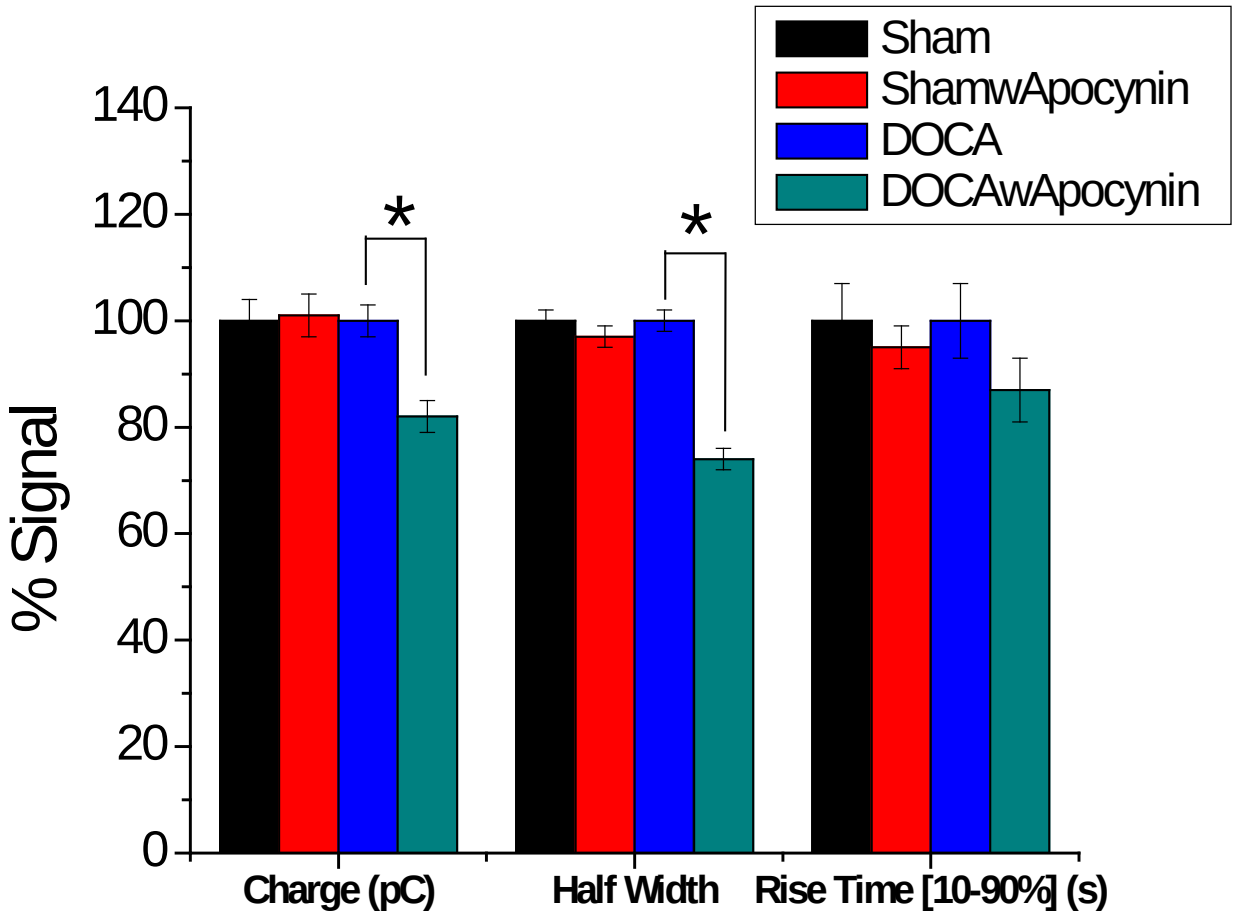

Figure 5-3. Summary of apocynin treatment on individual release events from chromaffin cells isolated from Sham and DOCA-salt animals. Apocynin treatment decreased the charge and half-width for individual secretory events from DOCA-salt chromaffin cells as compared to non-treated DOCA-salt cells. Apocynin treatment had no effect on individual secretory events from Sham chromaffin cells.

Taken together these data suggest that superoxide may not play a role in the alterations found in DOCA-salt chromaffin cell secretion. Apocynin treatment did not lower the blood pressure of DOCA-salt rats at least at the four-week point in the time course of the disease when these measurements were made. The data described in

this chapter also suggest that apocynin treatment causes a decrease in the quantal charge for individual release events in DOCA-salt cells. This decrease in charge detected is also evidenced over the course of secretion, which is evidenced by the decrease in total catecholamine molecules released per stimulus for untreated and treated DOCA-salt cells. These data show a decline in catecholamine packaging in DOCA-salt cells when treated with apocynin. Release frequency remains unchanged providing evidence that the alterations found in potassium channel function is most likely unrelated to elevated superoxide levels.

5.3 Discussion

The goals of this chapter were to further probe the causes for the impaired catecholamine secretion characteristic of DOCA-salt chromaffin cells. As mentioned earlier, calcium plays an important role in exocytosis. It is possible that an increase in calcium flux during depolarization is a cause for the increased secretion. Using the calcium fluorescence probe, Fluo-4 AM, to visualize calcium influx into chromaffin cells upon stimulation, we found no clear differences in calcium handling between the two cell types regardless of whether ACh and high potassium were used for stimulation. It should be noted these experiments suffered from high variability between samples that complicated the analysis. Our findings are not in agreement with similar studies performed using spontaneously hypertensive rats by the Garcia group[225]. They found that there are higher basal levels of calcium in the cytosol and mitochondria in adrenal slices from spontaneously hypertensive rats compared with normotensive controls. Garcia *et al.* also found that after stimulation with ACh or high potassium, spontaneously hypertensive rats show a greater peak in calcium levels and have a

slower time course of calcium clearance as compared to normotensive controls. The Garcia group employed an internal standard for calibration in each fluorescence experiment. We did not take these measures, which may have contributed to large variability in our measurements and lack of statistical difference between DOCA-salt and Sham chromaffin cell calcium handling. It is important to note that the slow time course of calcium clearance found by the Garcia group supports the impairment in potassium channel function found in our work.

Another possible explanation for the impaired secretion in DOCA-salt chromaffin cells that was tested was elevated superoxide levels in the cells which leads to oxidative stress. Elevated levels of superoxide have been linked to alterations in sympathetic neuroeffector transmission in DOCA-salt hypertension[36, 220, 226]. The NADPH oxidase inhibitor apocynin was given to Sham and DOCA-salt rats to inhibit the generation of superoxide. A complete investigation into blood pressures, animal weights, superoxide levels as measured with DHE fluorescence levels and chromaffin cell neurotransmission yielded interesting results. It was found that apocynin treatment, at least at the four-week point in time course of the disease, had no effect on the blood pressure in DOCA-salt or Sham rats. Previous work in our lab showed that chronic apocynin treatment of DOCA-salt rats lowered blood pressure at the two- and three-week points in the time course of the disease, as compared to untreated rats[223]. The antioxidant treatment was less effective at the four-week point in the time course of the disease[223]. The results reported herein for cells from animals at the four-week point in the time course of

the disease revealed no statistically significant difference in superoxide levels for apocynin-treated and untreated Sham or DOCA-salt rats. In retrospect, these studies should perhaps have been performed using two- or three-week animals. Continuous amperometric data indicated that apocynin treatment did not change the total amount of catecholamines released per secretion event, the number of release events per stimulus and the individual secretory event kinetics in Sham cells. Apocynin treatment did appear to affect some aspects of secretion from DOCA-salt chromaffin cells. Apocynin caused a decrease in the total number of catecholamine molecules released per stimulus in DOCA-salt cells as well as the total number released over a 60 s experiment as compared to untreated controls. There was no change in the release frequency however. One interpretation of the results is that by some mechanism, apocynin decreases the number of catecholamine molecules packaged into vesicles. It is unclear though if this is a direct effect of apocynin. Catecholamine packaging into chromaffin vesicles is dependent on the intercellular pH[199]. Any change in superoxide levels would change the intercellular pH. The most interesting finding was that antioxidant treatment had no effect on the number of release events per stimulus in DOCA-salt chromaffin cells. This suggests that the impairments found in potassium channel function are not linked to superoxide levels. A significant complicating effect was the fact that apocynin treatment did not reduce blood pressure in the DOCA-salt rats. Taking all the results together, it is concluded that at least in the four-week animals, elevated superoxide levels do not exist in DOCA-salt chromaffin cells, as compared to Sham controls, and that superoxide levels are not the cause for impaired potassium channel function.

5.4 Conclusions

1) There was no evidence of altered calcium handling in cells from Sham and DOCA-salt animals. These studies did not use a calibration standard.
2) Super oxide levels, based on DHE fluorescence intensities, were not elevated in cells from DOCA-salt animals.
3) Treatment with apocynin had no effect on the number of release events per stimulus, the oxidation charge per stimulus or the total number of catecholamine molecules oxidized in cells from Sham controls. Treatment did reduce the charge per stimulus, the total number of catecholamine molecules oxidized, individual secretory kinetics and quantal charge for individual release events in cells from DOCA-salt animals. Apocynin reduced secretion values to those characteristic of Sham controls. Since the apocynin treatment had no effect on superoxide levels and blood pressure for DOCA-salt rats, these findings are most likely due to intracellular pH being affected by apocynin treatment in DOCA-salt chromaffin cells. pH changes could cause alterations in packaging for individual chromaffin vesicles. Fewer catecholamines packaged into individual vesicles would explain the lower levels of catecholamines released per individual secretory event and over the total time-course of an amperometric recording.

Chapter 6

Fast-Scan Cyclic Voltammetric Detection of Norepinephrine and Epinephrine Secretion from Normotensive and DOCA-salt Hypertensive Chromaffin Cells

6.1 Introduction

Hypertension is associated with heightened sympathetic nerve activity[182-184]. Associated with this heightened activity, elevated levels of the vasoconstrictor, NE, have been measured by continuous amperometry at the adventitia of mesenteric blood vessels[34-35, 125, 149]. Adrenal chromaffin cells have been used in this work as a model for sympathetic neuroeffector transmission. The work provides new insight about how the quantal amount, secretion frequency and individual secretory event kinetics from these cells are altered in DOCA-salt hypertension. These cells release both NE and EPI; however, the continuous amperometric measurements provide information about total catecholamine concentrations secreted, not individual levels. It would be of interest to know if NE and EPI levels released are altered in DOCA-salt hypertension.

Measurements of whole tissue catecholamine levels in the adrenal medulla were made to determine NE and EPI levels. The assumption being that these levels would be reflective of the levels packaged in chromaffin cell vesicles. The results indicated that approximately 85% (8.5/1 ratio of EPI to NE) of the catecholamines in the medulla are EPI for both Sham and DOCA-salt tissues. While useful, these data may not reflect

the level of each transmitter secreted from individual chromaffin cells. To study this, we employed FSCV to distinguish NE and EPI released from individual Sham and DOCA-salt chromaffin cells.

Chromaffin cells are more than just a model for sympathetic neuroeffector transmission. The adrenal medulla is a significant source of circulating catecholamines, specifically EPI[48]. In fact, pheochromocytomas, which are rare tumors of the adrenal medulla, cause large amounts of catecholamines to be released into the blood stream. These tumors are associated with a number of side effects including elevated heart rate and blood pressure. The EPI released acts at alpha and beta adrenergic receptors expressed by the vascular smooth muscle cells and cardiac muscle cells to cause increased heart rate, blood vessel constriction and increased cardiac output, all of which lead to elevated blood pressure. Of particular relevance to this research is the observation that heightened sympathetic nerve activity produces greater release of catecholamines (approximately 25% NE and 75% EPI) into the circulation[227].

Given the significant effects of EPI on body homeostasis, an obvious question to consider is whether or not the levels of EPI and NE secreted from DOCA-salt chromaffin cells are different from the levels released from Sham cells. As mentioned above, rat chromaffin cells produce and secrete EPI at roughly 3x the level of NE[227]. Continuous amperometric experiments reported in Chapter 4 were performed by applying a potential sufficient to detect both NE and EPI released from chromaffin cells

via the oxidation of the hydroquinone moiety of each molecule. Continuous amperometry is an excellent technique for monitoring rapid transient changes associated with neurochemical signals of known origin[228]. Unfortunately, the technique does not provide qualitative information about the identity of the molecule(s) being detected. In other words, all molecules arriving at the recording electrode surface that are oxidizable or reducible will be detected, depending on the detection mode. An alternative approach is fast-scan cyclic voltammetry, which provides a good temporal resolution and allows for the identification of the molecules being detected based on their voltammetric signature.

FSCV has been successfully used to identify and quantify NE and EPI released from bovine and mouse adrenal chromaffin cells[121, 229]. These studies showed that the majority of chromaffin cells secrete primarily either NE or EPI. To date, there have been studies on the effects of hypertension on exocytosis from chromaffin cells[83, 102, 185, 206, 225]. These studies relied on amperometry and HPLC to detect catecholamines released and found a higher number of catecholamines secreted from hypertensive cells. In this chapter the use of *in vitro* fast-scan cyclic voltammetry to compare EPI and NE secretion from Sham and DOCA-salt rat adrenal chromaffin cells is reported.

Control measurements were made using cells from Sham animals. Release was evoked from individual cells using a nitrogen-pressurized, high potassium (70 mM K^+)

bolus, which depolarizes the cells. NE and EPI release were monitored as an oxidation current with a carbon fiber electrode placed adjacent to the cell. The hydroquinone moiety of both molecules is detected as an oxidation current at 0.600 V vs. Ag/AgCl while EPI is distinguished via the oxidation of the secondary amine at 1.425 V. The identification and quantification of NE and EPI is possible by recording cyclic voltammograms between 0.100 - 1.500 V vs. Ag/AgCl at intervals of 16.6 ms for a 30 s period after stimulation. It was hypothesized that the EPI/NE ratio from chromaffin cells is altered in DOCA-salt hypertension.

6.2 Results

6.2.1 Cyclic Voltammetry of Sham and DOCA-salt Chromaffin Cells

In section 4.2.2, continuous amperometric measurements revealed an increase in the levels of catecholamines secreted per release event and prolonged release events for cells from DOCA-salt animals as compared to Sham controls. The amperometric data are reflective of both NE and EPI oxidation and provided no differentiation. Continuous amperometry is a powerful tool for studying small temporal changes, such as individual vesicle secretion, but its use for molecule identification is limited. Cyclic voltammetry, on the other hand, can be used to identify molecules based on their oxidation potential (i.e., voltammetric signature). Scanning a potential range at high scan rates generates a series of voltammograms as a function of time during secretion event. This measurement enables identification of NE and EPI (Chapter 1, Fig. 1-7) as they are released from adrenal chromaffin cells[39, 121, 136]. Experiments were performed at 600 V/s between 0.1 and 1.5 V vs. Ag/AgCl at a frequency of 60 Hz

(16.6 ms per scan). Voltammograms were collected over 30 s and filtered using a two-pole Bessel filter at 2 kHz. 50 Sham cells and 49 DOCA-salt chromaffin cells were studied. The cells were isolated from Sham and DOCA-salt rats that had an average systolic blood pressure of 133 ± 23 mmHg (n=11) and 187 ± 7 mmHg (n=11) respectively.

Before investigating chromaffin cell secretion, 10 µM standards of NE and EPI were analyzed to verify that the identification of both molecules via these redox reactions is possible. Figure 6-2 shows background subtracted voltammograms (full details on background subtraction can be found in Chapter 2) of 10 µM NE and EPI (A & B). It can be seen that NE has only a single oxidation wave, which is associated with the oxidation of the hydroquinone moiety. However, EPI has two oxidation waves: the first is due to the hydroquinone oxidation, and the second is due to the oxidation of the secondary amine. These tests provided validation that it is possible to discriminate NE and EPI based on the presence of the secondary amine oxidation wave.

In Figure 6.1 A, two oxidation peaks are seen for EPI at 0.6 and 1.4 V. The lower potential peak is due to the $2e^-/2H^+$ oxidation of the hydroquinone moiety, while the higher potential peak is due to the $2e^-/2H^+$ oxidation of the secondary amine moiety for EPI. There is only the one oxidation peak at 0.6 V for NE (Fig. 6-1 B). These curves reveal different voltammetric signatures for these two molecules. Recording these voltammograms as a function of time after a stimulus allows for analysis of NE and EPI secreted from chromaffin cells.

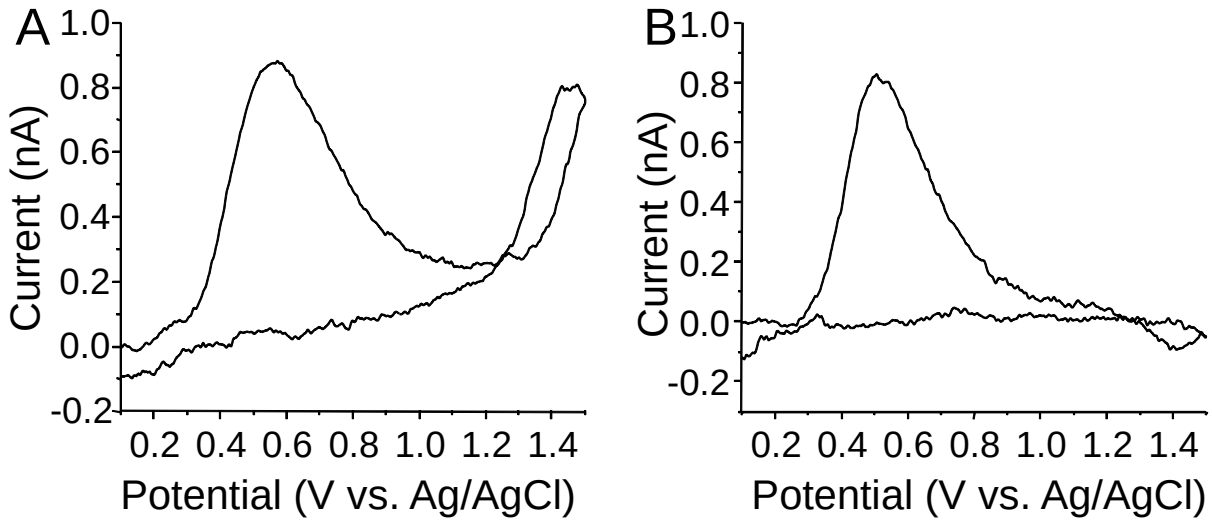

Figure 6-1. Fast-scan cyclic voltammetric curves for 10 µM EPI (A) and NE (B) recorded at 600 V/s from 0.1 – 1.5 V vs. Ag/AgCl at 60 Hz. The supporting electrolyte was Tris-HCl buffer. pH = 7.2.

The voltammetric measurements of single cell secretion were performed in a manner identical to the continuous amperometric experiments. The microelectrode was gently placed in contact with a single chromaffin cell and secretion was stimulated using a high concentration of potassium (70 mM) with voltammograms being collected for 30 s. After collection, the data were converted into an averaged current-time trace between the potentials of 0.55 – 0.65 V and 1.4 – 1.45 V vs. Ag/AgCl, as discussed in Chapter 2. Current-time traces revealed current spikes for hydroquinone and secondary amine oxidations at the two different detection potentials, 0.6 and 1.425 V. Current-time traces for Sham and DOCA-salt cells releasing primarily EPI (A and B) and cells primarily releasing NE (C and D) are shown in Figure 6-2. It can be seen that all current-time traces taken at 0.6 V vs. Ag/AgCl shows current spikes that are associated with the hydroquinone oxidation of both NE and EPI. Tracings, such as those in Figures

6-2 A and B, reveal overlapping current spikes at both potentials indicating this cell is releasing EPI. In contrast, the tracings in Figure 6-2 C and D show primary current spikes at 0.6 V but little at 1.425 V. This indicates this cell is releasing NE.

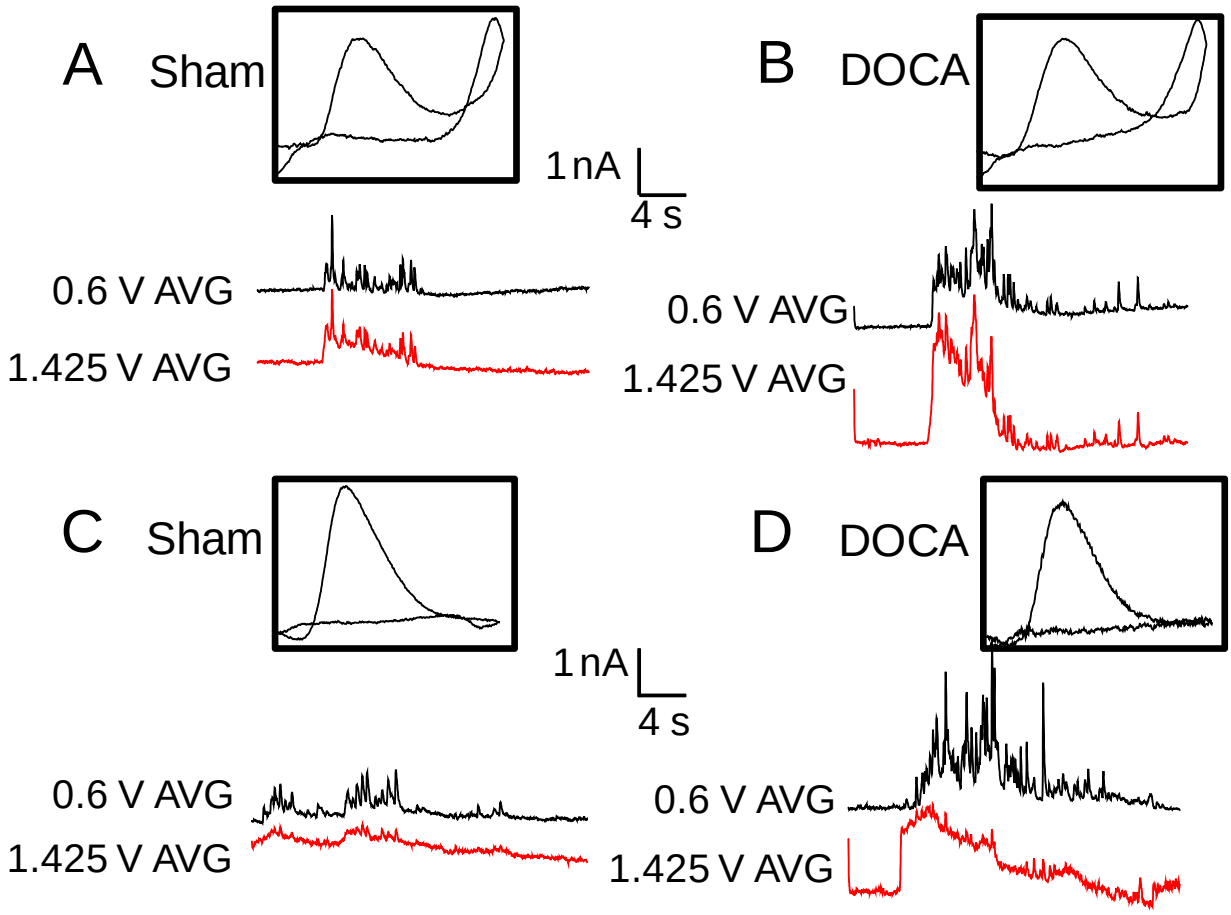

Figure 6-2. Current-time traces obtained via fast-scan cyclic voltammetry. Scale bars are for i-t traces. Representative cyclic voltammograms are shown above each trace to identify the neurotransmitter release from each cell.

It is important to briefly discuss the significance of the current-time traces as shown in Fig. 6-2. Firstly, the oxidation signatures for NE secreting cells appear to be ambiguous. There appears to be small oxidation spikes in the 1.425 V current-time trace seen in Fig. 6-2 C & D. Those spikes are not identified as peaks when the signal is run through the MatLab peak-finding algorithm. The appearance of these "false"-

peaks is the exact reason that the MatLab algorithm was used to select peaks that were significantly different from the baseline signal. By using the algorithm, human bias is removed from data analysis. Another important topic to cover is the magnitude of the current spikes. Prior to each cellular recording, the electrode was cycled in just the flowing buffer to ensure the background current did not change with time (Fig. 6-3). However, no control experiments were performed to calibrate spike intensities into a concentration. These studies were meant to be a qualitative investigation to identify to molecules secreted, but not quantify the amount. For this reason, comparing the relative amplitudes of current spikes between Sham and DOCA-salt cells is not reasonable.

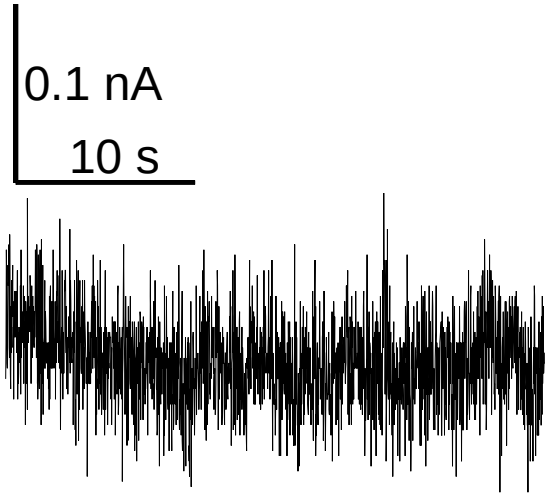

Figure 6-3. Background current-time trace obtained at 0.600 V vs. Ag/AgCl. A background current-time trace is shown for 0.600 V vs. Ag/AgCl reference electrode. The current-time trace was obtained in flowing Tris-HCl buffer prior to cellular recording with no cell near the electrode surface. The background current associated with the experimental conditions used to monitor NE and EPI secretion is roughly 0.1 nA.

A few remarks about how the oxidation spikes were identified relative to background current/noise. As shown in Fig. 6-3, the intrinsic background current

associated with the experimental is approximately 0.1 nA. Recognized current spikes obviously must be distinguishable from this background current. This was accomplished by setting a threshold for the MatLab algorithm that only identified spike that were at least twice the background noise (2x background rsd). A complete explanation of how the peaks associated with secretion events were distinguished from the background noise using MatLab can be found in Chapter 2. Spikes that were detected at both 0.600 V and 1.425 V vs. Ag/AgCl were attributed to EPI. Spikes that were only detected at 0.600 V were attributed to NE.

Cells were categorized as either releasing primarily NE or EPI. Cells were placed into each category if they were found to have at least 90% of the recognized current spikes (MatLab algorithm) assigned to either NE or EPI. 50 Sham cells and 49 DOCA cells were investigated. Table 6-1 shows an overview of the distribution of NE, EPI and mixed release cells. It was found that 26% of the Sham cells were primarily NE (>90% NE) secreting and 74% were primarily EPI (>90% EPI) secreting. Similarly, it was found that 29% of the DOCA-salt chromaffin cells were NE secreting, 69% were EPI secreting, but 2% (1 cell) showed evidence of both NE and EPI secretory spikes.

Data for the one single cell that appeared to be releasing both NE or EPI are shown in Figure 6-4 A-C. Figure 6-4 A shows the current-time traces from the voltammetric data at 0.600 V (top) and 1.425 V (bottom) vs. Ag/AgCl. Many of the current spikes seen at 0.6 V have a corresponding spike at 1.45 V (Fig. 6-4 C). These are attributed to EPI release. There are also a few current spikes at 0.6 V that have no

corresponding peak at 1.45 V which are attributed to NE (Fig. 6-4 B). This cell was determined to be releasing both NE and EPI. Such a cell was found only once out of the 99 cells investigated in this study.

Table 6-1. Summary of the blood pressure and weight of the Sham and DOCA-salt animals. Data for the type of catecholamine-releasing chromaffin cell identities.

	Animals Used	**Blood Pressure (mmHg)**	**Weight (g)**	**% NE Secreting**	**% EPI Secreting**	**% Mixed**
Sham n=50	11	133 ± 4*	422 ± 11*	26	74	0
DOCA n=49	11	188 ± 7	359 ± 18	29	69	2

No significant difference between the number of NE and EPI secreting cells was found between Sham and DOCA rats (p>0.05, Chi-squared Test), "n" = number of cells investigated.

The ratio of NE:EPI secreting cells was analyzed using a chi-squared test of association which yielded a value of 0.7 was obtained. This suggests that there is no change in the ratio of NE and EPI-releasing cells in DOCA-salt hypertension. In other words, the ratio of NE and EPI secreting cells does not differ between Sham and DOCA-salt chromaffin cells.

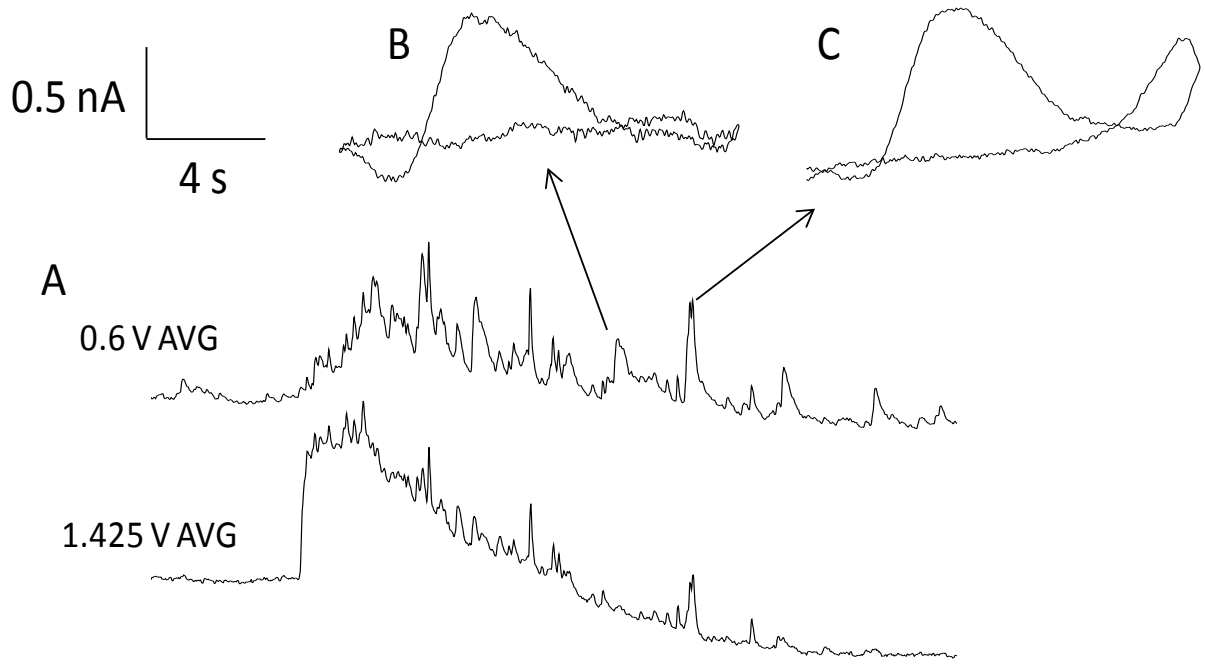

Figure 6-5. Averaged amperometric traces are shown (A) for a cell that was identified as secreting both NE (B) and EPI (C). This cell was found from a DOCA animal and was the only cell to be identified as not secreting primarily one catecholamine. (<90% of peaks identified were either NE or EPI).

6.3 Discussion

It has been well documented that in the spontaneous and DOCA-salt animal models of hypertension there are differences in the secretory responses of adrenal chromaffin cells[83, 102, 195, 205-206, 225]. Previous research has monitored NE and EPI using amperometry or HPLC. Such techniques do not provide real-time information on identification of NE and EPI released directly from adrenal chromaffin cells.

Identification of secreted NE and EPI in real-time has been performed by Wightman *et al.* in bovine and mouse chromaffin cells[121, 229]. These studies provided

significant details into how NE and EPI are secreted. An important finding was that the majority of cells primarily release either NE or EPI. There has also been work probing the effects of hypertension on the circulating catecholamine ratio in hypertension. Kubo *et al.*[230] found that the ratio of 0.61 NE/EPI in blood plasma for DOCA-salt rats. This translates to 62 % EPI and 38 % NE. These findings only indicate the ratio of catecholamines released into the blood by all sources.

The work presented in this chapter aimed at creating a profile of NE:EPI secretion for chromaffin cells in normotensive and hypertensive rats. Due to the adrenal glands' immense storage and release of EPI into the blood stream, it was hypothesized that significant changes in the ratio of NE and EPI secretion could play a role in established hypertension. The results presented provide evidence that it is possible to successfully use FSCV in order to profile cell populations isolated from the adrenal medulla into NE and EPI secreting categories. FSCV allowed for the creation of a detailed profile for catecholamine secretion from the adrenal medulla for the DOCA-salt model. This profile is novel due to the integration of unbiased cell identification via MatLab. The data analysis process made it possible to create the first true profile of randomly distributed chromaffin cells in culture. It was found that the ratio of NE to EPI secreted from isolated adrenal chromaffin cells was unaffected in DOCA-salt hypertension as compared to normotensive cells.

6.4 Conclusions

1) NE and EPI secreted from DOCA-salt chromaffin cells can be differentiated using FSCV using the secondary amine oxidation wave of EPI at 1.425 V as a discriminator.

2) Using FSCV, a breakdown of Sham chromaffin cells revealed 26% secreted only NE and 74% secreted only EPI. For DOCA-salt cells 29% secreted only NE, 69% secreted only EPI and 2% (1 cell) released both. These data suggest that DOCA-salt hypertension does not affect the ratio of NE:EPI secreting cells.

3) This study corroborates literature evidence that the majority of chromaffin cells are differentiated as either NE or EPI secreting[231-232]. A small population of chromaffin cells can secrete both catecholamines, as evidenced by our single DOCA-salt cell that released both NE and EPI[39, 121].

Chapter 7

Conclusions

It is well documented that sympathetic nerve activity plays an important role in blood pressure regulation[184]. Of particular relevance to this dissertation is neuroeffector signaling from sympathetic neurons to mesenteric blood vessels and the abnormalities in this signaling that arise in hypertension. Prior work in our group performed by Drs. Hua Dong, Stacie Demel and Jinwoo Park showed a number of abnormalities in neuroeffector signaling in the and DOCA-salt animal model[33, 125, 223]. These studies revealed higher overflow of norepinephrine from sympathetic nerves innervating mesenteric blood vessels in DOCA-salt rats. Further investigation led to the discovery that the increased neurotransmitter availability is due, in part, to impairments in the prejunctional auto-regulatory α_2-adrenoreceptor and the NET. This prior work did not address if there is in alteration in vesicular release in the DOCA-salt model of hypertension.

The goal of this dissertation was to address this last point, namely, to determine if there is altered vesicular release. Since these kinds of studies are difficult using *in vitro* blood vessel preparations, we chose to use adrenal chromaffin cells as a model for sympathetic transmission. The adrenal glands contain chromaffin cells that secrete norepinephrine and epinephrine by exocytosis is a manner presumably identical.

The adrenal gland, of which chromaffin cells are a constituent, is highly innervated by sympathetic nerves. These cells are often considered a type of specialized ganglia; therefore it is reasonable to use these as a model for release. Chromaffin cells have been widely studied to elucidate the steps involved in exocytosis [38, 40, 50-52]. Chromaffin cells were used to understand how DOCA-salt hypertension affects individual secretory secretion. The research involved the preparation of diamond and carbon fiber microelectrodes, establishment of single cell secretion measurement capabilities, the isolation and culturing of chromaffin cells from Sham and DOCA-salt hypertensive rats, continuous amperometric measurements of catecholamine secretion from single cells and fast scan voltammetric measurements for quantification of norepinephrine and epinephrine secreted from individual cells. The key findings can be summarized as follows:

1) **Successfully employing a NNP for preparing the Pt wire surfaces for the deposition of BDD. This preparation method decreased the growth time required for deposition of a continuous conductive polycrystalline film. Electrochemical characterization showed the coated wires exhibit good activity for several aqueous redox systems.**

Carbon fibers and BDD films were used as electrode materials for the oxidative detection of catecholamines. The carbon fiber used (pitch-base) has a relatively disordered microstructure with a significant fraction of exposed edge plane as shown via Raman spectra. Raman spectra obtained for our carbon fibers yielded a high D/G ratio

(≈1). The ratio of the D/G band provides information about the fraction of the carbon microstructure that is characterized as either basal or edge plane. Increased amounts of edge plane exposure can provide a larger area for oxide functional groups to adsorb. Oxygen functional groups are required for catecholamine adsorbtion[138]. This contributes to the high activity for NE and EPI oxidation[133].

On the other hand, the polycrystalline diamond microelectrodes are comprised of sp^3-bonded carbon rather than sp^2 carbon. BDD films have many positive attributes including low background current, microstructural stability, resistance to biofouling and a wide working potential window[145]. As compared to the carbon fibers, BDD microelectrodes are more laborious to prepare due to the sample preparation that is needed and the relatively to the long deposition times (8-10 h) required for complete film coverage. We applied a version of the NNP developed by Rotter that increases the initial nucleation density on the Pt wire substrate and this results in a reduced deposition for complete coverage[233]. Using the NNP procedure, the diamond deposition time was reduced to as little as 4 h. Importantly, the application of the NNP increases the number of wires in a batch that receive a uniform coating with diamond. This arises due to an increase in the nucleation density of diamond seeds on the pre-growth carbon layer, causing a reduction in deposition times as compared to simply seeding Pt wires via ultrasonication with diamond particles. A particularly interesting finding of this work was that nanocrystalline diamond readily nucleated on our platinum wires, which removes the need for seeding with nanodiamond particles all together.

2) Chromaffin cells isolated from DOCA-salt hypertensive rats secrete more catecholamine molecules per exocytotic vesicular release event more rapidly with more total events per stimulus than cells from Sham rats. The results suggest that neurotransmitter release in sympathetic nerves is altered in DOCA-salt hypertension.

Adrenal chromaffin cells were used as models for sympathetic neurotransmission. Using continuous amperometry, catecholamine secretion events were monitored as an oxidation current from single Sham and DOCA-salt cells isolated in culture. Secretion was evoked by the natural physiological stimulant, acetylcholine, and high extracellular potassium. Identical results were found for both ACh and high potassium. Individual secretory events were also analyzed to quantify the number of catecholamines released and time course of secretion for individual vesicle exocytosis. I found that chromaffin vesicles from DOCA-salt chromaffin cells contained a higher number of catecholamines than vesicles from Sham cells. The larger number of catecholamines in these vesicles is most likely due to increased vesicle diameters.

One piece of evidence for larger vesicle sizes is the elevated cubed root of the charge value obtained for DOCA-salt secretory events. The cubed root of the charge is proportional to a vesicle's diameter, so a larger cubed root is consistent with a larger vesicle size. This assumes that the concentration, or packing density of catecholamines, remains constant. Research suggests this in fact is the case, and that

as the quantal charge of a release event increases, the size of the vesicle also increases. This is due to self-regulating assembly of the vesicle membranes as more catecholamines are packaged into vesicles[208]. The HPCL studies also support the argument for larger vesicle sizes. The data suggest that dopamine, the precursor for NE and EPI synthesis, was present at similar levels in Sham and DOCA-salt adrenal medulla tissue. Also, the relative rate of catecholamine metabolism within adrenal chromaffin cells from Sham and DOCA-salt rats were not statistically different. These data suggest that the increased amount of catecholamines secreted from DOCA-salt cells is not due to an increase in NE or EPI synthesis. Also, the relative rate of metabolism does not explain the increased amounts of catecholamines secreted from DOCA-salt cells. Larger vesicles would explain the increased amount of NE and EPI levels found in medulla from DOCA-salt rats. Put together with the cubed root of the charge data, larger vesicle sizes appears to be a reasonable explanation for the increased quantal charge for DOCA-salt release events and the higher levels of NE and EPI found in DOCA-salt adrenal medulla as determined by HPLC.

3) The prolonged release (i.e., greater number of release events per stimulus) seen for DOCA-salt chromaffin cells is linked to impairment in BK and ATP-sensitive potassium channels.

To investigate the cause(s) for the enhanced secretion from DOCA-salt cells, the possibility of altered catecholamine metabolism was probed. One cause for the increased catecholamine secretion from these cells is down-regulation in the

intracellular metabolic degradation of NE and EPI HPLC analysis of whole tissue levels of catecholamines and their metabolites in adrenal medulla from Sham and DOCA-salt rats revealed there is no change in turnover for NE or EPI in DOCA-salt and Sham chromaffin cells. Another cause for the increased release is increase calcium influx into chromaffin cells. Ca imaging studies revealed no differences in the calcium handling in Sham and DOCA-salt cells.

During previous work in our group, it was found that increased superoxide levels in the sympathetic nerve terminals are linked to the impairments found in prejunctional α_2-ARs[36]. Therefore, the hypothesis was tested that increased reactive oxygen species may also play a role in some of the impairments found in secretion from DOCA-salt chromaffin cells. Sham and DOCA-salt rats were treated with the NADPH oxidase inhibitor, apocynin, for 4 weeks. Chromaffin cells were isolated from both animal models. Continuous amperometry was used to record catecholamine release and cells were stained for superoxide levels. Higher levels of superoxide were found in both apocynin-treated Sham cells as compared to DOCA-salt cells. This did not fit with the hypothesis and remains an unanswered question It was found, however, that chromaffin cells isolated from apocynin-treated DOCA-salt rats had a reduced number of secretion events per stimulus than did untreated DOCA-salt cells. For Sham cells, release frequency and individual secretory kinetics were unaffected by apocynin treatment. It cannot be stated for certain that these differences are due to apocynin treatment as blood pressure was unchanged DOCA-salt rats.

Finally, it was found that the prolonged secretion from DOCA-salt cells is linked to impaired potassium channel function. Pharmacological tools along with continuous amperometry were used to probe different potassium channel function. The application of BK and ATP-sensitive channel antagonists caused an increase in secretion from Sham chromaffin cells; however, they had no effect on DOCA-salt cells. This led to the conclusion that impaired BK and ATP-sensitive potassium channels are at least partially involved in the increased release frequency found in DOCA-salt chromaffin cells. Therefore, potassium channels might be a therapeutic target for the treatment of salt-sensitive hypertension.

4) The ratio of NE/EPI released from DOCA-salt cells is not changed as probed by fast-scan voltammetry.

Chromaffin cells have been previously investigated to determine if they secrete just NE or EPI, or both[121]. However, to the best of our knowledge there have been no studies into the profile of randomly distributed chromaffin cells secrete NE or EPI. After investigating nearly 50 cells from Sham and DOCA-salt rats using fast scan cyclic voltammetry, it was found that there is no difference in the ratio of NE secreting cells to EPI secreting cells in DOCA-salt hypertension. Approximately 30% of all chromaffin cells released NE, as where 70% of cells released EPI from both Sham and DOCA-salt rats. An interesting finding is that out of the nearly 100 cells investigated, only 1 cell was found to secrete both NE and EPI. These data lead to the conclusion that a higher number of NE and EPI molecules are secreted from DOCA-salt chromaffin cells per stimulus but the ratio of NE to EPI secreted remains the same.

Future Perspectives

Basic characterization of DOCA-salt chromaffin cell secretion was completed through the work presented in this dissertation along with some preliminary mechanistic studies to ascertain the causes of alterations in DOCA-salt secretion. Further mechanistic studies would provide more details into the cause of the impairments found in DOCA-salt chromaffin cells. Applying patch clamp electrophysiology to monitor and single out channel function during exocytosis could provide more information into the role calcium plays in altered secretion from DOCA-salt cells. It has also been shown that SNARE proteins can increase secretion frequency[72]. Possibly performing PCR or western blot experiments to determine the relative protein levels for SNARE may provide more details into the causes of impaired chromaffin cell secretion.

Bibliography

Bibliography

1. Chobanian, A. V.; Bakris, G. L.; Black, H. R.; Cushman, W. C.; Green, L. A.; Izzo, J. L.; Jones, D. W.; Materson, B. J.; Oparil, S.; Wright, J. T.; Roccella, E. J.; Natl High Blood Pressure Educ, P., Seventh Report of the Joint National Committee on Prevention, Detection, Evaluation, and Treatment of High Blood Pressure. *Hypertension* **2003,** *42* (6), 1206-1252.

2. Izzo, J. L., *Hypertension Primer*. Fourth Edition ed.; Lippincott Williams & Wilkins: 2008; p 640.

3. Carretero, O. A.; Oparil, S., Essential hypertension Part I: Definition and etiology. *Circulation* **2000,** *101* (3), 329-335.

4. Kassim, T. A.; Clarke, D. D.; Mai, V. Q.; Clyde, P. W.; Mohamed, S. K. M., Catecholamine-induced cardiomyopathy. *Endocr Pract* **2008,** *14* (Copyright (C) 2012 U.S. National Library of Medicine.), 1137-49.

5. Addison, W. L. T., THE USE OF SODIUM-CHLORIDE, POTASSIUM-CHLORIDE, SODIUM-BROMIDE, AND POTASSIUM-BROMIDE IN CASES OF ARTERIAL-HYPERTENSION WHICH ARE AMENABLE TO POTASSIUM-CHLORIDE. *Nutrition Reviews* **1988,** *46* (8), 295-296.

6. Peters, R. M.; Flack, J. M., Salt sensitivity and hypertension in African Americans: implications for cardiovascular nurses. *Prog Cardiovasc Nurs* **2000,** *15* (Copyright (C) 2012 U.S. National Library of Medicine.), 138-44.

7. Brooks, V. L.; Haywood, J. R.; Johnson, A. K., Translation of salt retention to central activation of the sympathetic nervous system in hypertension. *Clin Exp Pharmacol P* **2005,** *32* (5-6), 426-432.

8. Weinberger, M. H., Salt sensitivity of blood pressure in humans. *Hypertension* **1996,** *27* (3), 481-490.

9. Klabunde, R. E., *Cardiovascular Physiology Concepts*. Second ed.; Lippincott Williams & Wilkins: 2011.

10. Davis, G., Baroreflex and somato-reflex control of blood pressure, heart rate and renal sympathetic nerve activity in the obese Zucker rat. *Exp Physiol* **2011,** *96* (7), 623-634.

11. Cowley, A. W.; Liard, J. F.; Guyton, A. C., ROLE OF BARORECEPTOR REFLEX IN DAILY CONTROL OF ARTERIAL BLOOD-PRESSURE AND OTHER VARIABLES IN DOGS. *Circ Res* **1973,** *32* (5), 564-576.

12. Head, G. A., The sympathetic nervous system in hypertension: assessment by blood pressure variability and ganglionic blockade. *J Hypertens* **2003,** *21* (9), 1619-1621.

13. Zanutto, B. S.; Frias, B. C.; Valentinuzzi, M. E., Blood pressure long term regulation: A neural network model of the set point development. *Biomedical Engineering Online* **2011,** *10*.

14. Pfisterer, L.; Feldner, A.; Hecker, M.; Korff, T., Hypertension impairs myocardin function: a novel mechanism facilitating arterial remodelling. *Cardiovasc Res* **2012,** *96* (1), 120-129.

15. Carey, R. M., Primary aldosteronism. *J. Surg. Oncol.* **2012,** *106* (5), 575-579.

16. Ohicita, M.; Tawa, M.; Kitada, K.; Matsumura, Y., Pathophysiological Roles of Endothelin Receptors in Cardiovascular Diseases. *J. Pharmacol. Sci.* **2012,** *119* (4), 302-313.

17. Zuber, S. M.; Kantorovich, V.; Pacak, K., Hypertension in Pheochromocytoma: Characteristics and Treatment. *Endocrinol. Metabol. Clin. North Amer.* **2011,** *40* (2), 295-+.

18. Goodman, L. S.; Gilman, A. Z.; Editors, *The Pharmacological Basis of Therapeutics, Pt. 1. 8th Ed*. Hirokawa Publishing Co.: 1992; p 1132 pp.

19. Shoukas, A. A.; Bohlen, H. G., RAT VENULAR PRESSURE-DIAMETER RELATIONSHIPS ARE REGULATED BY SYMPATHETIC ACTIVITY. *American Journal of Physiology* **1990,** *259* (3), H674-H680.

20. Ozono, K.; Bosnjak, Z. J.; Kampine, J. P., EFFECT OF SYMPATHETIC TONE ON PRESSURE DIAMETER RELATION OF RABBIT MESENTERIC VEINS INSITU. *Circ Res* **1991,** *68* (3), 888-896.

21. Rummery, N. M.; Brock, J. A.; Pakdeechote, P.; Ralevic, V.; Dunn, W. R., ATP is the predominant sympathetic neurotransmitter in rat mesenteric arteries at high pressure. *J. Physiol. (Oxford, U. K.)* **2007,** *582* (Copyright (C) 2012 American Chemical Society (ACS). All Rights Reserved.), 745-754.

22. Charkoudian, N.; Joyner, M. J.; Sokolnicki, L. A.; Johnson, C. P.; Eisenach, J. H.; Dietz, N. M.; Curry, T. B.; Wallin, B. G., Vascular adrenergic responsiveness is inversely related to tonic activity of sympathetic vasoconstrictor nerves in humans. *J. Physiol. (Oxford, U. K.)* **2006,** *572* (Copyright (C) 2012 American Chemical Society (ACS). All Rights Reserved.), 821-827.

23. Victor, R. G.; Shafiq, M. M., Sympathetic neural mechanisms in human hypertension. *Curr. Hypertens. Rep.* **2008,** *10* (Copyright (C) 2012 American Chemical Society (ACS). All Rights Reserved.), 241-247.

24. Osborn, J. L.; Plato, C. F.; Gordin, E.; He, X. R., Long-term increases in renal sympathetic nerve activity and hypertension. *Clin. Exp. Pharmacol. Physiol.* **1997,** *24* (Copyright (C) 2012 American Chemical Society (ACS). All Rights Reserved.), 72-76.

25. Henriksen, J. H.; Moller, S., Liver cirrhosis and arterial hypertension. *World J Gastroenterol* **2006,** *12* (Copyright (C) 2012 U.S. National Library of Medicine.), 678-85.

26. Greenway, C. V.; Lister, G. E., Capacitance effects and blood reservoir function in the splanchnic vascular bed during non-hypotensive haemorrhage and blood volume expansion in anaesthetized cats. *J Physiol* **1974,** *237* (Copyright (C) 2012 U.S. National Library of Medicine.), 279-94.

27. Schlaich, M. P.; Lambert, E.; Kaye, D. M.; Krozowski, Z.; Campbell, D. J.; Lambert, G.; Hastings, J.; Aggarwal, A.; Esler, M. D., Sympathetic augmentation in hypertension: role of nerve firing, norepinephrine reuptake, and Angiotensin neuromodulation. *Hypertension* **2004,** *43* (Copyright (C) 2012 U.S. National Library of Medicine.), 169-75.

28. Greenway, C. V., Role of splanchnic venous system in overall cardiovascular homeostasis. *Fed Proc* **1983,** *42* (Copyright (C) 2012 U.S. National Library of Medicine.), 1678-84.

29. Lowe, A. W.; Madeddu, L.; Kelly, R. B., Endocrine secretory granules and neuronal synaptic vesicles have three integral membrane proteins in common. *J Cell Biol* **1988,** *106* (Copyright (C) 2012 U.S. National Library of Medicine.), 51-9.

30. Boeynaems, J. M.; Demolle, D.; Galand, N., Adrenergic stimulation of vascular prostacyclin: role of α1-receptors in smooth muscle cells. *Eur. J. Pharmacol.* **1987,** *144* (Copyright (C) 2012 American Chemical Society (ACS). All Rights Reserved.), 193-200.

31. Elliott, J., Alpha-adrenoceptors in equine digital veins: evidence for the presence of both alpha1 and alpha2-receptors mediating vasoconstriction. *J. Vet. Pharmacol. Ther.* **1997,** *20* (Copyright (C) 2012 American Chemical Society (ACS). All Rights Reserved.), 308-317.

32. Chan, C.-C.; Chang, C.-C.; Huang, H.-C.; Wang, S.-S.; Lee, F.-Y.; Chang, F.-Y.; Lin, H.-C.; Tai, C.-C.; Lee, S.-D., Effects of norepinephrine and acetylcholine on portal-systemic collaterals of common bile duct-ligated cirrhotic rat. *J.*

Gastroenterol. Hepatol. **2005,** *20* (Copyright (C) 2012 American Chemical Society (ACS). All Rights Reserved.), 1867-1872.

33. Dong, H. Disruption of norepinephrine release and clearance mechanisms in sympathetic nerves associated with mesenteric arteries but not veins in salt-sensitive hypertension. 2009.

34. Park, J.; Galligan, J. J.; Fink, G. D.; Swain, G. M., Alterations in sympathetic neuroeffector transmission to mesenteric arteries but not veins in DOCA-salt hypertension. *Auton Neurosci-Basic* **2010,** *152* (1-2), 11-20.

35. Park, J.; Galligan, J. J.; Fink, G. D.; Swain, G. M., Differences in sympathetic neuroeffector transmission to rat mesenteric arteries and veins as probed by in vitro continuous amperometry and video imaging. *J Physiol-London* **2007,** *584* (3), 819-834.

36. Demel, S. L.; Dong, H.; Swain, G. M.; Wang, X.; Kreulen, D. L.; Galligan, J. J., ANTIOXIDANT TREATMENT RESTORES PREJUNCTIONAL REGULATION OF PURINERGIC TRANSMISSION IN MESENTERIC ARTERIES OF DEOXYCORTICOSTERONE ACETATE-SALT HYPERTENSIVE RATS. *Neuroscience* **2010,** *168* (2), 335-345.

37. Dong, H.; Demel, S.; Fink, G.; Galligan, J.; Swain, G., Differential function of alpha(2)-adrenergic receptors in sympathetic neuroeffector transmission in mesenteric arteries in hypertension. *Hypertension* **2008,** *52* (4), E65-E65.

38. Schroeder, T. J.; Borges, R.; Finnegan, J. M.; Pihel, K.; Amatore, C.; Wightman, R. M., Temporally resolved, independent stages of individual exocytotic secretion events. *Biophys J* **1996,** *70* (2), 1061-1068.

39. Ciolkowski, E. L.; Cooper, B. R.; Jankowski, J. A.; Jorgenson, J. W.; Wightman, R. M., DIRECT OBSERVATION OF EPINEPHRINE AND NOREPINEPHRINE COSECRETION FROM INDIVIDUAL ADRENAL-MEDULLARY CHROMAFFIN CELLS. *J Am Chem Soc* **1992,** *114* (8), 2815-2821.

40. Jankowski, J. A.; Schroeder, T. J.; Ciolkowski, E. L.; Wightman, R. M., TEMPORAL CHARACTERISTICS OF QUANTAL SECRETION OF CATECHOLAMINES FROM ADRENAL-MEDULLARY CELLS. *J Biol Chem* **1993,** *268* (20), 14694-14700.

41. Wightman, R. M.; Jankowski, J. A.; Kennedy, R. T.; Kawagoe, K. T.; Schroeder, T. J.; Leszczyszyn, D. J.; Near, J. A.; Diliberto, E. J.; Viveros, O. H., TEMPORALLY RESOLVED CATECHOLAMINE SPIKES CORRESPOND TO SINGLE VESICLE RELEASE FROM INDIVIDUAL CHROMAFFIN CELLS. *P Natl Acad Sci USA* **1991,** *88* (23), 10754-10758.

42. Marquis, B. J.; McFarland, A. D.; Braun, K. L.; Haynes, C. L., Dynamic measurement of altered chemical messenger secretion after cellular uptake of nanoparticles using carbon-fiber microelectrode amperometry. *Analytical Chemistry* **2008,** *80* (9), 3431-3437.

43. Aspinwall, C. A.; Huang, L.; Lakey, J. R. T.; Kennedy, R. T., Comparison of amperometric methods for detection of exocytosis from single pancreatic beta-cells of different species. *Analytical Chemistry* **1999,** *71* (24), 5551-5556.

44. Watson, D. J.; Gummi, R. R.; Papke, J. B.; Harkins, A. B., Analysis of Amperometric Spike Shapes to Release Vesicles. *Electroanalysis* **2011,** *23* (12), 2757-2763.

45. Weiss, J. L., Ca2+ signaling mechanisms in bovine adrenal chromaffin cells. *Adv. Exp. Med. Biol.* **2012,** *740* (Copyright (C) 2012 American Chemical Society (ACS). All Rights Reserved.), 859-872.

46. Espat, N. J., Skandalakis' Surgical Anatomy: The Embryologic and Anatomic Basis of Modern Surgery, vois 1 & 2 edited by John E. Skandalakis. *JAMA, J. Am. Med. Assoc.* **2005,** *294* (Copyright (C) 2012 American Chemical Society (ACS). All Rights Reserved.), 1556.

47. Iwanami, J.; Mogi, M.; Horiuchi, M., RAA system and hypertension: recent topics. *Saibo* **2012,** *44* (Copyright (C) 2012 American Chemical Society (ACS). All Rights Reserved.), 4-7.

48. Aunis, D.; Langley, K., Physiological aspects of exocytosis in chromaffin cells of the adrenal medulla. *Acta Physiologica Scandinavica* **1999,** *167* (2), 89-97.

49. Kesse, W. K.; Parker, T. L.; Coupland, R. E., THE INNERVATION OF THE ADRENAL-GLAND .1. THE SOURCE OF PREGANGLIONIC AND POSTGANGLIONIC NERVE-FIBERS TO THE RAT ADRENAL-GLAND. *J Anat* **1988,** *157*, 33-41.

50. Amatore, C.; Arbault, S.; Bonifas, I.; Bouret, Y.; Erard, M.; Ewing, A. G.; Sombers, L. A., Correlation between vesicle quantal size and fusion pore release in chromaffin cell exocytosis. *Biophys J* **2005,** *88* (6), 4411-4420.

51. Amatore, C.; Arbault, S.; Bonifas, I.; Guille, M., Quantitative investigations of amperometric spike feet suggest different controlling factors of the fusion pore in exocytosis at chromaffin cells. *Biophys Chem* **2009,** *143* (3), 124-131.

52. Amatore, C.; Arbault, S.; Lemaitre, F.; Verchier, Y., Comparison of apex and bottom secretion efficiency at chromaffin cells as measured by amperometry. *Biophys Chem* **2007,** *127* (3), 165-171.

53. Finnegan, J. M.; Borges, R.; Wightman, R. M., Comparison of cytosolic Ca2+ and exocytosis responses from single rat and bovine chromaffin cells. *Neuroscience* **1996,** *71* (3), 833-843.

54. Haynes, C. L.; Siff, L. N.; Wightman, R. M., Temperature-dependent differences between readily releasable and reserve pool vesicles in chromaffin cells. *Biochimica Et Biophysica Acta-Molecular Cell Research* **2007,** *1773* (6), 728-735.

55. Eisenhofer, G., The role of neuronal and extraneuronal plasma membrane transporters in the inactivation of peripheral catecholamines. *Pharmacol. Ther.* **2001,** *91* (1), 35-62.

56. Rodwell, Conversion of Amino Acids to Specialized Products. In *Harper's Illustrated Biochemistry*, 29th Edition ed.; McGraw-Hill: New York, 2011.

57. Henry, J. P.; Sagne, C.; Bedet, C.; Gasnier, B., The vesicular monoamine transporter: from chromaffin granule to brain. *Neurochemistry International* **1998,** *32* (3), 227-246.

58. Garcia, A. G.; Garcia-De-Diego, A. M.; Gandia, L.; Borges, R.; Garcia-Sancho, J., Calcium signaling and exocytosis in adrenal chromaffin cells. *Physiol. Rev.* **2006,** *86* (4), 1093-1131.

59. Sala, F.; Nistri, A.; Criado, M., Nicotinic acetylcholine receptors of adrenal chromaffin cells. *Acta Physiologica* **2008,** *192* (2), 203-212.

60. Burgoyne, R. D., CONTROL OF EXOCYTOSIS IN ADRENAL CHROMAFFIN CELLS. *Biochimica Et Biophysica Acta* **1991,** *1071* (2), 174-202.

61. Bretou, M.; Anne, C.; Darchen, F., A fast mode of membrane fusion dependent on tight SNARE zippering. *J Neurosci* **2008,** *28* (34), 8470-8476.

62. Winkler, H.; Sietzen, M.; Schober, M., THE LIFE-CYCLE OF CATECHOLAMINE-STORING VESICLES. *Annals of the New York Academy of Sciences* **1987,** *493*, 3-19.

63. Winkler, H.; Schopf, J. A. L.; Hortnagl, H., BOVINE ADRENAL-MEDULLA - SUBCELLULAR DISTRIBUTION OF NEWLY SYNTHESIZED CATECHOLAMINES, NUCLEOTIDES AND CHROMOGRANINS. *Naunyn-Schmiedebergs Archiv Fur Pharmakologie* **1972,** *273* (1-2), 43-&.

64. Viveros, O. H.; Arqueros, L.; Kirshner, N., Mechanism of secretion from the adrenal medulla. VI. Effect of reserpine on the dopamine β-hydroxylase and catechol amine content and on the buoyant density of adrenal storage vesicles. *Mol. Pharmacol.* **1971,** *7* (Copyright (C) 2012 American Chemical Society (ACS). All Rights Reserved.), 434-43.

65. Baumgart.H; Gibb, J. W.; Hortnagl, H.; Snider, S. R.; Winkler, H., LABELING OF CHROMAFFIN GRANULES IN ADRENAL-MEDULLA WITH S-35 SULFATE. *Molecular Pharmacology* **1974,** *10* (4), 678-685.

66. Winkler, H.; Apps, D. K.; Fischercolbrie, R., THE MOLECULAR FUNCTION OF ADRENAL CHROMAFFIN GRANULES - ESTABLISHED FACTS AND UNRESOLVED TOPICS. *Neuroscience* **1986,** *18* (2), 261-+.

67. Caviston, J. P.; Holzbaur, E. L. F., Microtubule motors at the intersection of trafficking and transport. *Trends Cell Biol.* **2006,** *16* (Copyright (C) 2012 American Chemical Society (ACS). All Rights Reserved.), 530-537.

68. Neco, P.; Rossetto, O.; Gil, A.; Montecucco, C.; Gutierrez, L. M., Taipoxin induces F-actin fragmentation and enhances release of catecholamines in bovine chromaffin cells. *J Neurochem* **2003,** *85* (2), 329-337.

69. Oheim, M.; Stuhmer, W., Tracking chromaffin granules on their way through the actin cortex. *Eur Biophys J Biophy* **2000,** *29* (2), 67-89.

70. Trifaro, J. M.; Gasman, S.; Gutierrez, L. M., Cytoskeletal control of vesicle transport and exocytosis in chromaffin cells. *Acta Physiologica* **2008,** *192* (2), 165-172.

71. Vitale, M. L.; Delcastillo, A. R.; Tchakarov, L.; Trifaro, J. M., CORTICAL FILAMENTOUS ACTIN DISASSEMBLY AND SCINDERIN REDISTRIBUTION DURING CHROMAFFIN CELL STIMULATION PRECEDE EXOCYTOSIS, A PHENOMENON NOT EXHIBITED BY GELSOLIN. *Journal of Cell Biology* **1991,** *113* (5), 1057-1067.

72. Guzman, R. E.; Schwarz, Y. N.; Rettig, J.; Bruns, D., SNARE Force Synchronizes Synaptic Vesicle Fusion and Controls the Kinetics of Quantal Synaptic Transmission. *J Neurosci* **2010,** *30* (31), 10272-10281.

73. Xu, J. H.; Tang, K. S.; Lu, V. B.; Weerasinghe, C. P.; Tse, A.; Tse, F. W., Maintenance of quantal size and immediately releasable granules in rat chromaffin cells by glucocorticoid. *Am. J. Physiol.-Cell Physiol.* **2005,** *289* (5), C1122-C1133.

74. Pitchford, S.; Day, J. W.; Gordon, A.; Mochlyrosen, D., NICOTINIC ACETYLCHOLINE-RECEPTOR DESENSITIZATION IS REGULATED BY ACTIVATION-INDUCED EXTRACELLULAR ADENOSINE ACCUMULATION. *J Neurosci* **1992,** *12* (11), 4540-4544.

75. Huganir, R. L.; Greengard, P., CAMP-DEPENDENT PROTEIN-KINASE PHOSPHORYLATES THE NICOTINIC ACETYLCHOLINE-RECEPTOR.

Proceedings of the National Academy of Sciences of the United States of America-Biological Sciences **1983,** *80* (4), 1130-1134.

76. Gould, T. J.; Portugal, G. S.; Andre, J. M.; Tadman, M. P.; Marks, M. J.; Kenney, J. W.; Yildirim, E.; Adoff, M., The duration of nicotine withdrawal-associated deficits in contextual fear conditioning parallels changes in hippocampal high affinity nicotinic acetylcholine receptor upregulation. *Neuropharmacology* **2012,** *62* (5-6), 2118-2125.

77. Eisenhofer, G.; Kopin, I. J.; Goldstein, D. S., Catecholamine metabolism: A contemporary view with implications for physiology and medicine. *Pharmacol Rev* **2004,** *56* (3), 331-349.

78. Eisenhofer, G.; Esler, M. D.; Meredith, I. T.; Ferrier, C.; Lambert, G.; Jennings, G., NEURONAL REUPTAKE OF NORADRENALINE BY SYMPATHETIC-NERVES IN HUMANS. *Clinical Science* **1991,** *80* (3), 257-263.

79. Eisenhofer, G.; Keiser, H.; Friberg, P.; Mezey, E.; Huynh, T. T.; Hiremagalur, B.; Ellingson, T.; Duddempudi, S.; Eijsbouts, A.; Lenders, J. W. M., Plasma metanephrines are markers of pheochromocytoma produced by catechol-O-methyltransferase within tumors. *J Clin Endocr Metab* **1998,** *83* (6), 2175-2185.

80. Ellingson, T.; Duddempudi, S.; Greenberg, B. D.; Hooper, D.; Eisenhofer, G., Determination of differential activities of soluble and membrane-bound catechol-O-methyltransferase in tissues and erythrocytes. *Journal of Chromatography B* **1999,** *729* (1-2), 347-353.

81. Roth, J. A., MEMBRANE-BOUND CATECHOL-O-METHYLTRANSFERASE - A REEVALUATION OF ITS ROLE IN THE O-METHYLATION OF THE CATECHOLAMINE NEUROTRANSMITTERS. *Reviews of Physiology Biochemistry and Pharmacology* **1992,** *120*, 1-29.

82. Eisenhofer, G.; Huynh, T.-T.; Hiroi, M.; Pacak, K., Understanding catecholamine metabolism as a guide to the biochemical diagnosis of pheochromocytoma. *Rev. Endocr. Metab. Disord.* **2001,** *2* (Copyright (C) 2012 American Chemical Society (ACS). All Rights Reserved.), 297-311.

83. Lim, D. Y.; Jang, S. J.; Park, D. G., Comparison of catecholamine release in the isolated adrenal glands of SHR and WKY rats. *Auton. Autacoid Pharmacol.* **2002,** *22* (Copyright (C) 2012 American Chemical Society (ACS). All Rights Reserved.), 225-232.

84. Douglas, W. W.; Rubin, R. P., The role of calcium in the secretory response of the adrenal medulla to acetylcholine. *J Physiol* **1961,** *159* (Copyright (C) 2012 U.S. National Library of Medicine.), 40-57.

85. Baker, P. F.; Knight, D. E., CALCIUM-DEPENDENT EXOCYTOSIS IN BOVINE ADRENAL-MEDULLARY CELLS WITH LEAKY PLASMA-MEMBRANES. *Nature* **1978,** *276* (5688), 620-622.

86. Holz, R. W.; Bittner, M. A.; Peppers, S. C.; Senter, R. A.; Eberhard, D. A., MGATP-INDEPENDENT AND MGATP-DEPENDENT EXOCYTOSIS - EVIDENCE THAT MGATP PRIMES ADRENAL CHROMAFFIN CELLS TO UNDERGO EXOCYTOSIS. *J Biol Chem* **1989,** *264* (10), 5412-5419.

87. Heinemann, C.; Chow, R. H.; Neher, E.; Zucker, R. S., KINETICS OF THE SECRETORY RESPONSE IN BOVINE CHROMAFFIN CELLS FOLLOWING FLASH-PHOTOLYSIS OF CAGED CA2+. *Biophys J* **1994,** *67* (6), 2546-2557.

88. Heinemann, C.; Vonruden, L.; Chow, R. H.; Neher, E., A 2-STEP MODEL OF SECRETION CONTROL IN NEUROENDOCRINE CELLS. *Pflugers Archiv-European Journal of Physiology* **1993,** *424* (2), 105-112.

89. Vonruden, L.; Garcia, A. G.; Lopez, M. G., THE MECHANISM OF BA2+-INDUCED EXOCYTOSIS FROM SINGLE CHROMAFFIN CELLS. *Febs Letters* **1993,** *336* (1), 48-52.

90. Michelena, P.; Garciaperez, L. E.; Artalejo, A. R.; Garcia, A. G., SEPARATION BETWEEN CYTOSOLIC CALCIUM AND SECRETION IN CHROMAFFIN CELLS SUPERFUSED WITH CALCIUM RAMPS. *P Natl Acad Sci USA* **1993,** *90* (8), 3284-3288.

91. Dodge, F. A., Jr.; Rahamimoff, R., Cooperative action of calcium ions in transmitter release at the neuromuscular junction. *J. Physiol. (London)* **1967,** *193* (Copyright (C) 2012 American Chemical Society (ACS). All Rights Reserved.), 419-32.

92. Yamamoto, E.; Kataoka, K.; Dong, Y. F.; Koibuchi, N.; Toyama, K.; Sueta, D.; Katayama, T.; Yasuda, O.; Ogawa, H.; Kim-Mitsuyama, S., Calcium Channel Blockers, More than Diuretics, Enhance Vascular Protective Effects of Angiotensin Receptor Blockers in Salt-Loaded Hypertensive Rats. *Plos One* **2012,** *7* (6).

93. Magura, I. S.; Magura, O. I.; Dolga, O. V.; Bogdanova, N. A.; Ageev, S.; Pogorela, N. K., Signal function of potassium channels - clinical aspects. *Fiziol. Zh. (Kiev, Ukr.)* **2010,** *56* (Copyright (C) 2012 American Chemical Society (ACS). All Rights Reserved.), 19-24.

94. No, H.-J.; Woo, S.-C.; Lim, D.-Y., Influence of glibenclamide on catecholamine secretion in the isolated rat adrenal gland. *J. Appl. Pharmacol.* **2007,** *15* (Copyright (C) 2012 American Chemical Society (ACS). All Rights Reserved.), 108-117.

95. Prakriya, M.; Lingle, C. J., Activation of BK channels in rat chromaffin cells requires summation of Ca2+ influx from multiple Ca2+ channels. *Journal of Neurophysiology* **2000,** *84* (3), 1123-1135.

96. Akiyama, T.; Yamazaki, T.; Kawada, T.; Shimizu, S.; Sugimachi, M.; Shirai, M., Role of Ca2+-activated K+ channels in catecholamine release from in vivo rat adrenal medulla. *Neurochemistry International* **2010,** *56* (2), 263-269.

97. Patel, A. J.; Honore, E., Molecular physiology of oxygen-sensitive potassium channels. *Eur Respir J* **2001,** *18* (1), 221-227.

98. Brandt, B. L.; Hagiwara, S.; Kidokoro, Y.; Miyazaki, S., Action potentials in the rat chromaffin cell and effects of acetylcholine. *J. Physiol. (London)* **1976,** *263* (Copyright (C) 2012 American Chemical Society (ACS). All Rights Reserved.), 417-39.

99. Sun, L.; Xiong, Y.; Zeng, X. H.; Wu, Y.; Pan, N.; Lingle, C. J.; Qu, A. L.; Ding, J. P., Differential Regulation of Action Potentials by Inactivating and Noninactivating BK Channels in Rat Adrenal Chromaffin Cells. *Biophys J* **2009,** *97* (7), 1832-1842.

100. Grimm, P. R.; Sansom, S. C., BK channels and a new form of hypertension. *Kidney Int* **2010,** *78* (10), 956-962.

101. Sausbier, M.; Arntz, C.; Bucurenciu, I.; Zhao, H.; Zhou, X. B.; Sausbier, U.; Feil, S.; Kamm, S.; Essin, K.; Sailer, C. A.; Abdullah, U.; Krippeit-Drews, P.; Feil, R.; Hofmann, F.; Knaus, H. G.; Kenyon, C.; Shipston, M. J.; Storm, J. F.; Neuhuber, W.; Korth, M.; Schubert, R.; Gollasch, M.; Ruth, P., Elevated blood pressure linked to primary hyperaldosteronism and impaired vasodilation in BK channel-deficient mice. *Circulation* **2005,** *112* (1), 60-68.

102. Miranda-Ferreira, R.; de Pascual, R.; de Diego, A. M. G.; Caricati, A.; Gandia, L.; Jurkiewicz, A.; Garcia, A. G., Single-vesicle catecholamine release has greater quantal content and faster kinetics in chromaffin cells from hypertensive, as compared with normotensive, rats. *J Pharmacol Exp Ther* **2008,** *324* (2), 685-693.

103. van der Vliet, A., NADPH oxidases in lung biology and pathology: Host defense enzymes, and more. *Free Radical Bio Med* **2008,** *44* (6), 938-955.

104. Koshkin, V.; Lotan, O.; Pick, E., Electron transfer in the superoxide-generating NADPH oxidase complex reconstituted in vitro. *Biochim. Biophys. Acta, Bioenerg.* **1997,** *1319* (Copyright (C) 2012 American Chemical Society (ACS). All Rights Reserved.), 139-146.

105. Goldstein, S.; Czapski, G. In *Superoxide dismutase*, IRL Press: 1996; pp 241-255.

106. Takimoto, E.; Kass, D. A., Role of Oxidative Stress in Cardiac Hypertrophy and Remodeling. *Hypertension* **2007,** *49* (Copyright (C) 2012 American Chemical Society (ACS). All Rights Reserved.), 241-248.

107. Bondia-Pons, I.; Ryan, L.; Martinez, J. A., Oxidative stress and inflammation interactions in human obesity. *Journal of physiology and biochemistry* **2012,** *68* (4), 701-11.

108. Toporsian, M.; Jerkic, M.; Zhou, Y. Q.; Kabir, M. G.; Yu, L. X.; McIntyre, B. A. S.; Davis, A.; Wang, Y. J.; Stewart, D. J.; Belik, J.; Husain, M.; Henkelman, M.; Letarte, M., Spontaneous Adult-Onset Pulmonary Arterial Hypertension Attributable to Increased Endothelial Oxidative Stress in a Murine Model of Hereditary Hemorrhagic Telangiectasia. *Arterioscl Throm Vas* **2010,** *30* (3), 509-517.

109. Bouloumie, A.; Bauersachs, J.; Linz, W.; Scholkens, B. A.; Wiemer, G.; Fleming, I.; Busse, R., Endothelial dysfunction coincides with an enhanced nitric oxide synthase expression and superoxide anion production. *Hypertension* **1997,** *30* (4), 934-941.

110. Suzuki, H.; Swei, A.; Zweifach, B. W.; Schmidschonbein, G. W., IN-VIVO EVIDENCE FOR MICROVASCULAR OXIDATIVE STRESS IN SPONTANEOUSLY HYPERTENSIVE RATS - HYDROETHIDINE MICROFLUOROGRAPHY. *Hypertension* **1995,** *25* (5), 1083-1089.

111. Dohi, Y.; Thiel, M. A.; Buehler, F. R.; Luescher, T. F., Activation of endothelial L-arginine pathway in resistance arteries. Effect of age and hypertension. *Hypertension (Dallas)* **1990,** *16* (Copyright (C) 2012 American Chemical Society (ACS). All Rights Reserved.), 170-9.

112. Cuzzocrea, S.; Mazzon, E.; Dugo, L.; Di Paola, R.; Caputi, A. P.; Salvemini, D., Superoxide: a key player in hypertension. *Faseb Journal* **2004,** *18* (1), 94-101.

113. Pinto, Y. M.; Paul, M.; Ganten, D., Lessons from rat models of hypertension: from Goldblatt to genetic engineering. *Cardiovasc Res* **1998,** *39* (1), 77-88.

114. Perez-Rivera, A. A.; Hlavacova, A.; Rosario-Colon, L. A.; Fink, G. D.; Galligan, J. J., Differential contributions of alpha-1 and alpha-2 adrenoceptors to vasoconstriction in mesenteric arteries and veins of normal and hypertensive mice. *Vasc Pharmacol* **2007,** *46* (5), 373-382.

115. Iyer, A.; Chan, V.; Brown, L., The DOCA-Salt Hypertensive Rat as a Model of Cardiovascular Oxidative and Inflammatory Stress. *Current cardiology reviews* **2010,** *6* (4), 291-7.

116. Sun, Z. J.; Zhang, Z. E., Historic perspectives and recent advances in major animal models of hypertension. *Acta Pharmacol. Sin.* **2005,** *26* (3), 295-301.

117. Gupta, V., Mineralocorticoid hypertension. *Indian journal of endocrinology and metabolism* **2011,** *15 Suppl 4*, S298-312.

118. Bebarova, M., Advances in patch clamp technique: towards higher quality and quantity. *Gen. Physiol. Biophys.* **2012,** *31* (2), 131-140.

119. Rossier, M. F.; Burnay, M. M.; Vallotton, M. B.; Capponi, A. M., Distinct functions of T- and L-type calcium channels during activation of bovine adrenal glomerulosa cells. *Endocrinology* **1996,** *137* (11), 4817-4826.

120. Gonon, F.; Msghina, M.; Stjarne, L., KINETICS OF NORADRENALINE RELEASED BY SYMPATHETIC-NERVES. *Neuroscience* **1993,** *56* (3), 535-538.

121. Pihel, K.; Schroeder, T. J.; Wightman, R. M., RAPID AND SELECTIVE CYCLIC VOLTAMMETRIC MEASUREMENTS OF EPINEPHRINE AND NOREPINEPHRINE AS A METHOD TO MEASURE SECRETION FROM SINGLE BOVINE ADRENAL-MEDULLARY CELLS. *Analytical Chemistry* **1994,** *66* (24), 4532-4537.

122. Wang, N.; Lee, A. K.; Yan, L.; Simpson, M. R.; Tse, A.; Tse, F. W., Granule matrix property and rapid "kiss-and-run" exocytosis contribute to the different kinetics of catecholamine release from carotid glomus and adrenal chromaffin cells at matched quantal size. *Canadian Journal of Physiology and Pharmacology* **2012,** *90* (6), 791-801.

123. Brock, J. A.; Dunn, W. R.; Boyd, N. S. F.; Wong, D. K. Y., Spontaneous release of large packets of noradrenaline from sympathetic nerve terminals in rat mesenteric arteries in vitro. *British Journal of Pharmacology* **2000,** *131* (8), 1507-1511.

124. Dunn, W. R.; Brock, J. A.; Hardy, T. A., Electrochemical and electrophysiological characterization of neurotransmitter release from sympathetic nerves supplying rat mesenteric arteries. *British Journal of Pharmacology* **1999,** *128* (1), 174-180.

125. Park, J. Functional differences in sympathetic neural control mechanism of arteries and veins as probed by continuous amperometry and video microscopy. 2006.

126. Park, J.; Galligan, J. J.; Fink, G. D.; Swain, G. M., In vitro continuous amperometry with a diamond microelectrode coupled with video microscopy for simultaneously monitoring endogenous norepinephrine and its effect on the contractile response of a rat mesenteric artery. *Analytical Chemistry* **2006,** *78* (19), 6756-6764.

127. Perez, X. A.; Mathews, T. A.; Chisnell, A. C.; Andrews, A. M., Adaptations in dopamine neurochemistry in SERT knockout mice by microdialysis and chronoamperometry. *Abstr Pap Am Chem S* **2002,** *224*, U116-U116.

128. Zhang, B.; Adams, K. L.; Luber, S. J.; Eves, D. J.; Heien, M. L.; Ewing, A. G., Spatially and temporally resolved single-cell exocytosis utilizing individually addressable carbon microelectrode arrays. *Anal. Chem. (Washington, DC, U. S.)* **2008,** *80* (Copyright (C) 2012 American Chemical Society (ACS). All Rights Reserved.), 1394-1400.

129. Clark, R. A.; Ewing, A. G., Quantitative measurements of released amines from individual exocytosis events. *Mol. Neurobiol.* **1997,** *15* (Copyright (C) 2012 American Chemical Society (ACS). All Rights Reserved.), 1-16.

130. Maina, F. K.; Mathews, T. A., Functional Fast Scan Cyclic Voltammetry Assay to Characterize Dopamine D2 and D3 Autoreceptors in the Mouse Striatum. *ACS Chem. Neurosci.* **2010,** *1* (6), 450-462.

131. Quaiserova-Mocko, V.; Novotny, M.; Schaefer, L. S.; Fink, G. D.; Swain, G. M., Led with amperometric detection using a boron-doped diamond microelectrode: Validation of a method for endogenous norepinephrine analysis in tissue. *Electrophoresis* **2008,** *29* (2), 441-447.

132. Eisenhofer, G.; Lenders, J. W. M.; Timmers, H.; Mannelli, M.; Grebe, S. K.; Hofbauer, L. C.; Bornstein, S. R.; Tiebel, O.; Adams, K.; Bratslavsky, G.; Linehan, W. M.; Pacak, K., Measurements of Plasma Methoxytyramine, Normetanephrine, and Metanephrine as Discriminators of Different Hereditary Forms of Pheochromocytoma. *Clin. Chem.* **2011,** *57* (3), 411-420.

133. McCreery, R. L., Advanced carbon electrode materials for molecular electrochemistry. *Chemical Reviews* **2008,** *108* (7), 2646-2687.

134. Bard, A. J.; Editor, *Electroanalytical Chemistry. A Series of Advances, Vol. 17*. Dekker: 1991; p 393 pp.

135. dresselhaus, M. S., *Graphite Fibers and Filamnets*. Springer-Verlag: New York, 1988.

136. Baur, J. E.; Kristensen, E. W.; May, L. J.; Wiedemann, D. J.; Wightman, R. M., FAST-SCAN VOLTAMMETRY OF BIOGENIC-AMINES. *Analytical Chemistry* **1988,** *60* (13), 1268-1272.

137. Bath, B. D.; Martin, H. B.; Wightman, R. M.; Anderson, M. R., Dopamine adsorption at surface modified carbon-fiber electrodes. *Langmuir* **2001,** *17* (22), 7032-7039.

138. DuVall, S. H.; McCreery, R. L., Self-catalysis by catechols and quinones during heterogeneous electron transfer at carbon electrodes. *J Am Chem Soc* **2000,** *122* (28), 6759-6764.

139. Kelly, R. S.; Wightman, R. M., BEVELED CARBON-FIBER ULTRAMICROELECTRODES. *Analytica Chimica Acta* **1986,** *187*, 79-87.

140. Tuinstra, F.; Koenig, J. L., RAMAN SPECTRUM OF GRAPHITE. *J Chem Phys* **1970,** *53* (3), 1126-&.

141. Park, J.; Show, Y.; Quaiserova, V.; Galligan, J. J.; Fink, G. D.; Swain, G. M., Diamond microelectrodes for use in biological environments. *J Electroanal Chem* **2005,** *583* (1), 56-68.

142. Williams, O. A., Nanocrystalline diamond. *Diam. Relat. Mat.* **2011,** *20* (5-6), 621-640.

143. Patel, B. A.; Galligan, J. J.; Swain, G. M.; Bian, X., Electrochemical monitoring of nitric oxide released by myenteric neurons of the guinea pig ileum. *Neurogastroenterol. Motil.* **2008,** *20* (11), 1243-1250.

144. Wang, S. Structure-function relationship of boron-doped diamond thin-film electrodes and application for in vitro amperometric measurements. 2008.

145. Park, J.; Quaiserova-Mocko, V.; Peckova, K.; Galligan, J. J.; Fink, G. D.; Swain, G. M., Fabrication, characterization, and application of a diamond microelectrode for electrochemical measurement of norepinephrine release from the sympathetic nervous system. *Diam. Relat. Mat.* **2006,** *15* (4-8), 761-772.

146. Tachibana, T.; Yokota, Y.; Kobashi, K.; Yoshimoto, M., Heteroepitaxial growth of {111}-oriented diamond films on platinum {111}/sapphire{0001} substrates. *Journal of Crystal Growth* **1999,** *205* (1-2), 163-168.

147. Rotter, S., Applications of conformal CVD diamond films. *Isr. J. Chem.* **1998,** *38* (Copyright (C) 2012 American Chemical Society (ACS). All Rights Reserved.), 135-140.

148. Fink, G. D.; Johnson, R. J.; Galligan, J., Mechanisms of increased venous smooth muscle tone in desoxycorticosterone acetate-salt hypertension. *Hypertension* **2000,** *35* (1), 464-469.

149. Luo, M.; Hess, M. C.; Fink, G. D.; Olson, L. K.; Rogers, J.; Kreulen, D. L.; Dai, X. L.; Galligan, J. J., Differential alterations in sympathetic neurotransmission in mesenteric arteries and veins in DOCA-salt hypertensive rats. *Auton Neurosci-Basic* **2003,** *104* (1), 47-57.

150. Luo, M.; Fink, G. D.; Lookingland, K. J.; Morris, J. A.; Galligan, J. J., Impaired function of alpha(2)-adrenergic autoreceptors on sympathetic nerves associated with mesenteric arteries and veins in DOCA-salt hypertension. *Am J Physiol-Heart C* **2004,** *286* (4), H1558-H1564.

151. Ranganathan, S.; McCreery, R. L., Electroanalytical performance of carbon films with near-atomic flatness. *Analytical Chemistry* **2001,** *73* (5), 893-900.

152. Wang, S. H.; Swain, G. M., Spatially heterogeneous electrical and electrochemical properties of hydrogen-terminated boron-doped nanocrystalline diamond thin film deposited from an argon-rich CH4/H-2/Ar/B2H6 source gas mixture. *Journal of Physical Chemistry C* **2007,** *111* (10), 3986-3995.

153. Dong, H.; Wang, S. H.; Liu, A. H.; Galligan, J. J.; Swain, G. M., Drug effects on the electrochemical detection of norepinephrine with carbon fiber and diamond microelectrodes. *J Electroanal Chem* **2009,** *632* (1-2), 20-29.

154. Dong, Y.; Heien, M. L.; Maxson, M. M.; Ewing, A. G., Amperometric measurements of catecholamine release from single vesicles in MN9D cells. *J Neurochem* **2008,** *107* (6), 1589-1595.

155. Li, Y. F.; LaCroix, C.; Freeling, J., Cytisine induces autonomic cardiovascular responses via activations of different nicotinic receptors. *Auton Neurosci-Basic* **2010,** *154* (1-2), 14-19.

156. *Ion Channels and Their Inhibitors*. Springer-Verlag Berlin: Berlin, 2011; p 1-348.

157. Mathews, T. A.; Bosse, K. E.; Newman, B.; Apawu, A.; Rogalla, C., ALTERED STRIATAL DOPAMINE NEUROTRANSMISSION IN MICE WITH LOW ENDOGENOUS BDNF FOLLOWING DRINKING-IN-THE-DARK ETHANOL EXPOSURE. *Alcohol Clin Exp Res* **2012,** *36*, 177A-177A.

158. Takmakov, P.; Zachek, M. K.; Keithley, R. B.; Walsh, P. L.; Donley, C.; McCarty, G. S.; Wightman, R. M., Carbon Microelectrodes with a Renewable Surface. *Analytical Chemistry* **2010,** *82* (5), 2020-2028.

159. Dunn, W. R.; Hardy, T. A.; Brock, J. A., Electrophysiological effects of activating the peptidergic primary afferent innervation of rat mesenteric arteries. *British Journal of Pharmacology* **2003,** *140* (2), 231-238.

160. Brock, J. A.; Tan, J. H. C., Selective modulation of noradrenaline release by alpha(2)-adrenoceptor blockade in the rat-tail artery in vitro. *British Journal of Pharmacology* **2004,** *142* (2), 267-274.

161. Kawagoe, K. T.; Zimmerman, J. B.; Wightman, R. M., PRINCIPLES OF VOLTAMMETRY AND MICROELECTRODE SURFACE-STATES. *J. Neurosci. Methods* **1993,** *48* (3), 225-240.

162. Ge, S. C.; White, J. G.; Haynes, C. L., Quantal Release of Serotonin from Platelets. *Analytical Chemistry* **2009,** *81* (8), 2935-2943.

163. Cvacka, J.; Quaiserova, V.; Park, J.; Show, Y.; Muck, A.; Swain, G. M., Boron-doped diamond microelectrodes for use in capillary electrophoresis with electrochemical detection. *Analytical Chemistry* **2003,** *75* (11), 2678-2687.

164. Rotter, S. Z.; Madaleno, J. C., Diamond CVD by a Combined Plasma Pretreatment and Seeding Procedure. *Chemical Vapor Deposition* **2009,** *15* (7-9), 209-216.

165. Feng, J. X.; Brazell, M.; Renner, K.; Kasser, R.; Adams, R. N., Electrochemical pretreatment of carbon fibers for in vivo electrochemistry: effects on sensitivity and response time. *Anal. Chem.* **1987,** *59* (Copyright (C) 2012 American Chemical Society (ACS). All Rights Reserved.), 1863-7.

166. Ferrari, A. C.; Robertson, J., Is there a "nanocrystalline diamond" Raman peak in nanocrystalline diamond? *NATO Sci. Ser., II* **2001,** *24* (Copyright (C) 2012 American Chemical Society (ACS). All Rights Reserved.), 177-184.

167. Ferrari, A. C.; Robertson, J., Resonant Raman spectroscopy of disordered, amorphous, and diamondlike carbon. *Phys. Rev. B: Condens. Matter Mater. Phys.* **2001,** *64* (Copyright (C) 2012 American Chemical Society (ACS). All Rights Reserved.), 075414/1-075414/13.

168. Birrell, J.; Gerbi, J. E.; Auciello, O.; Gibson, J. M.; Johnson, J.; Carlisle, J. A., Interpretation of the Raman spectra of ultrananocrystalline diamond. *Diamond Relat. Mater.* **2005,** *14* (Copyright (C) 2012 American Chemical Society (ACS). All Rights Reserved.), 86-92.

169. Wang, S.; Swope, V. M.; Butler, J. E.; Feygelson, T.; Swain, G. M., The structural and electrochemical properties of boron-doped nanocrystalline diamond thin-film electrodes grown from Ar-rich and H2-rich source gases. *Diamond Relat. Mater.*

2009, *18* (Copyright (C) 2012 American Chemical Society (ACS). All Rights Reserved.), 669-677.

170. Hikavyy, A.; Clauws, P.; Maes, J.; Moshchalkov, V. V.; Butler, J. E.; Feygelson, T.; Williams, O. A.; Daenen, M.; Haenen, K., An investigation of structural and electrical properties of boron doped and undoped nanocrystalline diamond films. *Phys. Status Solidi A* **2006,** *203* (Copyright (C) 2012 American Chemical Society (ACS). All Rights Reserved.), 3021-3027.

171. Butler, J. E.; Sumant, A. V., The CVD of nanodiamond materials. *Chem. Vap. Deposition* **2008,** *14* (Copyright (C) 2012 American Chemical Society (ACS). All Rights Reserved.), 145-160.

172. Butler, J. E.; Sumant, A. V., The CVD of nanodiamond materials. *Chemical Vapor Deposition* **2008,** *14* (7-8), 145-160.

173. Wagner, J.; Wild, C.; Koidl, P., Resonance effects in Raman scattering from polycrystalline diamond films. *Appl. Phys. Lett.* **1991,** *59* (Copyright (C) 2012 American Chemical Society (ACS). All Rights Reserved.), 779-81.

174. Knight, D. S.; White, W. B., Characterization of diamond films by Raman spectroscopy. *J. Mater. Res.* **1989,** *4* (Copyright (C) 2012 American Chemical Society (ACS). All Rights Reserved.), 385-93.

175. Kim, D. Y.; Wang, J.; Yang, J.; Kim, H. W.; Swain, G. M., Electrolyte and Temperature Effects on the Electron Transfer Kinetics of Fe(CN)(6)(-3/-4) at Boron-Doped Diamond Thin Film Electrodes. *Journal of Physical Chemistry C* **2011,** *115* (20), 10026-10032.

176. Bard, A. J.; Faulkner, L. R., *Electrochemical Methods: Fundamentals and Applications*. Masson: 1982; p 808 pp.

177. Kinoshit.K; Bett, J., ELECTROCHEMICAL OXIDATION OF CARBON-BLACK IN CONCENTRATED PHOSPHORIC-ACID AT 135 DEGREES C. *Carbon* **1973,** *11* (3), 237-247.

178. Hu, I. F.; Karweik, D. H.; Kuwana, T., ACTIVATION AND DEACTIVATION OF GLASSY-CARBON ELECTRODES. *J Electroanal Chem* **1985,** *188* (1-2), 59-72.

179. Chen, Q. Y.; Swain, G. M., Structural characterization, electrochemical reactivity, and response stability of hydrogenated glassy carbon electrodes. *Langmuir* **1998,** *14* (24), 7017-7026.

180. Kuo, T.-C.; McCreery, R. L., Surface Chemistry and Electron-Transfer Kinetics of Hydrogen-Modified Glassy Carbon Electrodes. *Anal. Chem.* **1999,** *71* (Copyright (C) 2012 American Chemical Society (ACS). All Rights Reserved.), 1553-1560.

181. Strand, A. M.; Venton, B. J., Flame etching enhances the sensitivity of carbon-fiber microelectrodes. *Analytical Chemistry* **2008,** *80* (10), 3708-3715.

182. Dechamplain, J.; Farley, L.; Cousineau, D.; Vanameringen, M. R., CIRCULATING CATECHOLAMINE LEVELS IN HUMAN AND EXPERIMENTAL HYPERTENSION. *Circ Res* **1976,** *38* (2), 109-114.

183. Wallin, B. G.; Charikoudian, N., Sympathetic neural control of integrated cardiovascular function: Insights from measurement of human sympathetic nerve activity. *Muscle Nerve* **2007,** *36* (5), 595-614.

184. Esler, M.; Lambert, E.; Schlaich, M., POINT: CHRONIC ACTIVATION OF THE SYMPATHETIC NERVOUS SYSTEM IS THE DOMINANT CONTRIBUTOR TO SYSTEMIC HYPERTENSION. *J Appl Physiol* **2010,** *109* (6), 1996-1998.

185. Bouvier, M.; Dechamplain, J., INCREASED APPARENT NOREPINEPHRINE RELEASE RATE IN ANESTHETIZED DOCA-SALT HYPERTENSIVE RATS. *Clinical and Experimental Hypertension Part a-Theory and Practice* **1985,** *7* (11), 1629-1645.

186. Dietz, R.; Schomig, A.; Rascher, W.; Strasser, R.; Ganten, U.; Kubler, W., PARTIAL REPLACEMENT OF SODIUM BY POTASSIUM IN THE DIET RESTORES IMPAIRED NORADRENALINE INACTIVATION AND LOWERS BLOOD-PRESSURE IN STROKE-PRONE SPONTANEOUSLY HYPERTENSIVE RATS. *Clinical Science* **1981,** *61*, S69-S71.

187. Esler, M.; Kaye, D., Sympathetic nervous system activation in essential hypertension, cardiac failure and psychosomatic heart disease. *J Cardiovasc Pharm* **2000,** *35*, S1-S7.

188. Mosharov, E. V.; Sulzer, D., Analysis of exocytotic events recorded by amperometry. *Nature Methods* **2005,** *2* (9), 651-658.

189. Cuchillo-Ibanez, I.; Olivares, R.; Aldea, M.; Villarroya, M.; Arroyo, G.; Fuentealba, J.; Garcia, A. G.; Albillos, A., Acetylcholine and potassium elicit different patterns of exocytosis in chromaffin cells when the intracellular calcium handling is disturbed. *Pflugers Archiv-European Journal of Physiology* **2002,** *444* (1-2), 133-142.

190. Travis, E. R.; Wightman, R. M., Spatio-temporal resolution of exocytosis from individual cells (vol 27, pg 102, 1998). *Annual Review of Biophysics and Biomolecular Structure* **1999,** *28*, VII-VIII.

191. Cahill, P. S.; Wightman, R. M., SIMULTANEOUS AMPEROMETRIC MEASUREMENT OF ASCORBATE AND CATECHOLAMINE SECRETION

FROM INDIVIDUAL BOVINE ADRENAL-MEDULLARY CELLS. *Analytical Chemistry* **1995,** *67* (15), 2599-2605.

192. Donoso, M. V.; Steiner, M.; HuidobroToro, J. P., BIBP 3226, suramin and prazosin identify neuropeptide Y, adenosine 5'-triphosphate and noradrenaline as sympathetic cotransmitters in the rat arterial mesenteric bed. *J Pharmacol Exp Ther* **1997,** *282* (2), 691-698.

193. Almers, W., EXOCYTOSIS. *Annual Review of Physiology* **1990,** *52*, 607-624.

194. Young, W. F., Adrenal causes of hypertension: Pheochromocytoma and primary aldosteronism. *Reviews in Endocrine & Metabolic Disorders* **2007,** *8* (4), 309-320.

195. Zhang, W. G.; Thoren, P., Hyper-responsiveness of adrenal sympathetic nerve activity in spontaneously hypertensive rats to ganglionic blockade, mental stress and neuronglucopenia. *Pflugers Archiv-European Journal of Physiology* **1998,** *437* (1), 56-60.

196. Esler, M.; Jennings, G.; Lambert, G.; Meredith, I.; Horne, M.; Eisenhofer, G., OVERFLOW OF CATECHOLAMINE NEUROTRANSMITTERS TO THE CIRCULATION - SOURCE, FATE, AND FUNCTIONS. *Physiol. Rev.* **1990,** *70* (4), 963-985.

197. Niane, L. M.; Joseph, V.; Bairam, A., Systemic blockade of nicotinic and purinergic receptors inhibits ventilation and increases apnoea frequency in newborn rats. *Exp Physiol* **2012,** *97* (8), 981-993.

198. Fulop, T.; Radabaugh, S.; Smith, C., Activity-dependent differential transmitter release in mouse adrenal chromaffin cells. *J Neurosci* **2005,** *25* (32), 7324-7332.

199. Camacho, M.; Machado, J. D.; Montesinos, M. S.; Criado, M.; Borges, R., Intragranular pH rapidly modulates exocytosis in adrenal chromaffin cells. *J Neurochem* **2006,** *96* (2), 324-334.

200. Fulop, T.; Smith, C., Physiological stimulation regulates the exocytic mode through calcium activation of protein kinase C in mouse chromaffin cells. *Biochemical Journal* **2006,** *399*, 111-119.

201. Doreian, B. W.; Fulop, T. G.; Smith, C. B., Myosin II activation and actin reorganization regulate the mode of quantal exocytosis in mouse adrenal chromaffin cells. *J Neurosci* **2008,** *28* (17), 4470-4478.

202. Albillos, A.; Dernick, G.; Horstmann, H.; Almers, W.; deToledo, G. A.; Lindau, M., The exocytotic event in chromaffin cells revealed by patch amperometry. *Nature* **1997,** *389* (6650), 509-512.

203. Hu, Z.; Ma, A.; Tian, H.; Xi, Y.; Fan, L.; Wang, T., Activity and changed expression of calcium-activated potassium channel in vascular smooth muscle cells isolated from mesenteric arteries of spontaneous hypertensive rats. *Xi'an Jiaotong Daxue Xuebao, Yixueban* **2010,** *31* (Copyright (C) 2012 American Chemical Society (ACS). All Rights Reserved.), 424-428.

204. Xu, H.; Jackson, W. F.; Fink, G. D.; Galligan, J. J., Activation of potassium channels by tempol in arterial smooth muscle cells from normotensive and deoxycorticosterone acetate-salt hypertensive rats. *Hypertension* **2006,** *48* (6), 1080-1087.

205. Dechamplain, J.; Bouvier, M.; Drolet, G., ABNORMAL REGULATION OF THE SYMPATHOADRENAL SYSTEM IN DEOXYCORTICOSTERONE ACETATE SALT HYPERTENSIVE RATS. *Canadian Journal of Physiology and Pharmacology* **1987,** *65* (8), 1605-1614.

206. Bouvier, M.; Dechamplain, J., INCREASED BASAL AND REACTIVE PLASMA NOREPINEPHRINE AND EPINEPHRINE LEVELS IN AWAKE DOCA-SALT HYPERTENSIVE RATS. *Journal of the Autonomic Nervous System* **1986,** *15* (2), 191-195.

207. Feldberg, W.; Minz, B., The effect of acetylcholine upon the adrenal glands. *Arch. Exp. Pathol. Pharmakol.* **1931,** *163* (Copyright (C) 2012 American Chemical Society (ACS). All Rights Reserved.), 66-96.

208. Gong, L. W.; Hafez, I.; de Toledo, G. A.; Lindau, M., Secretory vesicles membrane area is regulated in tandem with quantal size in chromaffin cells. *J Neurosci* **2003,** *23* (21), 7917-7921.

209. Jahn, R.; Scheller, R. H., SNAREs - engines for membrane fusion. *Nature Reviews Molecular Cell Biology* **2006,** *7* (9), 631-643.

210. Chizmadzhev, Y. A.; Cohen, F. S.; Shcherbakov, A.; Zimmerberg, J., Membrane mechanics can account for fusion pore dilation in stages. *Biophys J* **1995,** *69* (6), 2489-2500.

211. Chizmadzhev, Y. A.; Kuzmin, P. I.; Kumenko, D. A.; Zimmerberg, J.; Cohen, F. S., Dynamics of fusion pores connecting membranes of different tensions. *Biophys J* **2000,** *78* (5), 2241-2256.

212. Tang, K. S.; Tse, A.; Tse, F. W., Differential regulation of multiple populations of granules in rat adrenal chromaffin cells by culture duration and cyclic AMP. *J Neurochem* **2005,** *92* (5), 1126-1139.

213. Lingle, C. J.; Solaro, C. R.; Prakriya, M.; Ding, J. P., Calcium-activated potassium channels in adrenal chromaffin cells. *Ion Channels (N. Y.)* **1996,** *4* (Copyright (C) 2012 American Chemical Society (ACS). All Rights Reserved.), 261-301.

214. Miranda-Ferreira, R.; de Pascual, R.; Caricati-Neto, A.; Gandia, L.; Jurkiewicz, A.; Garcia, A. G., Role of the Endoplasmic Reticulum and Mitochondria on Quantal Catecholamine Release from Chromaffin Cells of Control and Hypertensive Rats. *J Pharmacol Exp Ther* **2009,** *329* (1), 231-240.

215. Garcia, A. G.; Padin, F.; Fernandez-Morales, J. C.; Maroto, M.; Garcia-Sancho, J., Cytosolic organelles shape calcium signals and exo-endocytotic responses of chromaffin cells. *Cell Calcium* **2012,** *51* (3-4), 309-320.

216. Puertas, M. C.; Martinez-Martos, J. M.; Cobo, M. P.; Carrera, M. P.; Mayas, D.; Ramirez-Exposito, J., Plasma oxidative stress parameters in men and women with early stage Alzheimer type dementia. *Exp. Gerontol.* **2012,** *47* (8), 625-630.

217. Schaffer, S. W.; Jong, C. J.; Mozaffari, M., Role of oxidative stress in diabetes-mediated vascular dysfunction: Unifying hypothesis of diabetes revisited. *Vasc Pharmacol* **2012,** *57* (5-6), 139-149.

218. Mates, J. M.; Segura, J. A.; Alonso, F. J.; Marquez, J., Oxidative stress in apoptosis and cancer: an update. *Arch Toxicol* **2012,** *86* (11), 1649-1665.

219. Torok, J., Participation of Nitric Oxide in Different Models of Experimental Hypertension. *Physiol. Res.* **2008,** *57* (6), 813-825.

220. Cao, X.; Demel, S. L.; Quinn, M. T.; Galligan, J. J.; Kreulen, D., Localization of NADPH oxidase in sympathetic and sensory ganglion neurons and perivascular nerve fibers. *Auton Neurosci-Basic* **2009,** *151* (2), 90-97.

221. Chen, Q.; Marshall, J. C.; Weidner, R.; Fink, G. R., Zooming In and Zooming Out of the Attentional Focus: An fMRI Study. *Cereb Cortex* **2009,** *19* (4), 805-819.

222. Buchert, F.; Schober, Y.; Rompp, A.; Richter, M. L.; Forreiter, C., Reactive oxygen species affect ATP hydrolysis by targeting a highly conserved amino acid cluster in the thylakoid ATP synthase gamma subunit. *Biochim. Biophys. Acta-Bioenerg.* **2012,** *1817* (11), 2038-2048.

223. Demel, S. L. Impaired purinergic neurotransmission to mesenteric arteries in salt-sensitive hypertension. 2008.

224. Musicki, B.; Liu, T. Y.; Sezen, S. F.; Burnett, A. L., Targeting NADPH Oxidase Decreases Oxidative Stress in the Transgenic Sickle Cell Mouse Penis. *J Sex Med* **2012,** *9* (8), 1980-1987.

225. Miranda-Ferreira, R.; de Pascual, R.; Smaili, S. S.; Caricati-Neto, A.; Gandia, L.; Garcia, A. G.; Jurkiewicz, A., Greater cytosolic and mitochondrial calcium transients in adrenal medullary slices of hypertensive, compared with normotensive rats. *Eur J Pharmacol* **2010,** *636* (1-3), 126-136.

226. Chen, D. D.; Dong, Y. G.; Yuan, H.; Chen, A. F., Endothelin 1 Activation of Endothelin A Receptor/NADPH Oxidase Pathway and Diminished Antioxidants Critically Contribute to Endothelial Progenitor Cell Reduction and Dysfunction in Salt-Sensitive Hypertension. *Hypertension* **2012,** *59* (5), 1037-+.

227. Coupland, R. E., DETERMINING SIZES AND DISTRIBUTION OF SIZES OF SPHERICAL BODIES SUCH AS CHROMAFFIN GRANULES IN TISSUE SECTIONS. *Nature* **1968,** *217* (5126), 384-&.

228. Troyer, K. P.; Heien, M.; Venton, B. J.; Wightman, R. M., Neurochemistry and electroanalytical probes. *Current Opinion in Chemical Biology* **2002,** *6* (5), 696-703.

229. Walsh, P. L.; Petrovic, J.; Wightman, R. M., Distinguishing splanchnic nerve and chromaffin cell stimulation in mouse adrenal slices with fast-scan cyclic voltammetry. *Am. J. Physiol.-Cell Physiol.* **2011,** *300* (1), C49-C57.

230. Kubo, T.; Fukumori, R.; Kobayashi, M.; Yamaguchi, H., Enhanced cholinergic activity in the medulla oblongata of DOCA-salt hypertensive and renal hypertensive rats. *Hypertens. Res.* **1996,** *19* (Copyright (C) 2012 American Chemical Society (ACS). All Rights Reserved.), 213-219.

231. Morrison, S. F.; Cao, W. H., Different adrenal sympathetic preganglionic neurons regulate epinephrine and norepinephrine secretion. *Am J Physiol-Reg I* **2000,** *279* (5), R1763-R1775.

232. Cahill, A. L.; Eertmoed, A. L.; Mangoura, D.; Perlman, R. L., Differential regulation of phenylethanolamine N-methyltransferase expression in two distinct subpopulations of bovine chromaffin cells. *J Neurochem* **1996,** *67* (3), 1217-1224.

233. Shima, E. R.; Gouzman, I.; Folman, M.; Hoffman, A.; Rotter, S., Surface carbon saturation as a means of CVD diamond nucleation enhancement. *Diamond Relat. Mater.* **1999,** *8* (Copyright (C) 2012 American Chemical Society (ACS). All Rights Reserved.), 139-145.